Dissertation

To obtain
the academic degree
Doctor rerum humanarum (Dr. rer. hum.)
at the Medical Faculty, University of Rostock

Production and Characterization of Genetically Modified Magnetized Cells for Future Targeted Treatment of Cardiovascular Diseases

Submitted by
Natalia Voronina
born on 04.11.1989 in Novgorod, Russia

Rostock, 2016

urn:nbn:de:gbv:28-diss2018-0050-4

Reviewers:

1. Reviewer:
   Prof. Dr. Alexander Pfeifer,
   Institut für Pharmakologie und Toxikologie, Universitätsklinikum Bonn

2. Reviewer:
   Prof. Dr. Robert David,
   Referenz-und Translationszentrum für Kardiale Stammzelltherapie,
   Unversitätsmedizin Rostock

3. Reviewer:
   Prof. Dr. Michael O. Glocker,
   Proteomzentrum, Unversitätsmedizin Rostock

Date of submission: 14. Oktober 2016

Date of defence: 5. Juli 2017

CONTENTS

ORIGINAL PUBLICATIONS DESCRIBING DATA USED IN THIS DISSERTATION

Voronina N, Wiekhorst F, Kühn J-P, Rimmbach C, Steinhoff G & David R. "Non-Viral Magnetic Engineering of Endothelial Cells with microRNA and Plasmid-DNA-An Optimized Targeting Approach." *Nanomedicine : nanotechnology, biology, and medicine* 12.8 (2016): 2353–2364. Web. 15 Sept. 2016. (impact factor 5.67)

Müller P#, **Voronina N**#, Hausburg F#, Lux C, Steinhoff G & David R (#, authorship equally shared) "Magnet-bead based microRNA delivery system to modify CD133+ stem cells": Magnet-Bead Based MicroRNA Delivery System to Modify CD133 $^{+}$ Stem Cells. *Stem Cells Int.* **2016,** 1–16 (2016). (impact factor 3.687)

Voronina N, Lemcke H, Wiekhorst F, Kühn J-P, Steinhoff G & David R. "Manufacturing and *in vitro* characterization of magnetized miR-modified endothelial cells for regenerative medicine." Invited original publication: under revision in JoVE (impact factor 1.325)

Patent pending DE 102016216657.3: "Eukaryotische adulte Zellen umfassend ein Transfektionssystem und deren Herstellung und Verwendung". Invention is equally shared between Voronina N, Hausburg F, Müller P, Steinhoff G & David R.

Additional co-autorships and conference presentations are listed on p. 109-111.

ABBREVIATIONS

- AAV – adeno-associated virus
- ACE – angiotensin-converting-enzyme
- AC6 - adenylyl cyclase 6
- ADA-SCID – Adenosine Deaminase Severe Combined Immunodeficiency
- BM-MNCs - bone marrow mononuclear cells
- CABG - coronary artery bypass grafting
- CAD - coronary artery disease
- CMV - cytomegalovirus
- CRISPR – clustered regularly interspaced short palindromic repeat
- CSCs - cardiac stem and progenitor cells
- CVD – cardiovascular diseases
- Cx – connexin
- DMEM - Dulbecco's Modified Eagle's Medium
- DNA – deoxyribonucleic acid
- EdU - 5-ethynyl-2'-deoxyuridine
- EGFP – enhanced green fluorescent protein
- EPCs - endothelial progenitor cells
- ER – endoplasmic reticulum
- ESCs – embryonic stem cells
- FGF - fibroblast growth factor
- FRAP –fluorescence recovery after photobleaching
- GJ – gap junction
- GJIC - gap junctional intercellular communication
- HF – heart failure
- HIFα - hypoxia-specific transcription factor
- HSCs - hematopoietic stem cells
- HUVECs – human umbilical vein endothelial cells
- iPSCs - induced pluripotent stem cells
- LV – left ventricle
- LVEF - LV ejection fraction
- MI – myocardial infarction
- miR – microRNA

- MNPs - magnetic nanoparticles
- MSCs - mesenchymal stem cells
- MTT - 3-(4,5-Dimethylthiazol-2-yl)-2,5-diphenyltetrazolium bromide
- PAD – peripheral arterial disease
- PDGF - platelet-derived growth factor
- PEI – polyethyleneimine
- qRT-PCR – quantitative real-time polymerase chain reaction
- RISC - RNA-induced silencing complex
- SDF-1 – stromal derived factor-1
- SEM – standard error of mean
- SERCA2a - sarcoplasmic reticulum calcium ATPase
- shR – small hairpin RNA
- siR – small interfering RNA
- SKM - skeletal myoblasts
- TALENs – transcription activator-like effector nucleases
- VEGF - vascular endothelial growth factor
- WHO – World Health Organization
- ZFNs – zinc-finger nucleases

ZUSAMMENFASSUNG

CVD zählen nach wie vor zu den bedeutendsten und kostenintensivsten Erkrankungen, während das Ergebnis chirurgischer und pharmakologischer Interventionen hier limitiert und häufig palliativer Natur ist. Gleichzeitig bietet sich mit der Gentherapie ein viel versprechendes Instrument für die zukünftige kausale CVD-Behandlung an. Ihre breite klinische Anwendung ist jedoch durch das Fehlen von geeigneten gezielten Genvektor-Systemen noch sehr beschränkt.

Darüber hinaus wird die Entwicklung von multifunktionalen Gen-Vektoren, welche für die klinische Translation geeignet sind, eine Optimierung der Stammzelltypen ermöglichen, die derzeit bereits in klinischen Studien mit CVD-Behandlung angewendet werden.

Um dieses Ziel zu erreichen wurden im Rahmen dieser Arbeit nicht-virale Vektoren verwendet, bestehend aus Polyethyleneimin und magnetischen Nanopartikel n(PEI/MNP), die in unserer Gruppe entwickelt worden waren.

Zunächst wurde PEI/MNP an primären Endothelzellen (HUVECS) als in-vitro-Modell für die Angiogenese getestet, welche ein bedeutendes Therapieziel bei CVD darstellt. Optimale Transfektionsbedingungen wurden für MicroRNA (MiR) und Plasmid DNA definiert - dies führte zu ~ 95-98 % Aufnahme von markierter MiR sowie zu ~40-55 % Markergen-exprimierender Zellen nach Plasmid-Transfektion, was jeweils mittels Durchflusszytometrie ermittelt wurde.

Wenn funktionelle Anti-MiR transfiziert wurde, konnte ein vollständiger Knock-down der endogenen Ziel-miR erzielt werden und darüber hinaus eine entsprechende Hochregulation des Zielgens, was sich aus qRT-PCR-Analysen ergab. Dies gelang ohne Beeinträchtigung der Zellviabilität, wie die Beobachtung über 96h zeigte.

Darüber hinaus wurden zwei Targting-Modalitäten in vitro verglichen: 1) Direktes Vektor-Targeting, welches in lokaler Vektor-Aufnahme der Zellen in der Region des Magneten resultierte und 2) Modifikation von Zellen und deren anschließendes Targeting. Dabei dienten FACS, konfokale Mikroskopie, MACS© und Magnetpartikel-Spektroskopie als Analysetechnologien.

Ansatz 2, das magnetische Targeting miR-transfizierter Zellen erwies sich als sehr effizient: ~70 to 80% der Zellen, welche mit mindestens 0,16 pg Eisen pro Zelle geladen waren, konnten sowohl unter statischen als auch unter dynamischen Bedingungen *in vitro* magnetisch gezielt lokal gesteuert werden. Dagegen war Ansatz 1, also das direkte

Vektor-Targeting nur teilweise erfolgreich. Daher wurde im Folgenden der Fokus auf die zell-basierte Strategie gelegt, also die Verwendung miR/PEI/MNP-modifizierter, magnetisierbarer Zellen.

Hierbei konnte ein signifikant vorteilhafter Einfluss von MNP auf die Toxizität von PEI gezeigt werden, was normale Tubuli-Ausbildung der HUVECs widerspiegelte, die bei Verwendung von PEI alleine um ~50-80% zurückging. Zudem ergaben FRAP-Analysen die Ausbildung interzellulärer Zytoplasmaverbindungen („gap-junctions“), über welche möglicherweise miRs ausgetauscht werden können. Hier böten sich die modifizierten Zellen als gezielte miR-Vektoren an. Mikroskopische Analysen der miR/PEI/MNP Internalisierung ergaben für die miR keinen Unterschied zwischen An- und Abwesenheit von MNP bei der Transfektion. Daneben wurden die transfizierten Zellen hinsichtlich ihres Potentials zur MRT basierten Detektion untersucht, wobei bereits 10^4 Zellen bei einer Beladung mit ~0.37 pg Eisen pro Zelle nachweisbar waren.

Im Folgenden wurde diese optimierte Modifikationsstrategie auf einen für die Behandlung von CVD hoch relevanten Zelltyp übertragen - CD133-positive hämatopoetische Stammzellen. Auch hier wurde hoch effiziente Aufnahme von miR mittels PEI/MNP-Vektor erzielt (~80%), während die Zell-Viabilität erhalten blieb, wie durchfluß-zytometrisch nachgewiesen wurde. Darüber hinaus wurde stabile Expression charakteristischer Oberflächenmarker sowie das hämatopoetische Differenzierungs-potentials der Zellen *in vitro* belegt. Zudem konnten die Zellen *in vitro* effizient magnetisch zum Zielort gelenkt werden.

Zusammenfassend weisen die im Rahmend der Arbeit erzielten Daten eindeutig darauf hin, das transiente genetische Modifikation von Zellen mit miR/PEI/MNP einen attraktiven Ansatz darstellt und die Magnetisierung der Zellen sich für das Targeting sowie für MRT basiertes Monitoring der Zellen eignet. Der entwickelte Ansatz scheint besonders vielversprechend zur Optimierung von Zelltherapeutika im Bereich der kardiovaskulären Medizin.

ABSTRACT

CVD remain one of the most damaging and costly disease groups, whereas the outcome of surgical and pharmacological interventions is limited and often palliative. At the same time, gene therapy is a promising tool for CVD treatment. Its wide clinical application is, however, limited by the lack of suitable targeted gene delivery systems. Moreover, the development of multifunctional gene delivery vectors suitable for clinical translation can be used for modification of stem cells, currently applied in clinical trials of CVD treatment. This could improve their properties and allow overcoming current limitations of the concept.

To accomplish this objective, a non-viral vector was used composed by polyethyleneimine and magnetic nanoparticles (PEI/MNP) previously designed in our group.

First, PEI/MNP was tested with primary endothelial cells (HUVEC) as *in vitro* model for angiogenesis, which is a key target of CVD. Optimal transfection conditions were defined for microRNA and plasmid DNA, which resulted in ~95-98% uptake of tagged miR and ~40-55% of cells expressing an introduced marker gene, respectively (measured by flow cytometry). In addition, when functional anti-miR was transfected, a complete knock-down of its endogenous target miR was observed along with respective target gene upregulation as measured by qRT-PCR. This was achieved without affecting cell viability as 96h-observation has shown.

Further, two magnetic targeting modalities were compared *in vitro*: 1) direct vector guidance resulting in localized uptake above the magnet 2) modification of cells and their subsequent magnetic targeting. Flow cytometry, confocal microscopy, MACS© cell separation and magnetic particle spectroscopy served as analyzing tools for this purpose.

Modality 2), magnetic guidance of miR-transfected cells was proven to be very efficient: ~70 to 80% of cells, loaded with no less than 0,16 pg of iron per cell, were magnetically responsive under both, static and dynamic conditions *in vitro*. In contrast, the approach 1) based on direct vector guidance was restricted, presumably by the mechanism of PEI action during transfection. Hence, the focus of further investigation was on the cell-based strategy, i.e. miR/PEI/MNP-modified magnetized cells.

Furthermore, significant positive impact of MNP on the initial toxicity of PEI has been demonstrated (retained tube formation capacity of HUVECs vs ~50-80% decrease in

case of PEI only). In addition, FRAP technique demonstrated that miR/PEI/MNP-modified endothelial cells do maintain intercellular gap-junctional communication and potentially can exchange miR, thereby serving as its carrier to injured tissues. Microscopic investigation of the miR/PEI/MNP internalization mechanism revealed no difference introduced by MNP presence as compared to PEI only. Further, transfected cells were tested *in vitro* in terms of their MRI detection potential. As a result, as few as 10^4 cells could be detected when loaded with at least ~0.37 pg iron/cell.

Next, this optimized modification strategy was successfully transferred to a cell type highly relevant for the treatment of cardiovascular diseases (CVDs), namely, CD133-positive hematopoietic stem cells. In particular, efficient uptake of miR delivered by PEI/MNP was achieved (~80%) while retaining cell survival as measured by flow cytometry. Moreover, the capacity of CD133+ cells to maintain surface marker expression and *in vitro* hematopoietic differentiation capacity was shown. Importantly, these miR-modified cells were proven to be efficiently guided *in vitro* with a magnet.

Taken together, the obtained results indicate that transient genetic modification of cells with miR/PEI/MNP is feasible and results in their magnetization sufficient for targeting and MRI detection. This approach is particularly promising as a tool for improvement of cell therapeutics applied in the cardiovascular field.

INTRODUCTION

1.1 TREATMENT APPROACHES FOR CARDIOVASCULAR DISORDERS

1.1.1 CARDIOVASCULAR DISORDERS. BRIEF OVERVIEW

According to the statistics of the World Health Organization (WHO), cardiovascular diseases (CVD) are the major cause of mortality worldwide: in the United States alone, approximately 1 million of myocardial infarctions occur yearly and many of these patients develop heart failure which is currently diagnosed in 5 million patients[1]. It also represents a serious financial burden since the cost of the treatment is significantly higher than for any other disease group[2,3]. CVD include various disorders affecting heart and vessels: coronary heart disease, cerebrovascular disease, peripheral arterial disease, rheumatic heart disease, congenital heart disease, deep vein thrombosis and pulmonary embolism. Among these, the most frequent cases of tissue ischemia are associated with coronary heart disease, stroke and peripheral arterial disease (PAD), accounting for more than half of all CVD[2].

Until recently, the heart was thought to be a terminally differentiated tissue incapable of regeneration. However, the latest findings have proven that at the age of 20 the renewal rate for cardiomyocytes reaches 1%, whereas at 70 it decreases down to 0,4%[1]. At the same time, even without diagnosed heart disease cardiac overload or simple aging are associated with significant loss of cardiomyocytes – up to 20 million yearly (to compare, the left ventricle (LV) contains 2-4 billion cardiomyocytes). Furthermore, such an acute event as myocardial infarction (MI) cause loss of over a billion of cells, approximately 25% of the total heart mass[3]. Since cardiomyocytes are endogenously regenerated in a very limited degree, compensation of this cell loss is achieved by formation of fibrotic scar tissue[1].

1.1.2 EXISTING TREATMENT APPROACHES OF CVD

Currently, there are no efficient pharmaceutical or surgical strategies for complete prevention of such damage and full regeneration of the damaged tissue[3,4]. In addition to common treatment strategies, several groups of medicaments are applied for CVD prevention or as additives during treatment. For example, medications for the management of hypertension or dyslipidemia can reduce the risk of CVD approximately by 30% when applied separately and by 50% when used simultaneously[5].

In heart failure (HF), pharmacological treatment is principally palliative: ß-blockers, angiotensin-converting-enzyme (ACE) inhibitors, mineralcorticoid-receptor antagonists are mainly able to control metabolic symptoms. Together with cardiac resynchronization and LV assist devices, they are helpful in improving quality of life, however, not able to change the course of the disease[4]. Heart transplantation is known to provide the best therapeutic outcome[4] - yet, the current number of patients on the waiting list greatly exceeds the amount of available hearts according to recent annual Eurotransplant reports[6].

In case of MI, such options as angioplasty or thrombolysis are considered as a standard of care and intended to reverse the ischemia. In addition to these, certain medications are applied after MI to decrease the workload of the heart, eg diuretics and vasodilators[3]. Furthermore, ACE inhibitors, angiotensin receptor blockers and renin inhibitors are usually used to prevent renal dysfunction, which often accompany CVD[3]. Notably, even the most successful developments in surgery are restricted to an improvement of blood supply through large vessels. At the same time, one of the key mechanisms for inoperable heart conditions is microangiopathy, in which the lack of microcirculation is causing ischemia.

Taken together, currently applied pharmaceutic and surgical interventions help to reduce the rate of disease progression and mortality for patients with CVD[2]. However, they do not treat the underlying cause of disorders, creating thereby a necessity to design other treatments. Gene or cell therapy and their combination are the major promising strategies thereof[1,3].

1.1.3 OVERVIEW OF STRATEGIES FOR REPAIRING DAMAGED HEART USING GENE AND CELL THERAPY

Depending on the type of cardiovascular disorder and concomitant dysfunctions, several points can be targeted using gene and cell therapy: enhancement of regenerating capacity of damaged tissue; activation of cytoprotective mechanisms; suppression of disease-related apoptosis; improvement of angiogenesis; providing endogenous or exogenous precursor cells; replacing damaged myocardium with functional cells[1,3]. In cases where regeneration is a main target, it can be induced by overriding a cell cycle checkpoints using signaling factors. Cytoprotective mechanisms can be activated by stimulation of single or multiple cytokines or growth factors. Similarly, for the suppression of disease-triggered apoptosis, either inhibition or enhanced delivery of

cytokines or regulatory proteins can be exploited. Induction of angiogenesis, naturally occurring after ischemia serves to increase the supply of nutrients and oxygen to damaged tissues and to reduce thereby negative outcome of hypoxia[3]. Several of these mechanisms can be introduced by the delivery of precursor cells since they have been shown to secrete protective and antiapoptotic paracrine factors and to participate in the formation of new vessels[7]. Along with such indirect pathways, transplanted cells can participate in the regeneration of the injured organ directly, by differentiation into functional tissue[4].

1.2 GENE THERAPY FOR CVD

1.2.1 GENE THERAPY. INTRODUCTION TO CONCEPT AND APPROACHES.

In gene therapy, the prevention and treatment of diseases are accomplished by the delivery of functional genetic material into human cells, tissues and organs resulting in the correction of genetic defects or in new therapeutic functions[3]. Initially, gene therapy was designed as the replacement of a mutated gene for the treatment of monogenic diseases. Currently existing gene therapy strategies can be divided into 3 groups: gene transfer, gene silencing and gene editing (summarized in Figure 1)[8,9]. Gene transfer is aiming to restore or supplement specific therapeutic factors most often by utilizing complementary DNA or mRNA[9]. Gene silencing is achieved either by the introduction of dominant negative molecules or by RNA interference, which is accomplished by the delivery of small interfering RNA (siR), microRNA (miR) or small hairpin RNA (shR)[9]. Gene editing is based on the induction of DNA double-strand breaks at specific genomic loci, which subsequently stimulate the endogenous DNA-repair mechanisms to mediate genome editing *in situ*[10]. To date, such site-specific genome editing is being realized by delivery of 4 major classes of nucleases: meganucleases, zinc-finger nucleases (ZFNs), transcription activator-like effector nucleases (TALENs) or CRISPR (clustered regularly interspaced short palindromic repeat) associated nuclease Cas9 (reviewed in [10]).

Currently, after the successful marketing of the first gene therapeutic drug *Glibera*© in 2012 for the treatment of a rare form of familial dyslipidaemia[11], the second medication is very close to approval – stem cell gene therapy product *Strimvelis*© for the treatment of Adenosine Deaminase Severe Combined Immunodeficiency (ADA-SCID)[12]. At the same time, multiple phase I and II clinical trials have provided a strong evidence of gene therapy being safe for the treatment of other conditions: severe inherited diseases of the

blood, immune and nervous systems, including primary immunodeficiencies, leukodystrophies, thalassaemia and sickle cell disease, haemophilia B, inherited neurological disorders, retinal dystrophy and cancers (reviewed in [11,13]). Application of gene therapy for the treatment of CVD comprises 7.8% of total number of clinical trials, however, several of them progressed to phase II and III[14].

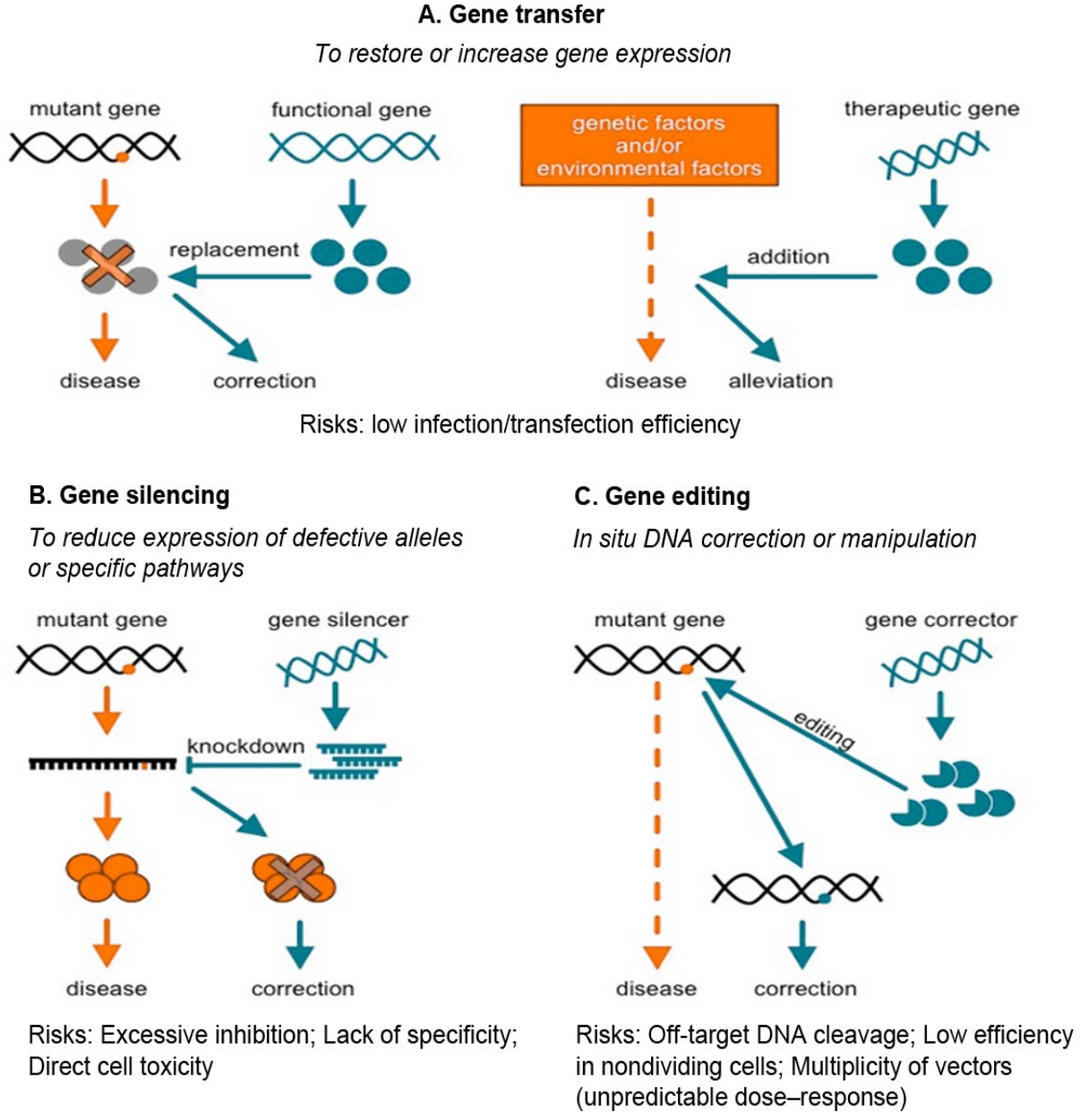

Figure 1. Schematic illustration of gene therapy strategies. (**A**) **Gene transfer.** Gene replacement therapy is based on correction of the mutated gene (orange dot on black helix) which led to disease via abrogated protein synthesis (a cross over circles representing target protein).
Gene addition treatment is ensured by supplementing therapeutic genes which interfere with specific aspects of disease (caused by various factors).
B) **Gene silencing** strategy is based on small noncoding RNA (blue combs) which are capable of inhibiting the aberrant disease-causing mRNA.
(**C**) **Gene editing** relies on the targeted change of a disease-promoting sequence (orange dot) into a disease-preventing sequence (blue dot) by using chimeric nucleases (circle and pie). (adapted from Wang *et al*, 2014[8])

1.2.2 GENE THERAPY FOR CARDIAC PATIENTS

For CVDs, more than 150 clinical trials involving gene therapy are completed or running according to the GeneMed Database[15]. Thus far, the targets include such growth factors as vascular endothelial growth factor (VEGF) and fibroblast growth factor (FGF), stromal derived factor-1 (SDF-1), hypoxia-specific transcription factor HIFα, sarcoplasmic reticulum calcium ATPase (SERCA2a) and adenylyl cyclase 6 (AC6)[3,16,17].

The majority of these studies involve overexpression of growth factors (e.g. VEGF, FGF, G-CSF, platelet-derived growth factor (PDGF), HGF, etc) which are primarily known by the ability to stimulate vasculogenesis and angiogenesis[18]. Often, they possess other beneficial properties: VEGF (through binding to VEGFR2 receptor) has been proven to increase cell survival, permeability and recruitment of local cardiac stem cells to ischemic areas; FGF influences cell proliferation, migration, and production of proteases in endothelial cells and cardiomyocytes, etc[17,19]. In clinical trials, growth factors are mainly aimed to treat angina and coronary artery disease (CAD), the most common form of heart disease, which along with other causes can lead to HF. Several studies using VEGF reported no major adverse events and inconsistent positive outcomes, including improvements in myocardial perfusion (phase II KAT201, GENESIS-I and VIF-CAD); in regional wall motion (EUROINJECT-ONE); in functional class and exercise tolerance (VIF-CAD where VEGF and FGF were applied together); in angina severity and frequency (VIVA)[3,16–18]. Another target, hHGF, was tested in the "Phase I intracoronary administration of Ad-Hhgf" study, resulting in improved activity tolerance; FGF – in the FIRST trial, where a trend towards symptomatic improvement was recorded. In addition, the AGENT III/IV study using FGF overexpression (after successful AGENT I & II in terms of safety and improved myocardial perfusion) was aiming to treat angina pectoris, however, no difference between placebo and treatment was reported[17].

Preclinical and clinical trials using HIFα were initiated as it is a regulator of cellular responses to hypoxia and is able to influence angiogenesis, cell survival, migration and stem cell behavior[17]. To date, it was tested for safety (NCT00117650 & "Multicentre Phase I and Safety Study") with no resulting concerns reported[16,17]. SDF-1, was introduced to clinical trials due to its capacity to maintain cardiac repair: one phase I study was carried out with patients suffering from ischemic HF and as a result its safety, improvement of 6-minute walk test, quality of life, and NYHA class were reported[16].

Another promising therapeutic agent, introduced in 2007 into phase I and II clinical trials
(CUPID & CUPID-2b), is sarcoplasmic reticulum calcium ATPase (SERCA2a) to treat advanced HF. The loss of SERCA2a activity and corresponding impairment in calcium homeostasis is one of the components of the disease[3]. During the phase I/II trials, a single injection of the vector has been shown to significantly improve cardiac function, symptoms and reduce hospitalization of patients, but recent results of a phase IIb study did not confirm the initially reported therapeutic outcome[17,20].
One phase I/II clinical trial (NCT00787059) involving virally-mediated transfer of AC6, which is a regulator of calcium cycling in cardiomyocytes and SERCA2a activity, has started in 2008 and results have not been published yet. This study is aiming to test the safety of therapy in patients with congestive HF and its efficiency in improving LV contractility[21].

Arrhythmias represent another prevalent class of CVDs, which is being evaluated for therapeutic benefit of gene therapy. In this case, however, clinical trials have not yet started despite multiple successful pre-clinical investigations(reviewed in [9]).

In clinical studies for CVDs, most often viruses (adeno-associated viruses (AAV) 1, 6 & 9 & adenoviruses with cardiac-specific cytomegalovirus (CMV) promoter) and sometimes naked plasmid are employed as delivery vectors[3,17,18]. Notably, main risks of gene therapeutics are related to these vehicles: immune reaction of host to viral particles and insertional mutagenesis, inadequate duration or expression and off-target activity[16].
In addition, certain trauma can be caused by the administration procedure since local intracardiac routes are most efficient in terms of gene delivery and avoiding off-target expression. In particular, myocardial injection can physically damage healthy tissue, cause inflammation and scarring or in some cases ventricular perforation; aortic cross-clamp LV cavity infusion can cause similar myocardial injury; pericardial delivery bears minimal risk of pericardial effusion and pneumothorax[16,17]. At the same time, development and wider accessibility of such image-guided injection strategies as NOGA® based on electromechanical mapping of the heart helps to maximally prevent negative events associated with the administration route[22].

1.2.3 PROMISING MOLECULAR TARGETS FOR GENE THERAPY OF CVD

In addition to results of clinical trials, pre-clinical studies suggest that, among others, the following targets bear significant translational potential: S100A1; G protein α subunit; ribonucleotide reductase[23]; ADCY1; βARKct-carboxy terminal peptide from GRK2; b-Adrenergic receptor; KCNH2-G628S; Cardiac sodium channel 4a (SCN4a); connexins 40, 42 and 43; Kir2.1[9,16,17].

In particular, G protein α subunit was reported to control heart rate and remodeling, whereas S100A1, in addition to reversed LV remodeling, also normalizes metabolism of calcium and improves contractility[16,17]. In addition to SERCA itself, which is already being tested in clinical studies, related proteins also regulate myocardial contractility and cardiac function[16]. Application of βARKct-carboxy terminal peptide from GRK2 leads to improvements in β-adreno-receptor signaling and in contractile dysfunction, to heart failure rescue[16]. In addition, for HF treatment, β-adrenergic receptors are proposed as targets: they are downregulated in many patients with HF and their upregulation in rats and rabbits significantly improved LV function[21]. Cardiac inherited myopathies can be influenced by enzymes or sarcomeric proteins (myosin, ribonucleotide reductase)[23]. The following targets were proven efficient *in vivo* for arrhythmia correction: KCNH2-G628S for prolonging refractory period and eliminating arrhythmia inducibility; SCN4a as reducing arrhythmia inducibility and decreasing electrogram fragmentation; connexins 40, 42 and 43 as improving conduction and reducing arrhythmia susceptibility; Kir2.1 was shown to improve pacemaking[16].

Importantly, many of the therapeutic targets for CVD are regulated by miR as pre-clinical studies have demonstrated[21]. In particular, miR25 and miR22 are known to regulate SERCA2a; miR 499 was proven to be a promoter of ventricular hypertrophy, along with miR 23a and 208; miR 1, 9, 98, 133 & 378 were shown to inhibit hypertrophy; circulating miR4235p can be used as a predictor of HF, whereas miR 34, 192 and 194 – of development of HF in patients with MI. Several miR are participating in regulation of fibrosis: miR-24, 299, 30c, 101a or b, 214. AntimiR21 expressed in cardiac fibroblasts suppresses fibrosis together with miR29[21]. Among others, such miRs as miR-21[24], 92a, 34a, 126, 210, 503, 16, 130a and miR-23~27~24 cluster were defined as angiogenesis regulators by having multiple targets (PNUTS, VEGFR2, FGFR1, ITGA5, eNOS, MKK4, Spred-1, etc)[24–32]. Importantly, various miR are known to modulate the

fate of stem cells applied for transplantation, e.g. for HSCs miR-125 family and miR-29a[33].

To date, according to clinicaltrials.gov the safety of miR / antago-miR administration was shown in patients with hepatitis, whereas the majority of trials is testing miRs as potential biomarkers and predictors of various diseases (including cancers, metabolic disorders, sepsis, CVD, etc.)[34].

1.2.4 CURRENT DIFFICULTIES AND POSSIBLE SOLUTIONS

Main obstacles for wide clinical application of gene therapy are shaped by its nature. Any kind of gene therapy implies a transfer of various therapeutic constructs in order to directly or indirectly influence protein structure or expression. By definition, this requires appropriate delivery strategies, which becomes a critical component of success. As discussed above, currently obtained pre-clinical data defined several molecular targets, which have been successfully used in animal models[16,17]. However, clinical trials have not demonstrated as successful or consistent outcome as *in vivo* studies have. This mismatch can be partly explained by the difficulty of modelling human disorders in animals and possible inaccurate prediction of human responses in respective clinical settings[35]. At the same time, targeting of therapeutic molecules to the cells of interest in sufficient quantities remains a highly challenging. Therefore, current directions in which gene therapy is being developed are: selection of proper genetic targets, development of optimized delivery methods and adjustment of administration routes.

1.3 CELL THERAPY FOR CVD

Another major direction within alternative treatment modalities for CVD is cell-based therapy. In general, effects of applied cells are expected to influence the entire course of disease: from vasculature dysfunction to damaged myocardial tissue, which together may lead to improved heart function.

In order to define a proper cells source and population for cardiac regeneration, multiple cell types have been tested in preclinical trials: embryonic stem cells (ESCs), induced pluripotent stem cells (iPSCs), neonatal cardiomyocytes, skeletal myoblasts (SKMs), endothelial progenitor cells (EPCs), cardiac stem and progenitor cells (CSCs), bone marrow mononuclear cells (BM-MNCs), hematopoietic stem cells (HSCs) and mesenchymal stem cells (MSCs)[1]. By now, all these have progressed to clinical studies for CVDs treatment, except neonatal cardiomyocytes and iPSCs[1,36] (summarized

in Figure 2). Initially, clinical cell transplantations started with skeletal myoblasts due to the ability of quiescent satellite cells located under the basal membrane to proliferate and thereby regenerate skeletal muscle. Although preclinical tests for MI were successful resulting in improved LV function, clinical trials including MAGIC (phase I) and MARVEL (Phase II/III) did not show functional improvement in the treatment group as compared to placebo. Importantly, elevated incidence of arrhythmias in myoblast-treated patients was registered, which is thought to be caused by lack of connexins 43 (Cx43) and, therefore, electromechanical integration [1,37,38]. Taken together, the lack of significant clinical improvement and pro-arrhythmicity discredited skeletal myoblasts as a promising therapeutic product[1].

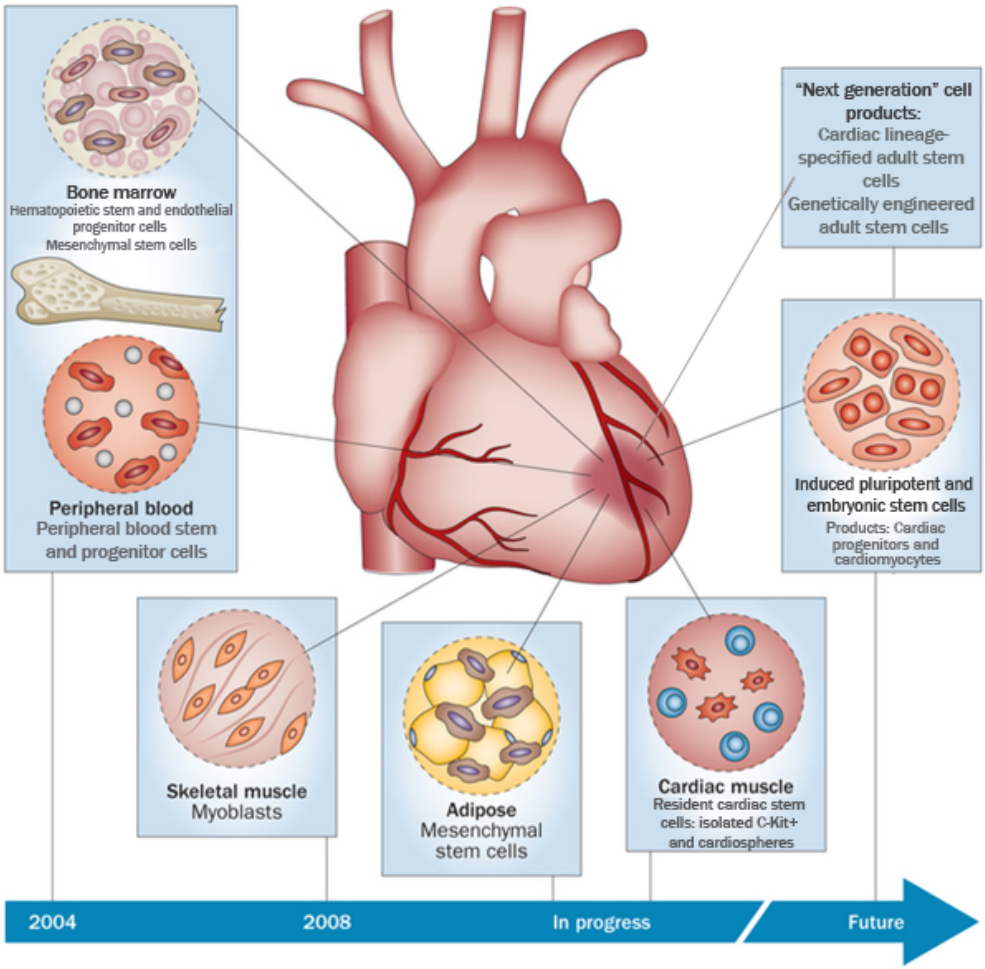

Figure 2. Overview of cell therapeutics applied in clinical trials for cardiac regeneration. To note: products from embryonic stem cells have been already transplanted to a first patient with heart failure; lineage-specified MSCs were tested during the C-CURE trial which promoted future CHART trials. (adapted from Fuster, 2014[39])

Currently, the main focus of regenerative therapy for CVD is persisting on different types of stem and progenitor cells.

1.3.1 STEM AND PROGENITOR CELL APPLICATION FOR CARDIAC REGENERATION

Stem cells carry the capacity for self-renewal as well as directed differentiation[38]. 3 main categories of stem cells are exploited for cardiac regenerative medicine: adult stem cells; embryonic (ESCs) and induced pluripotent stem cells (iPSCs) where either differentiated derivatives are being explored for transplantation or cells are differentiated *in situ* after transplantation[36,38,40]. As potential therapeutic agents, all these cell types carry certain advantages and disadvantages[38,40].

In particular, ESCs and iPSCs share several similar risks: teratome formation due to possible co-transplantation of remaining pluripotent cells together with the final therapeutic product or impaired *in situ* differentiation; cancerogenic potential defined by upregulation of miRNAs commonly found in cancers and possible development of tumorogenic mutations during prolonged culture; possibility of genetic and epigenetic abnormalities[40]. In addition, the use of ESCs has led to serious ethical debates and is risky in terms of immune system reaction to the allogenic cells[40].To date, one clinical trial for CVD treatment has been initiated involving pluripotent cells: ESC-derived cardiac progenitors with a reported purity of 99% were transplanted into an infarct area of a patient with severe heart failure. As a result, at 3 months follow-up an improvement of symptoms from NYHA class III to I and increase in LV ejection fraction (LVEF) of 10% were reported followed by no complications such as arrhythmias or tumor formation[36]. However, as promising as these results are, much better developed protocols, more data and long-term proofs of safety are required to bring early progenitors to wide clinical practice[38,41].

On the contrary, the clinical development of adult stem and progenitor cells for the treatment of cardiac patients is much more advanced: these are the only cells which have undergone most of the clinical translation path up to now. The main risks related to their transplantation are rare, usually manageable and similar for all cell products: immunogenicity and possible occurrence of arrhythmias (the latter particularly for MSCs)[1,38]. The class of adult stem cells consists of different populations of stem and progenitor cells, isolated from various sources, including bone-marrow, circulating blood or solid resident tissues.

Autologous bone marrow represents the most widely applied source of cells for cardiac regeneration. Unselected BM-MNCs (or peripheral blood MNCs) have been extensively studied in pre-clinical and clinical settings. MNCs are beneficial since they are easy to

harvest in large numbers, can be transplanted without *in vitro* expansion and contain different fractions of stem and progenitor cells[42]. In patients with MI, several primary trials including BOOST, REPAIR-AMI and FINCELL have reported early improvements, i.e. increase in LVEF of 5-6% in the cell-treatment group[4]. In contrast, such trials as ASTAMI, HEBE, TIME and Late-TIME have reported that BM-MNC have no effect on myocardial function as compared to placebo[4]. In patients with HF, among others 2 large trials were carried out TOPCARE-CHD (I/II) and FOCUS-CCTRN (II). TOPCARE-CHD compared the influence of circulating progenitor cells and BM-MNC and as a result, in the BM-MNC group a 2.9% increase of LVEF was observed, whereas control and circulating progenitor cells did not cause any improvement. The FOCUS-CCTRN trial demonstrated positive impact of BM-MNC in patients with symptomatic HF and LVEF≤45% (LVEF increase of 2.7% vs control group)[4,22].

In case further III trials with large patient cohorts (e.g. ongoing BAMI study) prove the positive outcome of BM-MNC therapy, it can be considered as an adjuvant to standard-of-care treatment[4]. At the same time, the concept can be improved, in particular by removing its intrinsic variability due to heterogeneity of BM-MNC cell population[22]. In order to achieve this, uniform progenitor or stem cell fractions were isolated from BM-MNC and tested in pre-clinical and clinical trials.

Hematopoietic stem cells (HSCs) represent a subset of bone marrow, which composes less than 0.1% of BM-MNC. They are usually identified by the expression of CD34, CD45 and/or CD133 antigens and were shown to induce angiogenesis and prevent LV remodeling in ischemic conditions *in vivo*[43]. Completed clinical trials for patients with MI or HF (I, II, III phase) have reported inconsistent outcomes: CD133+ cell intramyocardial injection to patients with MI in some cases resulted in improved LVEF (~5%) and myocardial perfusion; in some studies no difference towards the control group was reported[22,44].

Endothelial progenitor cells (EPCs), a subset of BM-MNC, are closely related to HSCs: they express the CD34 marker, the endothelial marker protein (VEGF-R2/KDR) and CXCR-4 receptors (after several weeks in culture, EPCs start to express VE-cadherin and von Willebrand factor)[42]. Preclinical studies have demonstrated that EPCs home to the site of tissue injury and participate directly by forming new vessels and indirectly by secreting proangiogenic cytokines and growth factors; CD34+ cells delivered after MI significantly improved cardiac function in small and large animals[1,42]. Several clinical

trials were initiated on this basis including ACT34-CMI (Ib/II), REGENT (II) and RENEW (III), where the safety of EPC therapy was proven and evidence of efficiency was shown[4]. In particular, the ACT34-CMI trial showed that the intramyocardial injection of low-dose circulating CD34+ EPC had significantly reduced the rate of angina in patients and improved tolerance of exercise[4]. In the REGENT trial, patients with reduced LV function were treated either with unselected BM-MNC or with CD34+/CXCR4+ cells. As a result, a similar improvement of LVEF of 3% was observed in both cell-treated groups and remained unchanged in the control group[22]. The RENEW study has reported an improvement in exercise tolerance as a result of CD34+ EPC transplantation to patients with chronic myocardial ischaemia[1].

From bone marrow stroma, (along with such sources as adipose tissue, lung, liver, peripheral and umbilical cord blood, etc), MSCs can be isolated which are currently defined by following criteria: ability to adhere to plastic under normal culture conditions and display a fibroblast-like morphology; ability to differentiate to osteoblasts, chondrocytes and adipocytes *in vitro;* expression of surface markers CD73, CD90 and CD105 in the absence of CD11b, CD14, CD19, CD34, CD45, Cd79a and HLA-DR (Human leukocyte antigen)[1]. The regenerative potential of MSCs is still under investigation; to date, their capacity for multilineage differentiation is demonstrated (controversial reports in terms of transdifferentiation to cardiomyocytes), as well as ability to control stem cell niches (in HCS & bone marrow), secrete angiogenic paracrine factors (VEGF, bFGF and PDGF) and immunomodulatory properties[1,42]. Large-animal studies have reported that MSCs decrease infarct size and improve ventricular function[1]. Interestingly, POSEIDON trial compared autologous and allogenic BM-MSC and reported no difference between these groups in terms of immunosensitization, although no significant improvement of LVEF was observed, either[4]. In addition, several trials including STEMI (II) and STEM-104-M-CHF (II) showed the safety of allogenic MSC transplantation[1]. In such trials as Prochymal® (II), improvement of LV and end systolic volume was demonstrated for patients with AMI after allogenic MSC transplantation; in PROMETHEUS (I/II) improvement of global LV function occurred after autologous MSC transplantation; in phase I trial PRECISE, adipose tissue-derived stem cell transplantation was safe and improved total LV mass by 20g in patients with ischemic cardiomyopathy[1,45,46].

In post-natal hearts, different subtypes of tissue-resident cardiac stem and progenitor cells have been identified with shared properties of clonality, multipotency and self-renewal [1,22]. Therapeutic effects of these populations are being explored (incl. Sca-1$^+$, Isl-1$^+$, SSEA-1$^+$, side-population cells and telocytes), however, to date c-kit$^+$ cells and cardiosphere-derived cells (CDC) demonstrated highest translational potential[1,44].

C-kit$^+$ cells lack hematopoietic lineage markers and are able to differentiate in cardiomyocytes, endothelial and smooth muscle cells[1]. Preclinical studies in mice and pigs have reported that after transplantation these cells can successfully engraft and improve cardiac function after MI. In phase I clinical trial SCIPIO autologous c-kit$^+$ cells were isolated from patients undergoing coronary artery bypass grafting (CABG) and infused back 113 days after; as a result, ~12.3% improvement of LV function vs baseline value was recorded[4].

CDCs are obtained by the expansion of heart biopsy samples using spheroid culture technique, which results in the formation of heterogenous cell aggregates expressing such stem cell markers as c-kit, Sca-1 and CD34. Preclinical studies in pigs have confirmed the ability of CDC to improve cardiac function and reduce the infarct size after MI[1]. Furthermore, CADUCEUS phase I clinical study have tested therapeutic benefits of CDCs in patients with AMI. The general safety and feasibility of isolated and expanded SCFR$^+$ were reported. At the same time, no effect of this transplantation on LVEF was recorded, although decreased scar size and positive influence on LV volumes were observed in the cell-treatment group[4]. In order to further prove the efficiency of CSCs, the phase I/II study ALLSTAR is currently recruiting patients with MI and further phase III trials will be necessary[1].

1.3.2 CURRENT STATE AND CHALLENGES OF ADULT STEM CELL TRANSPLANTATION FOR CVD TREATMENT

Together, preclinical and clinical trials have led to serious positive outcomes within the field of adult stem and progenitor cell transplantation for CVD therapy. First, as discussed in detail above, the therapeutic regeneration using cell products has been demonstrated (RENEW, Prochymal, SCIPIO, FINCELL, etc). In addition, different advanced delivery strategies were developed (e.g. 3D MyoStar®Injection Catheter combined with NOGA®electromechanical mapping system; 2D fluoroscopic guidance systems Helix™ infusion catheter and the MyoCath™). Notably, the possibility of safe allogenic cell therapy without immunosensitization has been proven for MSCs and CSCs

(POSEIDON, STEMI, Prochymal, ALLSTAR), which enables the generation of "off the shelf" products. Moreover, since such cell types as BM-MNC, HSC, EPC, MSC and CSC have been proven safe for transplantation, with a certain evidence of clinical efficacy, further phase II and III trials can be initiated. In addition, an optimal match between cell product and patient's cohort can be established: BM derived progenitor cells were positively influencing patients with most extensive MI-induced damage including low baseline of LVEF (REPAIR-AMI, FINCELL, REGENT). For other patients emerging cell types such as CSCs may be suitable which will be defined in planned and ongoing clinical trials[41].

At the same time, analysis of carried trials reveals current problems and challenges, which cell therapy for CVD is facing. In particular, in the majority of conducted trials, the criteria of patient selection are inconsistent, which might in part explain some controversies in the reported results. In addition, the intrinsic biological variability of such applied cell products as unselected MNCs can be another factor resulting in the inconsistent outcomes of clinical trials, which is less pronounced in more uniform cell fractions (e.g. positive functional outcomes in BOOST, REPAIR-AMI and FINCELL vs no outcome in ASTAMI, HEBE, TIME and Late-TIME).

Other limitations of currently available cell therapeutics are the following: available numbers of fractioned BM-derived cells are low, replicative capacity of adult stem cells *in situ* is limited compared to ESCs and iPSCs, and cells are restricted to a certain lineage. Moreover, the regenerative capacity of cells declines with age and progenitors mobilized in the body may also lack capability with age[41,47,48].

Delivery of sufficient cell numbers to the site of interest also remains a challenging issue: currently reported rates of cell retention drop below 5-10% as soon as several minutes to hours post application, regardless of administration routes[49–51]. After delivery, the regenerative potential of cells is often compromised by poor engraftment and survival in the ischemic tissue[52,53]. These factors may explain, at least in part, why the therapeutic benefit of adult stem cell application is so limited (~4-5% functional improvement except primary studies of CSCs)[54].

1.3.3 THERAPEUTIC VALUE OF CELL ENGINEERING PRIOR TO TRANSPLANTATION

Main directions, which are currently trying to address the challenges of cell therapy of CVD, are following: selection of particular cell types, development of pluripotent cells for

cardiac regeneration and improvement of administration strategies as discussed above (1.2.2 & 1.3.1.); cell preconditioning for functional and survival improvement[55–57]; control over adhesion molecules and growth factors[58]; enhancement of homing and engraftment, including development of supportive biomaterials[59,60]. At the same time, genetic cell engineering can be a complex answer to these objectives. In particular, by genetic modification or delivery of non-peptidic molecules, either innate cell properties can be improved or additional therapeutics agents can be incorporated. Moreover, using magnetic particles or surface modification with targeting moieties (enzymatic modification, chemical conjugation or non-covalent interactions) external targeting or increased homing can be achieved, respectively. Importantly, during adjustment and improvement, the balance between obtained therapeutic enhancement and minimized loss of stem cells' intrinsic functions must be maintained[61].

Among the mentioned engineering approaches, genetic modification of cells is the most promising, mainly because of its multimodality and ability to cover several challenges for stem cell therapy simultaneously[62]. Introduction of reporter genes can be applied to isolate highly purified cell populations by flow cytometry or to track transplanted cells (e.g. as a result of expression of fluorescent or luminescent proteins)[63,64]. Forced expression of certain factors with high cardiogenic potential can be achieved in transplanted cells[65]. Introduction of factors, which are responsible for such innate cell properties as mobilization, adhesion, migration or integration, can enhance their retention and activity in the desired area[58,66,67]. A similar outcome can be achieved by enhancing intrinsic cell properties, i.e. their survival in an ischemic environment or their paracrine potential[58,62,68]. Furthermore, a broad spectrum of therapeutic agents can be incorporated in order to specifically complement and promote regenerative properties of delivered cells[69,70].

Genetic cell engineering can be done based on different strategies to manipulate cell properties are described above: gene correction, gene silencing and gene editing (Figure 1 & section 1.2.1). There are various methods that enable delivery of genetic material.

1.4 DELIVERY VECTORS FOR GENETIC MATERIAL

Delivery strategies aim to protect the delivered therapeutics from degradation by serum nucleases, to selectively accumulate in the tissue of interest, to ensure cellular internalization followed by appropriate intracellular trafficking and functionality, e.g.

intranuclear transport for pDNA or uptake into RNA-induced silencing complex (RISC) for miR. Broadly, delivery systems can be divided in two main groups by their origin: viral and non-viral[71,72].

1.4.1 VIRAL VS NON-VIRAL

To date, in terms of efficiency viral vectors greatly exceed non-viral systems, which has led to their wider application in clinical trials (~67%)[14]. The most successful vectors which have entered clinical trials belong to adenoviruses, retroviruses (incl. lentiviruses), vaccina virus, adeno-associated viruses (AAV), poxviruses and herpes simplex virus, whereas development and application of such types as human foamy virus, Eppstein-Barr virus, cytomegalovirus, etc. is less advanced[14,72]. Among non-viral delivery systems, the application of naked/plasmid DNA and lipofection are mainly present in clinical studies[14].

Viral vectors enable highly efficient sustainable delivery of genetic material and their application allows both, long-term (years) and short-term (weeks to months) expression for integrating and non-integrating viruses, respectively. To compare the efficiency of viral and non-viral delivery for pDNA: in MSCs, viral delivery easily provides more than 90% gene expression, whereas non-viral usually does not exceed 50-60%; similarly, in CD34+ HSCs transduction ensures efficient expression of transgene by 80-90% of cells whereas non-viral strategy is considered successful already if more than 30-50% of cells start to overexpress the protein of interest[73–77].

However, viruses as delivery vehicles carry serious risks: their pronounced immunogenicity causes inflammatory response leading to severe complications including degeneration of the transducted tissue; limitations in size of the carried genetic material; risk of insertion possibly causing oncogene activation or tumor-suppressor gene inactivation[72].

Therefore, the use of non-viral systems is currently of great interest due to these safety concerns, difficulties and high costs of viral vector production. It is particularly reasonable in such cases as expression of growth factors controlling angiogenesis or delivery of vaccines, where transient genetic correction is required. For such situations virus-free systems pose more attractive options as they are non-pathogenic, non-immunogenic and not limited by the size of delivered genetic material. Notably, significant progress has been achieved in enhancing their efficiency – yet not reaching the level of viral vectors - and producing more advanced vectors[71,78].

1.4.2 MAGNETIC NANOPARTICLES AS A TOOL FOR ADVANCED GENETIC MANIPULATION

As the development of non-viral vectors progresses, many advanced strategies are being explored: including the design of stimuli-responsive vectors; targeted delivery; co-delivery of several molecules; production of biodegradable vectors and noninvasive monitoring of delivered systems[79]. Advanced strategies mostly require the production of hybrid vectors to consolidate their benefits and improve the quality and functionality of the final product. Often nanoparticles, particularly of inorganic origin, become the basis of these hybrid vectors[79].

Responsiveness of gene delivery systems to physicochemical stimuli allows for controlled release of cargo at certain time points and at targeted sites[80]. Recently numerous magnetically-, ultrasound-, light- and redox-triggered systems based on inorganic nanoparticles were reported by different research groups[81–84].

Targeted delivery of the vectors improves specificity of therapy, reduces off-target effects and toxicity. External guidance of magnetic nanoparticle-based vectors by a magnetic field is one of the options[80,85]. Cell surface modification with targeting moieties represents another possible approach and nowadays, various targeting ligands are being successfully applied. These include peptides (e.g., RGD peptide, TAT peptide), folate and other small molecules, glycoproteins (e.g. lactoferrin, transferrin), antibodies, aptamers (peptide- and nucleic acid-based), etc.[80,86,87].

Such advanced concepts as combinations of two or more therapeutic molecules with synergy effects, are widely used for cancer treatment due to its complicated drug resistance mechanisms. In this case, simultaneous delivery of chemotherapeutic agents and molecules for genetic manipulation to the tumors are shown to result in efficient cancer treatment in vivo[88]. In addition, co-delivery of nucleic acids can be used, e.g. siRNA and DNA. It is particularly valuable for the treatment of such disorders, where knockdown of expression and a transient increase in the amount of different proteins are required in parallel (e.g., immunodeficient states, certain types of cancer, cystic fibrosis)[89].

Biodegradability is a beneficial property of some modern gene delivery systems. It can reduce toxicity and side effects of the vector, thus facilitating the approval of the vector

for clinical use. Inorganic nanoparticles are known to be poorly metabolized *in vivo*, therefore their further development towards biodegradable vectors would be an important step forward[86].

Another important feature - for any gene delivery system - is the possibility to noninvasively monitor its post application fate and biodistribution. Magnetic nanoparticles and quantum dots can fulfill this requirement due to their magnetic and fluorescent properties, respectively[90,91].

Only few nanoparticle-based vectors combine several beneficial properties, and magnetic nanoparticles are among those[79]. They share common characteristics of inorganic nanoparticles, such as easy preparation, wide availability, storage stability and high functionality. Moreover, they possess several advantageous properties depending on the nature of magnetic response: magnetic guidance or cell sorting can be achieved in a permanent magnetic field; temperature increase can be produced in an oscillating magnetic field (a combination of both is also applicable)[92,93]. In addition, several studies have shown a positive impact of magnetic nanoparticles on transfection efficiency[93,94]. Importantly, magnetic nanoparticle-based vectors can be non-invasively visualized using conventional MRI or such developing techniques as magnetic particle imaging[81,95].

1.4.3 PROPERTIES OF PEI/MNP DELIVERY VECTOR

In our group, a non-viral vector based on streptavidine-coated superparamagnetic nanoparticles (MNP), bound to biotin-coated polyethyleneimine (PEI) by biotin-streptavidine interaction, was designed[96] as a potential tool for magnetically guided nucleic acid (NA) delivery for induction of angiogenesis in the clinic (vector structure is schematically represented in Figure 3).

In this case, PEI as a highly protonated polyamine ensures nucleic acid condensation and thus protection from degrading factors, vector internalization in cells and endosomal escape[97]. The nucleic acid (NA) is condensed due to electrostatic interactions between its negatively charged phosphates and positively charged protonated amino groups of PEI. The resulting positive charge of complexes ensures their unspecific interaction with the cell surface[14]. Next, cationic particles are endocytosed: for PEI clathrin- and caveolae-mediated uptake has been demonstrated, however, PEI modification can shift the balance between these two processes[98,99]. The details of the next step in transfection – endosomal escape – are still debated, but the most commonly accepted mechanism is the so-called “proton sponge effect”. Briefly, the low pH of the endosomal environment

leads to PEI protonation, which resists to further acidification leading, in turn, to influx of ions and water into endosomes and resulting in osmotic swelling and endosomal disruption[14]. Once in the cytoplasm or nuclei, the release of bound NA is thought to mainly occur as exchange of polycations for surrounding protein components[14]. Notably, the role of free uncondensed PEI in different stages of transfection and its resulting efficiency has been extensively demonstrated[100,101]. In the PEI/MNP vector, MNPs are meant to reduce PEI toxicity, which has already been demonstrated by our group in terms of enhanced survival of hMSCs[94]. Moreover, the presence of a magnetic component allows for exploration of targeted delivery and, therefore, minimized dosages and off-target effects as well as detection with MRI or the advanced imaging modality magnetic particle imaging (MPI) [81,92,95].

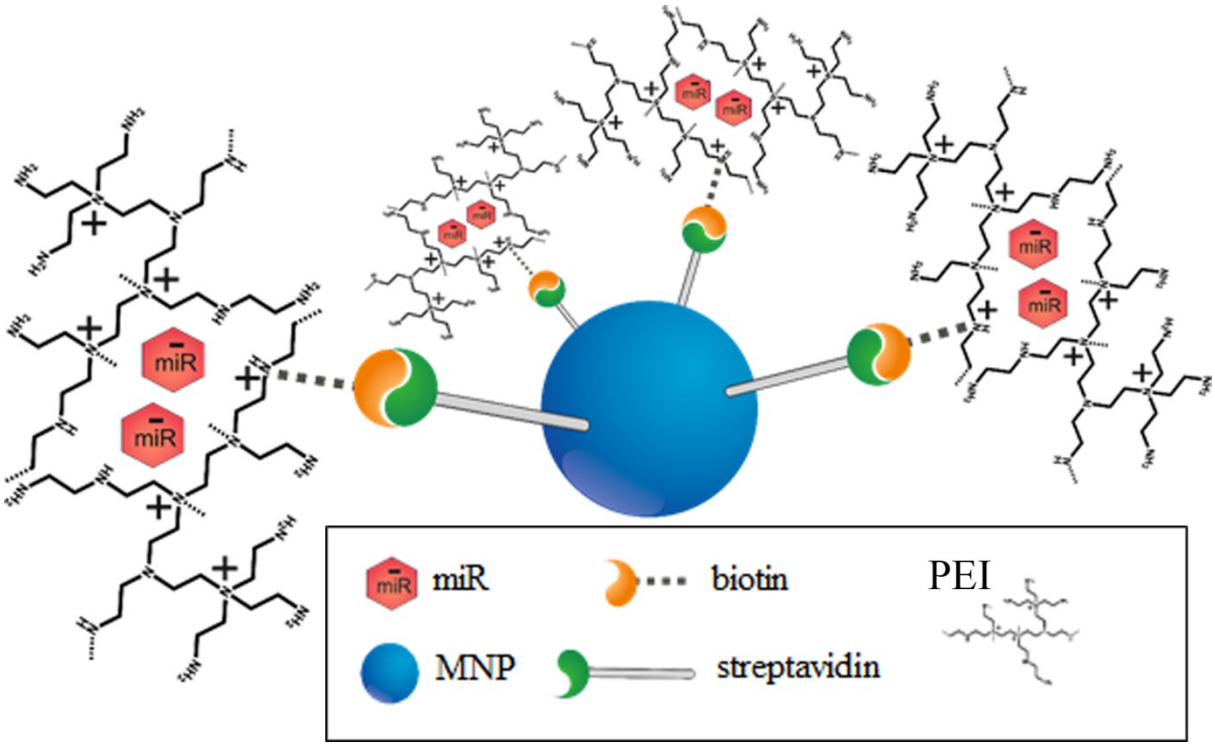

Figure 3. Structure of transfection complexes. A superparamagnetic nanosized core (MNP) is attached to polyethyleneimine (PEI), which condenses nucleic acid (miR is shown as an example here). Binding of the two structural vector components is ensured by biotin – streptavidine interaction resulting from respective PEI and MNP coating.

1.4.4 KNOWN AND UNKNOWN CHARACTERISTICS OF THE VECTOR

Previous studies of our group have demonstrated that, according to size and zeta potential measurements, NA/PEI/MNP complexes are stable in terms of aggregation and are small enough not to cause embolism after injection[94,97,102]. However, the magnetic component of the vector has not been described before in terms of morphology or

magnetic properties. At the same time, proper vector characterization and standardized production is an important step towards the clinic.

Using the PEI/MNP vector, both, pDNA (EGFP, Luciferase reporter constructs) and miR (tagged non-functional miR, therapeutic miR-335), can be efficiently delivered into fibroblasts and hMSCs[94,96,97]. Interestingly, highly increased transfection efficiency of plasmid was demonstrated in the presence of MNP compared to PEI only[94,96]. Since the PEI/MNP vector has been proven efficient for transfection of proliferating cells, it would be of high interest to define if the vector is likewise successful for the modification of non-proliferating clinically relevant cells.

In case of pDNA, the positive influence of MNP on cell survival was also shown in hMSCs. In order to explain this observation, superresolution imaging of internalized DNA/PEI/MNP complexes was performed. It revealed that MNP are preventing PEI from binding to nuclear DNA, which, in turn, might be the reason for improved cell survival[94]. On the other hand, the investigation of another crucial component of transfection, endocytosis, might prove another explanation. In addition, the knowledge about transfection regulators on cellular uptake level could be useful for clinical translation.

A preliminary attempt to achieve targeted gene expression in the murine heart was made[96]. As a result, localized thoracic vector uptake (left lung and endothelium of the heart) has been demonstrated after i.v. vector administration and epicardial magnet application. However, such direct vector targeting *in vivo* was proven to be incomplete: gene expression was observed also in off-target tissues, which are known to accumulate PEI – liver, spleen and kidneys. Detailed investigation of two possible targeting approaches – direct vector targeting and magnetic engineering of cells – could define the optimal one.

Moreover, the superparamagnetic part of the vector offers a highly beneficial potential for non-invasive MRI tracking. Testing this opportunity is of great importance.

1.5 AIM OF THE THESIS

Based on the background described above, the aim of the present study was to investigate the potential of a non-viral PEI/MNP based vector for magnetic targeting and non-invasive monitoring *in vitro*. In particular, the following questions were addressed:

- Can vector production be highly standardized?

- Is a direct vector guidance approach well suited for the current vector design, since its previous *in vivo* performance was not entirely successful?

- Can NA/PEI/MNP-modified cells be magnetically guided in static and dynamic conditions? And if yes, which amount of iron loading is sufficient for cell targeting? Does the application of static magnetic field negatively affect the modified cells?

- Does magnetic engineering of cells with NA/PEI/MNP influence their initial functional capacities? Does transfection affect their ability to maintain intercellular communication, which is crucial for cellular therapeutics intended for transplantation?

- How does the presence of MNP interfere with the toxicity known for PEI? Can this be associated with the impact of iron oxide particles on the intracellular processing?

- Will magnetically-responsive cells – modified at conditions optimal for transfection and targeting – be detectable using MRI? What are the limits of detection?

2 MATERIALS AND METHODS

2.1 CELL ISOLATION AND CULTURE

2.1.1 FIBROBLAST-LIKE CELL LINE (COS7)

The African green monkey kidney fibroblast-like cell line (COS7) was obtained from American Type Culture Collection (VA, USA) and cultured in Dulbecco`s Modified Eagle Medium (DMEM, Pan Biotech GmbH, Aidenbach, Germany), supplemented with 10% fetal bovine serum (FBS, Pan Biotech), non-essential amino-acids (Merck Millipore, Billerica, MA, USA), 100 U/ml Penicillin and 100 µg/ml Streptomycin (both Gibco, Thermo Fisher Scientific, Waltham, MA, USA). Cell cultures were maintained according to the manufacturer's protocol.

2.1.2 ENDOTHELIAL CELLS (HUVEC)

Human umbilical cords for cell isolation were obtained directly *post partum* from informed healthy women, who gave written consent to the use of this material for research according to the Declaration of Helsinki. The ethical committee of the University of Rostock has approved the presented study (reg. No. A 2011 06, prolonged 23 September, 2013).

Human umbilical vein endothelial cells (HUVEC) were isolated from cords by collagenase digestion from the interior of the cord vein following a previously developed protocol[103] - a modification of the procedure described by Jaffe *et al*[104]. Obtained cells were either stored long-term in liquid nitrogen or cultured in the endothelial growth medium (EGM-2, Lonza, Basel, Switzerland), supplemented with 100U/ml penicillin and 100 µg/ml streptomycin at 37C in a humidified atmosphere containing 5% CO2. For all experiments HUVEC were pooled (5 patients) and their passage did not exceed 4. Characterization of obtained cells was carried out by staining for an endothelial marker CD31 (platelet *endothelial* cell adhesion molecule, PECAM-1). For this purpose, cells were grown on Gelatine-coated (Sigma Aldrich, St Louis, MO, USA) coverslips, fixed with 4% PFA (Merck) for 10 minutes and immunofluorescently stained using PECAM-1 as a primary antibody (Santa Cruz Biotechnology Inc, Dallas, Texas, USA) and Alexa Fluor Alexa Fluor ® 647 (Thermo Scientific) as a secondary antibody. In addition, tube formation assay was performed: $3.5x10^4$ HUVECs were seeded in 24 well-plates (Greiner Bio-One, Kremsmünster, Austria), coated with 140 µl Matrigel Basement Membrane

Matrix (BD Biosciences, Heidelberg, Germany) and formation of tubes was observed after 24h.

2.1.3 HEMATOPOIETIC CD133+ STEM CELLS

Bone marrow (BM) was obtained from informed donors, who gave their written consent to use of their samples for research according to the Declaration of Helsinki. The study was approved by the ethical committee of the University of Rostock in 2010 and renewed in 2015 (registration number A 2010 23). Sternal BM aspirates were taken from cardiac patients undergoing coronary artery bypass grafting at the Department of Cardiac Surgery (University Hospital Rostock, Germany). To prevent coagulation in samples, heparin sodium (250 i.E./ml BM) (Rathiopharm GmbH, Ulm, Germany) was used.

First, mononuclear cells (MNCs) were isolated by layering patient derived BM on Pancoll human separation solution (Pan Biotech) and subsequent density gradient centrifugation. Next, $CD133^+$ cells were magnetically enriched using the MACS CD133 MicroBead Kit (Miltenyi Biotec GmbH, Teterow, Germany) following the manufacturer´s instructions. Quality control was carried out with all batches of CD133+ immediately after isolation and only cell fractions with viability and purity higher than 80% were used for further experiments (for the description of the assessment methods see the respective sections below). Obtained cells were treated immediately with transfection complexes and further cultured in humidified atmosphere at 37 °C and 5% CO_2 in DMEM supplemented with 1% penicillin/streptomycin and 2% fetal bovine serum. The only exception was made in the set of experiments carried out to further optimize culture conditions for $CD133^+$ cells. In this case, StemSpan™ H3000 culture medium (Stemcell Technologies Inc, Canada) supplemented with StemSpan™ CC100 (Stemcell Technologies Inc) was used for incubation (see Fig. 8).

2.2 PREPARATION AND CHARACTERIZATION OF TRANSFECTION COMPLEXES

Biotin-Streptavidine interaction was used to create a stable binding of vector components.

2.2.1 BIOTINYLATED POLYETHYLENEIMINE

Biotinylated polyethyleneimine (PEI) was obtained as a product of 25 kDa branched Polyethyleneimine (Sigma) reaction with EZ-Link Sulfo-NHS-LC-Biotin (Biotin, Thermo Scientific) as described in the manufacturers' protocol and previous reports [96]. Several

changes, however, were introduced to a previously developed protocol and characterization strategy in order to standardize the biotinylation procedure. Briefly, polyethyleneimine and biotin were diluted in the amine-free water (Gibco) and appropriate amount of Biotin solution was dropwise added to Polyethyleneimine. Obtained mixture was incubated for 16h under stirring at RT and unreacted Biotin was removed by size-exclusion chromatography with PD-10 Desalting columns (GE Healthcare, Little Chalfont, United Kingdom) as described elsewhere [105]. After purification, biotinylated polyethyleneimine (PEI) was characterized by primary amine group concentration (Ninhydrin assay, Ninhydrin was purchased from Sigma). For this purpose, the standard curve generated for Glycine during each repeated measurement and subsequent definition of PEI concentration was performed. Further, the degree of biotinylation was defined in a so-called HABA assay (Pierce Biotin Quantitation Kit, Thermo Scientific) following previously reported protocols [105,106] and manufacturers' recommendations.

2.2.2 STREPTAVIDINE-COATED SUPERPARAMAGNETIC NANOPARTICLES

The second component of the vector construct - MNP – was prepared as reported before [94] by filtration of Streptavidin MagneSphere® Paramagnetic Particles (Promega, Madison, Wisconsin, USA) through 0,45µm Millix-HV PVDF syringe driven filter (Merck) in order to exclude bigger toxic aggregates.

Obtained nanoparticles were characterized using a commercial dc-magnetometer (MPMS-XL, Quantum Design, San Diego, CA, USA). The magnetization curve $M(H)$ (magnetic moment normalized to iron content) of the MNPs as a function of the external magnetic field (up to 5 T) was determined at room temperature T=295 K. For the measurement, 30 µL of the suspension were placed into a polycarbonate capsule.

Core morphology of MNPs was characterized by transmission electron microscopy (TEM). For this purpose, 16µl of nanoparticle suspension was diluted with 40µl of distilled water, sonicated and vortexed. A small drop of the obtained solution (approx. 3 µl) was placed onto a 300 mesh formavar-carbon coated copper grid. The liquid was dried completely by placing the grid onto a glass slide on a heating plate. Subsequently, the specimen was analyzed in a Zeiss Libra 120 transmission electron microscope at 120 KV and digital images were recorded with a 2x2k Proscan camera (TRS, Moorenweis, Germany) using iTEM camera control and imaging software (Olympus Soft Imaging

Solutions, Münster, Germany). In addition, elemental composition of the specimen was verified using an X-ray detector (Sapphire / EDAX-Ametek, Weiterstadt, Germany).

2.2.3 DELIVERED NUCLEIC ACIDS

The delivery capacity of PEI/MNP vector was tested with both, pDNA and miR, and for this purpose several test NA were selected.

Commercially available fluorescent Cy™3 labeled Pre-miR™ Negative Control #1 (Cy3-miR) (Thermo Scientific) was used to define optimal miR delivery and targeting conditions. Pre-miR™ miRNA Precursor Molecules - Negative Control #1 (Thermo Scientific) served for flow cytometry gating controls, colony forming unit (CFU) assays, surface marker expression analysis and intracellular visualization of transfection complexes. For the real-time PCRs, a synthetic inhibitor against hsa-miR-92a-3p was used: Anti-miR™ miRNA Inhibitor (Thermo Scientific) (mature miR sequence as provided by manufacturer: UAUUGCACUUGUCCCGGCCUGU).

To investigate the delivery and magnetic guidance of plasmid, pEGFP-N3 and pcDNA3.1-Luc plasmids were transformed in *E. coli* DH5α-strain and amplified (long-term storage of bacteria at -80 C). Their following isolation and purification were performed using Plasmid DNA Purification Kit (Macherey-Nagel, Düren, Germany) in accordance with manufacturer's instructions.

2.2.4 FLUORESCENT LABELING OF TRANSFECTION COMPLEXES FOR MICROSCOPY

The previously developed protocol for 3-colour labeling of NA/PEI/MNP was applied [94], using different set of dyes. Briefly, PEI was labeled with NHS-Esther Atto 488 (ATTO-TEC GmbH, Siegen, Germany), purified by size-exclusion chromatography (PD-10 Desalting columns) and characterized by Ninhydrin assay for amine group concentration (see above); miR and DNA were labeled with Cy®5 using respective Label IT® kit (Mirus Bio, WI, USA) and their concentration was measured spectrophotometrically by NanoDrop ND-1000 (Thermo Scientific); MNP were labeled every time freshly during NA/PEI/MNP complex formation with Biotin Atto 565 or 488 (ATTO-TEC) in 1:1000 w/w dye to MNP ratio.

2.3 TRANSFECTION

In all experiments, COS7 were seeded in a multiwell plate (Greiner) suitable for the assay 24 h before transfection. HUVEC were cultured for 48 hours prior to transfection (TPP, Trasadingen, Switzerland, unless indicated otherwise) until 70-80% confluence. In

case of CD133+, cells were treated directly after their isolation and seeding in 24 well-plates (Greiner). Seeding formats and applied cell amounts are specified in the Table 1.
NA/PEI or NA/PEI/MNP complexes were prepared fresh before adding to the cell culture medium as previously described [94,97]. Briefly, to form NA/PEI complexes PEI and NA were pre-diluted in appropriate amounts of 5% Glucose solution (MP Biomedicals, Germany), mixed together, vortexed and incubated for 30 minutes. In order to prepare the NA/PEI/MNP formulation MNP were first incubated in an ultrasonic bath for 20 min and afterwards added to pre-prepared NA/PEI complexes. To form different complex compositions, various amounts of nucleic acid (µg or pmol per cm^2 of cell growth surface for pDNA and miR, respectively), molar ratios of PEI nitrogen and NA phosphate (NP ratio, NP) and amounts of iron (µg iron per ml of prepared NA/PEI) were used.
Obtained complexes were further added to the cell culture medium and incubated for different time-periods: in all experiments with HUVEC the transfection medium was replaced with fresh culture medium 6 hours after; treated CD133+ were always incubated with complexes for at least 18h and either directly used for measurements or fresh medium was supplied.

2.4 ANALYSIS OF TRANSFECTION RESULTS

2.4.1 VIABILITY ASSESSMENT

Trypan blue exclusion assay (concentration 0.4%; Sigma) was applied both, during manual cell counting and when T20 automated cell counter (Bio-Rad, Hercules, CA, USA) was used in the experiments with MACS© separation of transfected cells (see the 2.5 section for more information).
In case of COS7 transfection with Luc pDNA, the viability assessment was performed by MTT [3-(4,5-dimethylthiazol-2-yl)-2,5-diphenyl-2H-tetrazolium bromide] assay[94]. For this purpose, 24h after transfection the working solution 5 mg/ml of MTT in phosphate buffered saline (PBS, Pan Biotech) was added to each well for further incubation for 4 h at 37°C, 5% CO2. After the removal of reaction medium, crystals of purple formazan formed in cells were dissolved in 100 µl of DMSO. Absorbance was measured by Bio-Rad Model 680 microplate reader (Bio Rad Laboratories GmbH, Munich, Germany) at a 550 nm using 655 nm wavelength as a reference. Cell viability was calculated and normalized to control, where cells were treated with 5% Glucose equal in volume to the

Table 1. Description of experimental formats

Cell type	Experiment type	Seeding format: Cell number/well	Applied magnet	Evaluation strategy
Cos 7	**Transfection optimization**	48 well-plate: $1.5*10^4$	-	Flow cytometry for cell viability & transfection efficiency
		96 well-plate: $7.5*10^3$		MTT assay for viability Luciferase assay for efficiency
HUVEC	**Transfection assessment**	24 well-plate: $2.5*10^4$ 12 well-plate: $5*10^4$	-	Flow cytometry Proliferation & tube formation assays Real-time PCR
	Intracellular iron quantification	24 well-plate: $2.5*10^4$	B_{drive} = 25 mT, frequency f_0 = 25 kHz	Magnetic Particle Spectroscopy
	NA/PEI/MNP targeting on seeded cells	pDNA/ 6 well-plate: $1*10^5$	Magnetic plate (OZ Biosciences, Marseille, France). Field strength and gradient: 70-250 mT and 50-130 T/m, respectively [81].	Microscopy (confocal LSM)
		miRNA/ Gelatine-coated Lab-Tek 4-well chamber slide or 6 well-plate with 4 Gelatine-coated coverlips: 2 placed over magnet, 2 – without.: $2.5*10^4$ and $10*10^4$, respectively		
	Cell targeting 24h after transfection	24 well-plate (transfection): $2.5*10^4$ 12 well-plate (targeting after detachment): $5*10^4$	Ring Neodym Magnet (magnets4you GmbH Lohr a. Main, Germany), ø 10 mm; remanescence is ~1.3T, coercivity ≥ 955 kA/m.	Microscopy (conventional light)
			MACS cell separation system (Miltenyi). Field strength is 0.4-1T, gradient is up to 10^4 T/m [107]	Flow cytometry for negative and positive fractions after MACS sorting
	MRI visualization of transfected cells	6-well plate (transfection): $1*10^5$	7.1T (animal MRI system)	
	Intercellular communication evaluation	Gelatine-coated Lab-Tek 4-well chamber slide: $2.5*10^4$	-	Microscopy (FRAP)
CD133+	**Transfection optimization**	24 well-plate: $5*10^4$	-	Flow cytometry
	Cell targeting 24h after transfection	24 well-plate (transfection): $2.5*10^4$ 12 well-plate (targeting): all collected	Magnetic plate (OZ Biosciences, Marseille, France).	Microscopy (LSM)

transfection mixture. In all other cases, cell viability was evaluated using flow cytometry (FACS). To perform the measurement, cells were collected at the appropriate time point, stained with Near-IR LIVE/DEAD® Fixable Dead Cell Stain Kit (Molecular Probes) and

fixed with 4% PFA in accordance with standard procedures[97]. These cells were subsequently analyzed using BD FACS LSRII™ flow cytometer (BD Biosciences) with BD FACSDiva Software 6 (BD Biosciences, 2007) using untreated cells as negative control, whereas cells transfected with scrambled NA were used to form adequate gating strategy (a sample gating strategy applied for Cy3-miR or EGFP transfected HUVECs is illustrated in Figure 4).

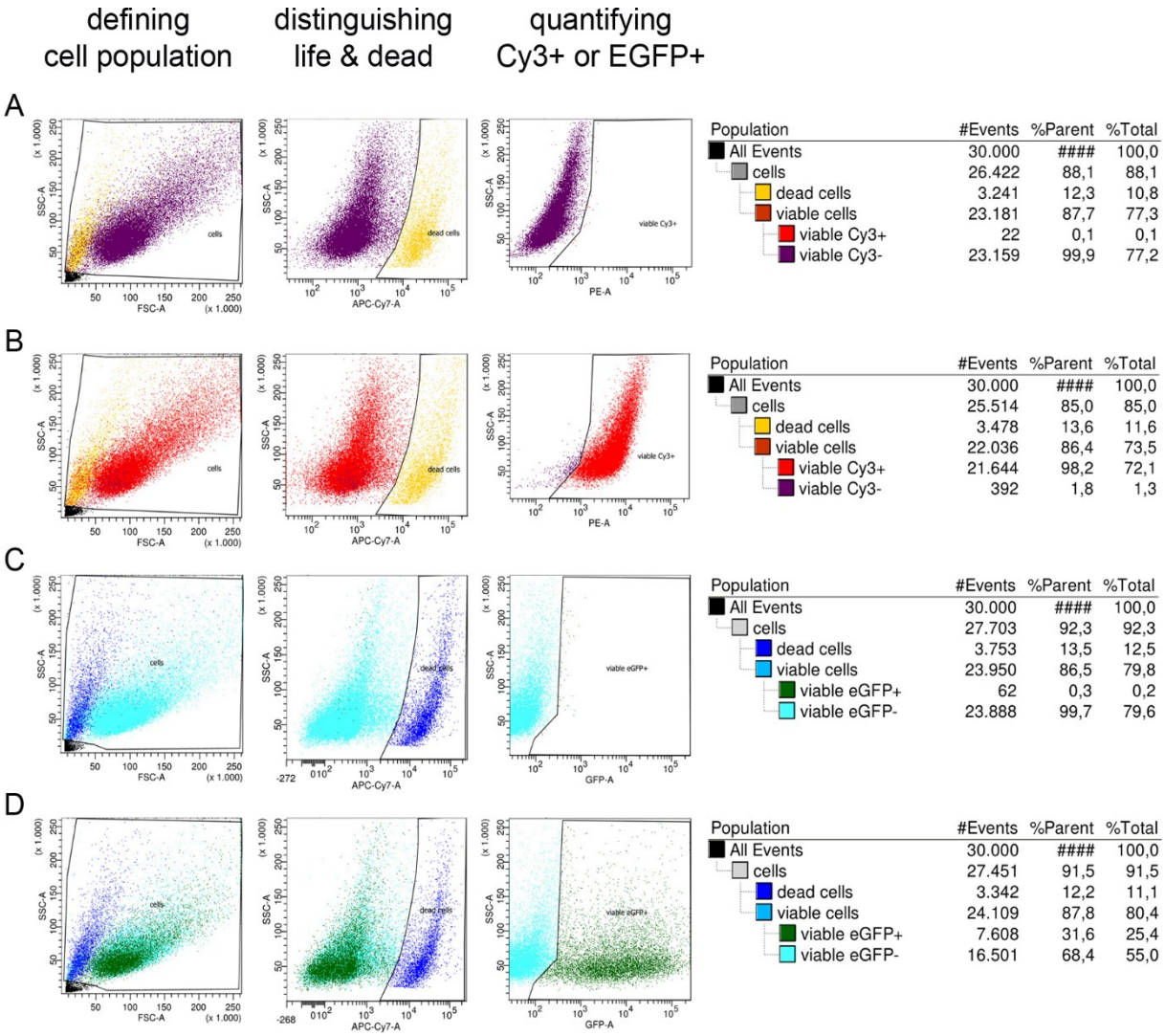

Figure 4. Representative flow cytometry data obtained for HUVEC, which illustrates the gating strategy used for analysis of transfection results.
Scrambled miR (A) or pDNA (C) were applied for transfection to form an adequate gating strategy. First, a dot plot of side scatter (SSC-A) and forward scatter (FSC-A) served to define cell populations and discriminate them from debris. Next, the amount of life and dead cells was defined by plotting cell population within coordinates SSC-A versus APC-Cy7-A. Further, the amount of Cy3-positive or EGFP-positive cells was analyzed (B & D, respectively) by plotting the signal from the excitation of cells with 561-nm laser for Cy3 detection (PE-A, log) or 488-nm laser for EGFP detection (GFP-A), against SSC-A scatter.

2.4.2 TRANSFECTION EFFICIENCY EVALUATION

Transfection efficiency for Luciferase plasmid was examined as reported previously using the Bright-Glo Luciferase Assay System (Promega)[94]. Relative light units were normalized against protein concentration determined by the BCA Protein Assay Kit (Thermo Scientific).

Efficiency of delivery of EGFP plasmid or Cy3-miR were assessed by flow cytometry. Probes for the measurement were prepared and examined as described above (2.4.1).

Real-time PCR was performed to quantify the level of miR silencing (92a, normally expressed in HUVEC) after transfection with inhibiting miR (anti-92a) delivered by miR/PEI or miR/PEI/MNP complexes. In addition, the expression of a target gene (ITGA V as a direct target for miR 92a [32]) was assessed. To perform these measurements, cells were transfected as described above and incubated for 48 h. After that, either total RNA was isolated with the NucleoSpin® RNA Kit (Macherey-Nagel, Düren, Germany) or miR - with mirVana™ miRNA Isolation Kit (Thermo Scientific). Reverse transcription was performed using the TaqMan® MicroRNA Reverse Transcription Kit (Thermo Scientific) and High Capacity cDNA Reverse Transcription Kit (Thermo Scientific). Further, human mature miR-92a and ITGA V transcripts were quantified by the StepOnePlus Real-Time PCR System (Applied Biosystems™) using the corresponding TaqMan Assays (Thermo Scientific).

To calculate the relative expression ratio (R) the ΔΔCT method was used (see equations 1, 2 below). Therefor RNU6B (Assay ID 001093) and Human 18s Endogenous Control (Thermo Scientific) were used as endogenous normalization controls for miR and protein coding genes, respectively. Untransfected cells were used as a reference. The obtained data are representative of 3 independent biological experiments (n = 3), each of which was measured in qPCR-triplicates.

Applied equations:

$$\Delta CT = CT\ target - CT\ endogenous\ control \quad (1)$$

$$R = 2^{-(\Delta CT\ sample - \Delta CT\ reference)} \quad (2)$$

2.4.3 SURFACE MARKER EXPRESSION OF CD133+ CELLS

The expression of surface markers is a crucial parameter for the characterization of stem cells and stability of marker expression after cell modification indicates

preservation of cell type and function. For the CD133+ cell characterization, the following antibodies were used: anti-CD34-FITC (clone: AC136), anti-CD133/2-PE (clone: 293C3), isotype control mouse IgG 2b-PE (Miltenyi), anti-CD45-APC-H7 (clone: 2D1) and 7-AAD (BD Biosciences). To reduce unspecific binding, FcR blocking reagent (Miltenyi) was added. After incubation for 10 min at 4 °C samples were measured with LSR-II flow cytometer (BD Biosciences) and data analysis was performed on FACSDiva software (BD Bioscience). For evaluation Boolean gating strategy was arranged based on the ISHAGE guidelines for $CD34^+$ cells analysis[108] in the following order: cell population, viable $CD45^+$ cells, viable $CD45^+/CD34^+$ cells, viable $CD45^+/CD34^+/CD133^+$ cells (Figure 5).

Calculation of surface marker expression was based on following equation:

$$\text{Surface marker pattern}[\%] = \frac{\text{Viable CD45} + /\text{CD34} + /\text{CD133} + \text{cells}}{\text{Viable CD45} + \text{cells}} \times 100$$

The procedure was carried out with freshly isolated CD133+ to control the quality of cells obtained from BM and also 18h after transfection.

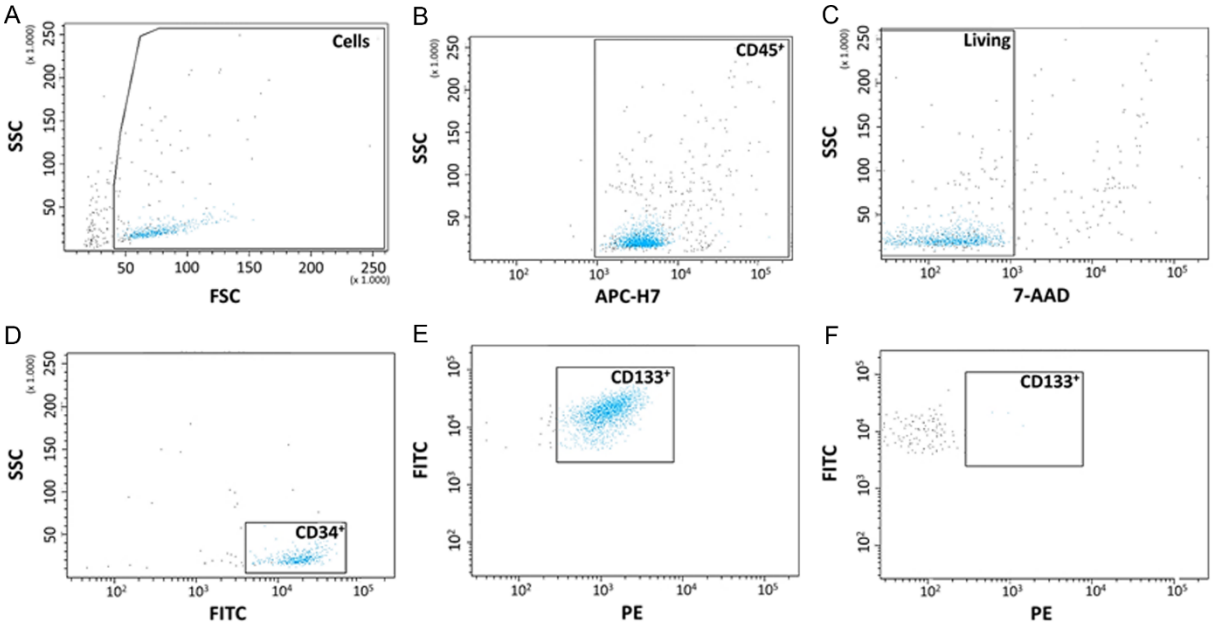

Figure 5: Application of Boolean gating strategy for the flow cytometry of CD133+ cells
(A) A dot plot of side scatter (SSC-A) and forward scatter (FSC-A) was built to exclude debris from the intact cell population. (B) $CD45^+$ cell population is defined in coordinates SSC-A/APC-H7 and subsequently viable (C) cells (7-AAD neg.) are detected in this population. Next, (D) $CD34^+$ cells (FITC pos.) are distinguished from viable $CD45^+$ population and, further, (E) $CD133^+$ cells (PE pos.) – out of viable $CD45^+/CD34^+$ population; (F) PE – isotype control.

2.4.4 MONITORING OF FUNCTIONAL PROPERTIES OF MODIFIED HUVEC AND CD133+

The proliferative capacity of HUVEC was examined in DNA synthesis-based proliferation assay using the Click-iT Plus EdU Imaging Kit (Thermo Scientific). The assay was carried

out 24h after transfection following the manufacturer's instructions. The result - 5 random fields in each well - was recorded with LSM 780 ELYRA PS.1 (Carl Zeiss) and evaluated using ImageJ (NIH). In particular, EdU stained and total nuclei (Hoechst-stained) numbers were defined and the rate of proliferating cells was calculated. To evaluate the influence of miR/PEI or miR/PEI/MNP complexes, the rate of proliferating transfected cells was divided by the rate of EdU-positive cells in untreated control and expressed in %.

To assess functional capacities of HUVEC, a tube formation assay was performed following standard protocols[32]. Briefly, cells were transfected with miR/PEI or miR/PEI/MNP as previously described and incubated for 48 h. After that, $3.5x10^4$ of modified HUVECs were seeded in 24 well-plates (Greiner), coated with 140 µl Matrigel© as described before (2.1.2). Images of 10 random fields in each well were recorded on the LSM 780 ELYRA PS.1 system (Carl Zeiss) and analyzed using ImageJ software, upgraded with an AngiogenesisAnalyzer (NIH). Parameters such as total length of branches, number of branches and number of junctions were used to compare different transfection conditions. Final plotted values were calculated as % of respective parameters vs untreated control.

In order to monitor the hematopoietic differentiation capacity of miR-modified $CD133^+$ cells, CFU assays were performed. After transfection, $1x10^3$ cells were mixed with MethoCult H4434 Classic (STEMCELL Technologies, Germany) and seeded in a 35 mm dish. Formed colonies were identified (CFU-erythroid (CFU-E) (A), Burst-forming unit-erythroid (BFU-E) (B), CFU-granulocyte, erythroid, macrophage, megakaryocyte (CFU-GEMM) (C) and CFU-granulocyte, macrophage (CFU-GM)) and counted for the assessment after 14 d of incubation at 37 °C and 5% CO_2. As recommended by the manufacturer, all samples for each repetition were prepared in duplicates.

2.4.5 INTRACELLULAR LOCALIZATION OF TRANSFECTION COMPLEXES

Qualitative analysis of cells transfected with Cy3-labeled miR was carried out using confocal LSM. This allowed to define whether miR was internalized during transfection or attached to the cell surface, whereas for pDNA this point was adressed by the presence or absence of protein expression.

CD133+ cells, transfected with miR/PEI/MNP were prepared 18 h post-treatment by washing with 2 % FBS in PBS and fixation with 4 % FA for 20 min. Afterwards, cells were spun down to a coverslip and washed with PBS. Prepared coverslip was mounted

with Fluoroshield™ containing DAPI (Sigma-Aldrich) on microscope slides. Obtained samples were visualized on the ELYRA PS.1 LSM 780 system in the tile-scan mode in order to acquire larger areas of 1062.33 µm x 1062.33 µm (40x oil immersion objective, 514 nm excitation laser, differential interference contrast). To identify the intra- or extracellular localization of Cy3 signal, z-stacks of approx. 7 µm depth were recorded.
In case of HUVECs, cells transfected with Cy3-labeled miR were repeatedly washed with PBS 24 h post-treatment, fixed by 4% PFA and their nuclei were counterstained with DAPI. Visualization of prepared samples was similar to CD133+ cells.

Detailed information on intracellular localization of transfection complexes was obtained after cell transfection with 3-colour labelled NA/PEI/MNP (for both, miR and pDNA). In particular, cells were transfected at previously optimized conditions with labeled complexes, where each component carried a fluorescent tag (see 2.2.4. section for detailed description). 24h after transfection cells were washed twice with 2% BSA in PBS in order to remove non-internalized MNPs and complexes [109] and fixed by incubation with 4% PFA solution for 15 min. Nuclei were counterstained by 1.25 nM DAPI (Molecular probes) in PBS and washed thoroughly to remove the excess of the dye. Coverslips prepared this way were mounted with FluorSave™ Reagent (Calbiochem, Darmstadt, Germany) on microscopic slides. Similar strategy was applied in case of CD133+, except several changes, mainly introduced due to the suspension character of cell culture. In particular, cells fixed with 4% PFA cells were spun down on to a coverslip. After washing, the coverslip was mounted with Fluoroshield™ with DAPI (Sigma-Aldrich, Germany) on microscopic slides.
All SIM observations were carried out on the ELYRA PS.1 LSM 780 system with ZEN Software (Carl Zeiss). Using a 63x alpha Plan-Apochromat or 100x alpha 1.46 Plan Apochromat® (Carl Zeiss) objective with oil immersion, Z-stacks were recorded in SIM mode with a 16bit depth at 3 or 5 angles, with averaging 4; 23 µm grid was applied for 405 laser line, 34 µm – 488, 42 µm – 561, 51 µm – 633. These SI raw datasets were computationally reconstructed by ZEN software. Presented final images were obtained as a result of alignment of Maximum projections created separately for each channel.

2.4.6 INVESTIGATION OF VECTOR UPTAKE MECHANISM

A specific inhibitor of dynamin, Dynasore[110] (Abcam, Cambridge, UK), was applied to verify the character of pathways involved in the internalization of transfection

complexes. In this setup, cells were pre-treated with Dynasore (6.8mg/ml[111]) for 1h, transfected with Cy3-miR/PEI or Cy3-miR/PEI/MNP as described above and incubated for 4h. The obtained probes were subsequently investigated by flow cytometry for viability and amount of Cy3-positive HUVEC (see above). Untransfected cells treated with Dynasore served to define the appropriate gating strategy, whereas HUVEC transfected, but untreated with the inhibitor, were used for comparison. The efficiency of uptake blockage was calculated in each experiment using the following equation:

$$efficiency\ of\ blocking = 100\% - \frac{Nr\ of\ Cy3 + Dynasore\ treated}{Nr\ of\ Cy3 + Dynasore\ untreated} * 100\%$$

Further, vector uptake studies were carried out at different time-points (30 minutes, 1h and 4h) after transfection with miR. In these experiments, Atto-565 labelled PEI was used to investigate its colocalization either with early endosomes (EEA1 marker), lysosomes (LAMP1 marker) or endoplasmic reticulum (Calnexin). For early endosome staining, cells were fixed with 4% PFA, permeabilized with 0.1% Triton ™ X-100 (Sigma Aldrich), blocked in 1% BSA (Cell Signalling Technology, Danvers, MA) for 1 hour at RT and incubated with primary anti-EEA1 antibody (Abcam), diluted 1:200 in suitable buffer (0.1% Tween + 1%BSA in PBS). Alexa Fluor ® 647 was used as a secondary antibody (1:300 in 1%BSA in PBS). Lysosomes were stained after cell fixation with 4% PFA for 10 minutes, permeabilization with 0.5% Saponin in PBS (Sigma Aldrich) and blocking of non-specific protein-protein interactions with 5% BSA in PBS for 1 hour. Primary anti-LAMP1 antibody was diluted in buffer (0.01% Saponin + 1%BSA in PBS), incubated on cells for 1h and Alexa Fluor ® 647 was used as a secondary antibody as described before. For staining of endoplasmic reticulum, cells were fixed with 4% PFA for 10 minutes, washed with 0.01% Tween in PBS, permeabilized with 0.2% Triton ™ X-100 for 5 minutes and incubated with 5% BSA in PBS to block unspecific antibody binding. After that antibody against Calnexin (Abcam) diluted 1:300 was added for 90 min and subsequently stained with secondary antibody Alexa Fluor ® 647. Prepared coverslips were further mounted on microscopic slides with Fluoroshield™ with DAPI (Sigma-Aldrich, Germany).

2.4.7 INTERCELLULAR COMMUNICATION OF MODIFIED CELLS THROUGH GAP-JUNCTIONS AS ASSESSED BY FRAP

Fluorescence recovery after photo-bleaching (FRAP) experiments were carried out to assess the ability of transfected endothelial cells to maintain gap-junctional intercellular

communication (GJIC). For this purpose, HUVEC were treated with 2.5 pmol/cm^2 miR NP 25 combined MNP 5 µg/ml & 25 µg/ml 24h prior to microscopy as described above. Directly before measurement these cells were loaded with gap-junction permeable fluorescent dye CellTrace Calcein red-orange AM (Thermo Scientific) as described elsewhere [112]. Prepared samples were placed in the CO_2 cage incubator of ELYRA PS.1 LSM 780 (Carl Zeiss) and visualized over time using 40x objective (oil immersion), LSM mode. Intracellular calcein was photobleached with 561 nm excitation light in the defined regions (selected cell within a cluster of cells). Subsequent fluorescence recovery due to communication with neighboring cells was recorded during the following 15 min by obtaining z-stacks (10-15 images per each) every 60 seconds. In each measurement, unbleached HUVEC were used as a reference for unspecific photobleaching during scanning process. In addition, wild-type HeLa cells, known to establish no GJIC [113], served as controls. All FRAP measurements were performed with 5-10 cells per experiment and repeated at least 3 times.

2.5 TARGETING EXPERIMENTS

2.5.1 MAGNETIC TARGETING OF TRANSFECTION VECTOR

In order to assess the possibility of the vector to be magnetically guided in HUVEC, LSM was performed. For this purpose, cells were placed on the magnet (Table 1) right after adding transfection complexes. In case of plasmid targeting, 24 hours after transfection with EGFP cells were fixed, stained with DAPI and visualized (10x & 20x objectives, air immersion, 405 and 488 nm excitation lasers) using using tile-scan acquisition mode to record images of bigger areas (1699 µm x 1699 µm). Afterwards the nuclei and EGFP-positive cells were counted using ImageJ software and transfection efficiency in % was calculated.

When miR guided uptake was assessed, higher resolution was applied (40x objective, oil immersion, 514 nm excitation laser, differential interference contrast) in order to detect also diffused or weak signal of miR-Cy3 in the cytoplasm. Subsequently, the total amount of cells per field and amount of Cy3-positive cells were examined. To quantitatively assess miR/PEI/MNP targeting, cells were seeded on Gelatine coated coverslips placed in a 6-well-plate (4 coverslips per well). After 2 days in culture, these cells were transfected with miR/PEI or miR/PEI/MNP complexes using previously optimized conditions and including different amounts of iron (half of the original dose of

complexes). Right after transfection, the 6-well-plates were located on the magnet in such manner that 2 coverslips per each well were placed above the magnetic plate and the other two remained without magnetic influence. After incubation, the cells on coverslips influenced by the magnetic field were analyzed independently from cells which remained out of the magnet range. In both cases, flow cytometry was used for quantification of Cy3+ HUVEC (for the FACS protocol see above).

2.5.2 MAGNETIC TARGETING OF MODIFIED CELLS IN STATIC AND DYNAMIC CONDITIONS

To examine the targeting potential of transfected cells (HUVEC & CD133+) in static conditions, they were treated with various complex formulations defined during the optimization step, incubated for 24h (HUVEC) or 18h (CD133+), collected and seeded again with the magnet attached locally under the culture well-plate (Table 1. 24h thereafter (total of 48h or 42h after transfection) the images of areas with and without magnetic field were acquired using LSM (differential interference contrast) or conventional light microscopy. In case of CD133+, cell numbers in the area with and without magnet were counted using ImageJ software. Magnetic targeting ratios were calculated by dividing obtained cell numbers of both areas.

During the examination of the targeting potential of modified endothelial cells, the properties of magnetically responsive and non-responsive cell fractions were analyzed independently. For this purpose, MACS© separation was applied to divide modified cells 24h after transfection. Each of the obtained fractions were further split in 4 parts: 1) for cell counting on the T20 automated cell counter (Bio-Rad, Hercules, CA, USA) and viability evaluation with Trypan blue exclusion assay (concentration 0.4%; Sigma-Aldrich); 2) for immediate preparation of FACS probes; 3&4) for culture and further flow cytometry analysis 24 and 72 hours after magnetic separation (48 and 96 hours after transfection, respectively). Untreated cells and cells transfected with NA/PEI complexes served as controls in all described experiments.

In order to more extensively verify the possibility of miR/PEI/MNP-modified cells to be guided, we have simulated dynamic conditions *in vitro*. For this purpose, transfected cells (Cy3-miR/PEI/MNP and Cy3-miR/PEI as control) were placed in suspension in the wells of a 12 well-plate rotating on a shaker (150 RPM)[114]. After 12h of incubation, the cells were fixed with 4% PFA and stained with DAPI as previously described. Obtained probes were visualized using LSM.

2.5.3 IRON CONTENT MEASUREMENT OF TRANSFECTED CELLS

Magnetic Particle Spectroscopy (MPS) was applied in order to quantify the loading of HUVEC with superparamagnetic iron oxide MNP. MPS is a sensitive magnetic detection method that allows for the specific quantification of the magnetic nanoparticle iron content without being affected by cells or suspension medium[115]. After incubation with transfection complexes for 24h cells were washed twice with 2% BSA in PBS, collected and the measurements were carried out employing a commercial MPS device (Bruker Biospin, Germany) operating at a magnetic field B_{drive} = 25 mT and a frequency f_0 = 25 kHz. For iron quantification of the samples the third harmonic A_3 of the MPS-spectrum was normalized to the corresponding $A_{3,\text{ref}}$ of a MNP reference sample of known iron amount of 2.1 µg as described before[116]. Untreated cells and cells transfected with NA/PEI complexes served as controls in all described experiments.

A similar MPS measurement strategy was applied for transfected CD133+ cells to quantify their iron loading. Briefly, 18 h post-treatment cells were collected, washed with 2% FBS in PBS, resuspended in PBS, fixed with 4% PFA and transferred into 0.1 ml PCR tubes for the measurement. The third harmonic A_3 of the MPS-spectrum was normalized to the corresponding $A_{3,\text{ref}}$ of a MNP reference sample of known iron amount (3.2 µg for MNPs only reference and 2.5 µg for the CD133 MicroBeads reference). The ratio of the fifth to third harmonic A_5/A_3 was used as a characteristic finger print to identify the magnetic nanoparticle type (MNPs or CD133 MicroBeads) in the sample.

2.6 MAGNETIC RESONANCE IMAGING

The possibility to non-invasively track modified cells was tested on HUVEC *in vitro* using magnetic resonance imaging (MRI).

2.6.1 PHANTOM PREPARATION

Agar gel phantoms were constructed using previously described protocols [117]. Briefly, various numbers of transfected cells were embedded in different layers of 2% agarose in order to define the detection limits. Air bubbles, which could be a source of false-positive signals, were removed in each layer by placing the 50ml tube with sample in the ultrasound bath and its following centrifugation at 500g for 1 minute. The compositions of NA/PEI/MNP complexes used for transfection were defined as a result of previously conducted targeting experiments. Phantoms containing $5.5*10^5$ HUVEC treated with non-magnetic NA/PEI complexes served as controls.

2.6.2 MR IMAGING

All examinations of obtained phantoms were carried out on a high-field 7.1 Tesla animal MRI system (ClinScan, Bruker Corp., Billerica, MA, USA) after placing the phantom centrally in the used coil parallel to the z-axis of the magnetic field. The following sequence parameters were applied for a gradient-echo sequence acquisition: TR: 66 ms; $TE_1/TE_2/TE_3/TE_4/TE_5/TE_6$: 1.44/2.88/4.51/6.11/7.60/9.01 ms; flip angle: 3°; matrix: 128×128 interpolated to 256x256; field of view: 42 mm; 100%; averages: 1, echo train length: 1; slice thickness: 1.5 mm; 16 slices. Further, signal decay of all four echo times were assessed and a R2* maps (R2*=1/T2*) were calculated using Matlab (Mathworks, Natik, MA, USA) [118]. Images were analyzed using the freeware Osirix (Pixmeo, Bernex, Switzerland). For each sample, a rectangular region of interest (ROI) based measurement of the R2* was performed. ROIs were placed over the whole container of each iron concentration. Image analysis was carried out using the freeware Osirix (Pixmeo, Bernex, Switzerland). For each sample a rectangular region of interest (ROI) based measurement of the R2* was performed. ROIs were placed over the whole container of each iron concentration. Artifacts, which typically appear in the boundary of the containers, were excluded.

2.7 STATISTICAL ANALYSIS

Presented graphs were created using GraphPad Prism 5 software (GraphPad Software, San Diego, Calif), except all experiments on CD133+ cells where SigmaPlot 11.0 software was applied (Systat Software, Inc., San Jose, CA, USA). To perform statistical analysis, SigmaPlot 11.0 software was used. All the data are presented as mean ± SEM (n is specified for each experiment). For normally distributed variables significant differences between groups were defined applying Student's *t*-test (2 groups) or 1-way ANOVA (multiple groups), for non-normally – by Mann-Whitney test (2 groups) and ANOVA on ranks (multiple groups, *Student Newman Keuls post-hoc test*). A *p-value* of $p < 0.05$ was considered as denoting statistical significance and marked with an asterisk (increase) or "#" (decrease) in figures (*p<0.05, **p<0.01, ***p<0.001; $^{\#}$p<0.05, $^{\#\#}$p<0.01, $^{\#\#\#}$p<0.001).

3 RESULTS

3.1 STANDARDIZATION OF VECTOR PRODUCTION AND ITS EXTENDED CHARACTERIZATION

Standardized production of the delivery vectors in the laboratory is an important step towards meeting GLP guidelines, which is a prerequisite for a clinical translation. Therefore, in this work, a number of efforts were dedicated to establishing well described protocols and detailed characterization of vector components.

First, the magnetic properties of the nanoparticle component, MNPs, were defined as they were not addressed previously by our group[94,97] (Figure 6A). According to the obtained magnetization curve, MNP demonstrate typical superparamagnetic behaviour. Saturation magnetization was 86 Am^2/kg Fe, usual for magnetite MNP. The Langevin model with log-normal distribution of MNP moments was used to extract a median magnetic moment of 940(+/- 90) μ_B (Bohr Magneton) of a single MNP at a distribution width of s=1.7. This corresponds to a mean particle size of about 4.3(3) nm. The latter was confirmed via TEM images. In addition, the morphology of filtered nanoparticles was defined: MNPs are formed by multiple round-shaped cores embedded in a single matrix (Figure 6B).

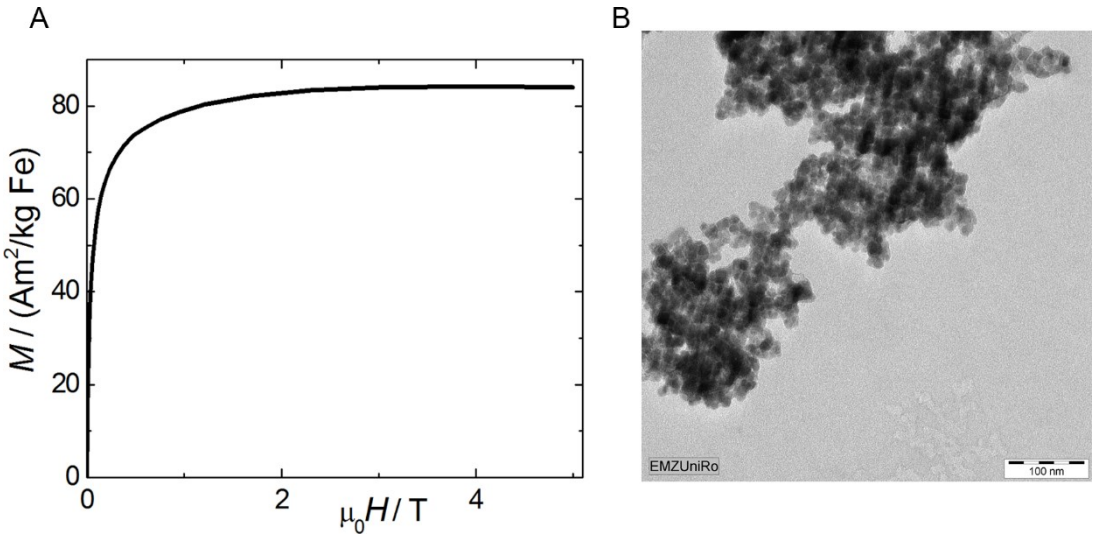

Figure 6. Characterization of magnetic nanoparticles (MNPs).
The magnetization curve obtained for MNPs characterizes them as a typical superparamagnetic material with a mean particle size of 4.3(3) nm. The demonstrated saturation magnetization of approximately about 86 Am^2/kg Fe is standard for magnetite material. (B) TEM micrographs revealing core characteristics and morphology of MNPs.
Magnetic properties of MNPs were analysed by Dr. F. Wiekhorst[131]; TEM images of filtered MNPs were obtained by Dr. M. Frank in the Electron Microscopy Center, University of Rostock, Germany.

The two parts of the introduced PEI/MNP vector are brought together by the strong interaction between biotin attached to PEI and streptavidin in the MNP coating. Whereas MNPs are available commercially and only require filtration to exclude bigger toxic aggregates[94], PEI has to be biotinylated in the laboratory. This procedure must be well defined and repeatable. Therefore, existing protocol was updated taking into account recent changes in availability of reagents on the market; in addition, the chemical and biological characterization of the final product were extended and its similarity to the PEI/MNP complexes previously used in our group was defined.

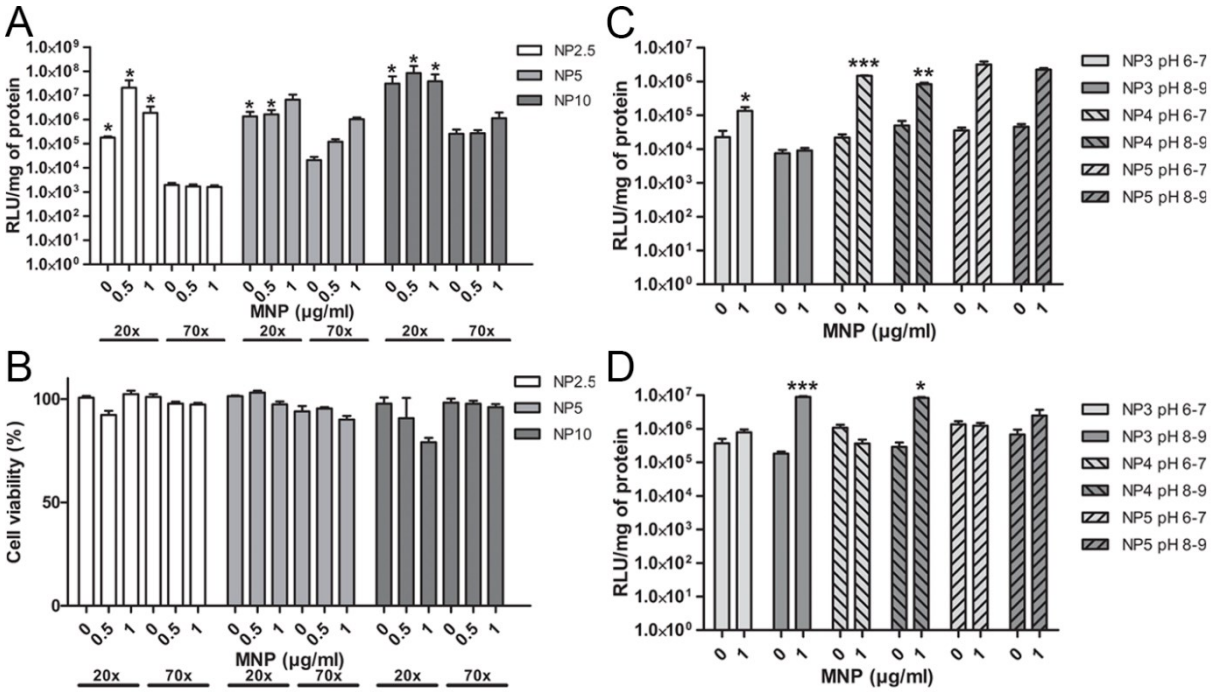

Figure 7. Selection of optimal degree of biotinylation for PEI. (A & B) Cos7 were transfected with pDNA/PEI or pDNA/PEI/MNP complexes where either PEI70x or PEI20x was included, which differ in the degree of biotinylation. For both of these, various complex formulations were applied: DNA amount 1 µg/cm^2; nitrogen/phosphate ratio of 2.5, 5 or 10 and 0.5 or 1 µg/ml of MNP iron. Transfection efficiency **(A)** was evaluated 24h after by luciferase reporter gene assay: RLU calculated per mg of total cell protein is depicted. Viability of cells **(B)** was evaluated using MTT assay and is reflected in the % of viable cells on the plot. Cell viability **(B)** was evaluated by MTT assay. Next, the influence of pH on the activity of PEI70x **(C)** and PEI20x **(D)** was assessed in the luciferase reporter gene assay. All results are representative of three independent experiments, each involved eight replicates (n = 8). The values are shown as mean ± SEM.
* **(A)** Statistically significant difference in transfection efficiency between PEI20x and PEI70x as compared for each complex formulation; **(B)** Significant increase in Luciferase expression caused by the presence of MNPs as defined for each NP ratio and pH value (*p<0.05, **p<0.01, ***p<0.001).
MTT assay: 3-(4,5-dimethylthiazol-2-yl)-2,5-diphenyltetrazolium bromide; RLU: Relative light unit.

During the biotinylation 2 different ratios of biotin to PEI were tested in accordance with the manufacturer's instructions: 70-fold excess of biotinylating reagent and 20-fold – "70x" and "20xPEI", respectively. After the reaction and following purification, the

concentration of primary amino groups in obtained solutions was 32.61± 3.205668 mM for 70x PEI; 34.76± 2.599481 for 20x vs 41.6 ± 1.122394 mM for the initial unbiotinylated PEI (mean ± SEM, n=3). Next, resulting products were characterised by the degree of biotinylation, which for 70x PEI was 2.36 ± 0.016997 molecules of Biotin per 1 molecule of PEI and for 20x - 1.35 ± 0.018346 (mean ± SEM, n=3).

Furthermore, we have tested the obtained PEI 70x and 20x in the fibroblast-like cell line, cos7, a common cellular model for transfection previously used by our group[94].

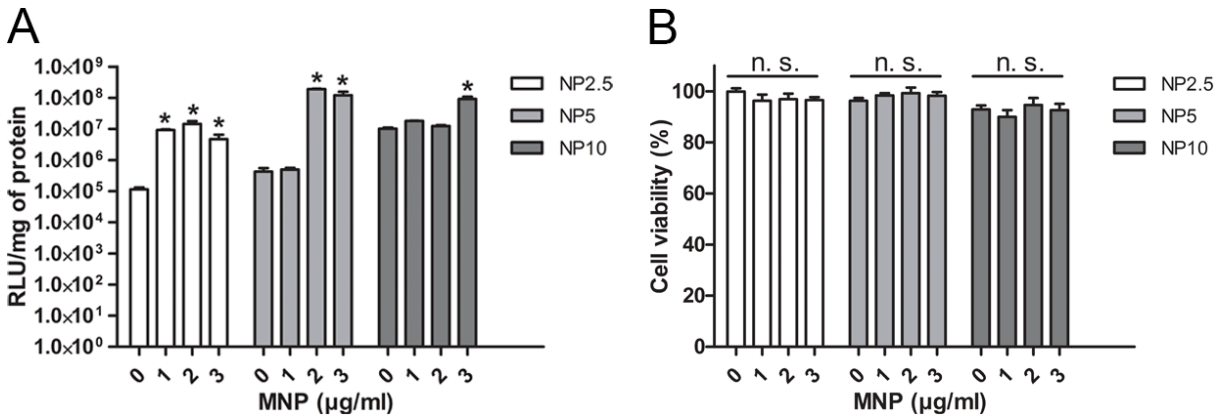

Figure 8. Testing different iron concentrations to form PEI/MNP with optimally biotinylated PEI. Transfection complexes were obtained using different amount of components: DNA 1 µg/cm^2; NP ratio of 2.5, 5 or 10 complemented by 0.5 or 1 µg/ml of MNP iron. The efficiency of transfection in cos7 **(A)** was evaluated after 24h of incubation using luciferase reporter gene assay. Bars represent RLU calculated per mg of total cell protein. Viability of cells **(B)** was evaluated using MTT assay. The plot reflects the % of viable cells in total cell population. All results are representative of three independent experiments, whereas in each experiment eight replicates were included (n = 8). The values are shown as mean ± SEM.
*Significant difference in transfection efficiency between pDNA/PEI complexes vs pDNA/PEI/MNP defined within each NP ratio (*p<0.05). n.s. no significant difference.
MTT assay: 3-(4,5-dimethylthiazol-2-yl)-2,5-diphenyltetrazolium bromide; RLU: Relative light unit.

As a result, PEI 70x was almost 100 fold less efficient in transfection than PEI 20x, with and without MNPs (Figure 7 A) with cell viability remaining unaffected for both cases (Figure 7 B). An increase in pH of the reaction mixture from physiological 6-7 to 8-9 – in order to possibly influence protonation and transfection activity - did not enhance the efficiency of PEI 70x, whereas addition of MNPs improved transfection efficiency for certain complex formulations (Figure 7 C & D). However, the resulting level of protein expression remained significantly lower than PEI 20x. Thus, PEI 20x – with 1.35 molecules of Biotin per 1 molecule of PEI – was preferred for further investigations (named "PEI" below).

During the following transfection tests with Luc pDNA, different amounts of MNPs were added and the level of target protein expression was measured along with cell viability.

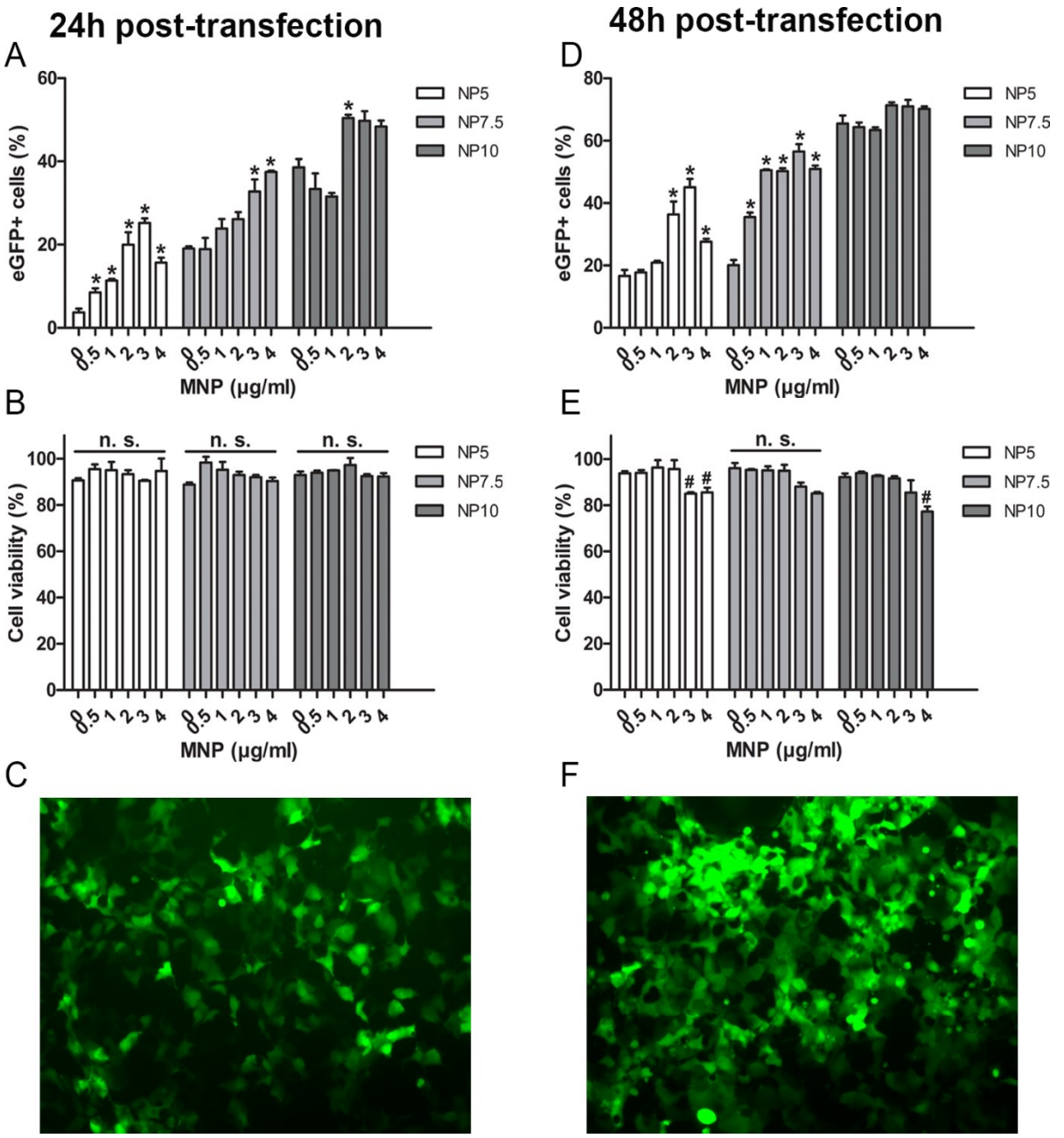

Figure 9. Transfection of cos7 with EGFP using optimized magnetic polyplexes. Transfection efficiency and cell viability were assessed 24h **(A-C)** and 48h **(D-F)** after delivery of EGFP-encoding plasmid by PEI or PEI/MNP using flow cytometry. Resulting average number of EGFP+ cells relative to the whole cell population was plotted **(A, D)** as mean ± SEM (n = 3). On the graphs illustrating cell viability after transfection **(B & E)**, bars represent the ratio between the average number of viable cells and the whole cell population (n=3; error bars: SEM). Representative fluorescence microscopy images depict EGFP-expressing cos7 24h **(C)** and 48h **(F)** post-transfection. Scale bars = 10 µm.
Significant difference in transfection efficiency between pDNA/PEI and pDNA/PEI/MNP complexes as compared within different NP ratios ($p<0.05$). n.s. no significant difference.
Significant negative change in cell viability vs untransfected control (#$p<0.05$).

Resulting numbers were comparable to the previously published data[94], thereby confirming the similarity of the obtained biotinylated PEI product. In particular, presence of MNPs significantly increased the transfection efficiency up to 100-fold for

the following complex compositions: NP ratio 2.5 complemented by 1, 2 & 3 µg/ml of MNPs and NP ratio 5 with 2 & 3 µg/ml MNPs (Figure 8 A) with cell survival remaining high (Figure 8B).

At the same time, the use of Luc as a test plasmid is limited as measured relative light units (RLU) depend on the portion of transfected cells in the whole population as well as the number of protein produced per transfected cell[35]. We have, therefore, extended the biological characterisation of PEI/MNP complexes by using EGFP plasmid and flow cytometry analysis to estimate the correct percentage of transfected cells (Figure 9).
The values obtained for EGFP/PEI – up to ~40% of cells were transfected – corresponded with values previously reported in the literature for bPEI 25kDa[119]. In general, the obtained results correlated with those of Luc transfection: the presence of certain amounts of MNPs significantly enhanced transfection efficiency up to ~50-55% 24h after transfection (Figure 9 A, C). Follow–up monitoring of transfected cells at the time-point 48h showed that the overall transfection efficiency increased, reaching ~60-70% of EGFP-positive cells for certain complex compositions (Figure 9 D, F). In all described experiments cell survival remained level with untreated cells except the highest MNP concentrations at 48 h post-transfection: NP 5 MNP 3 & 4, NP 10 MNP 4 (Figure 9 B, E).
To conclude, we observed strong evidence that the proposed strategy - including parameters previously published by our group[94,97] and newly reported assays and characteristics - is sufficient to maintain a standardized production of biotinylated PEI and resulting PEI/MNP transfection complexes.

3.2 SELECTION OF OPTIMAL TARGETING STRATEGY

Human umbilical vein endothelial cells (HUVEC) are recognized as one of the most appropriate and commonly used cell types to study angiogenesis *in vitro*: human primary cells which are relatively easy to isolate (compared to e.g. bone-marrow derived HSCs) performing all key functional assays related to angiogenesis. In addition, being difficult to transfect and susceptible to toxic influence, they are very well suited to test new therapeutic agents[120–122]. Therefore, the investigation for PEI/MNP magnetic vector was initiated using HUVEC as a model.

First, we defined optimal transfection conditions for both, plasmid and microRNA. Next, two targeting approaches were assessed *in vitro*: direct vector guidance and magnetic targeting of transfected cells. As a result, an optimal strategy was selected for further detailed investigation (schematically illustrated in Figure 10).

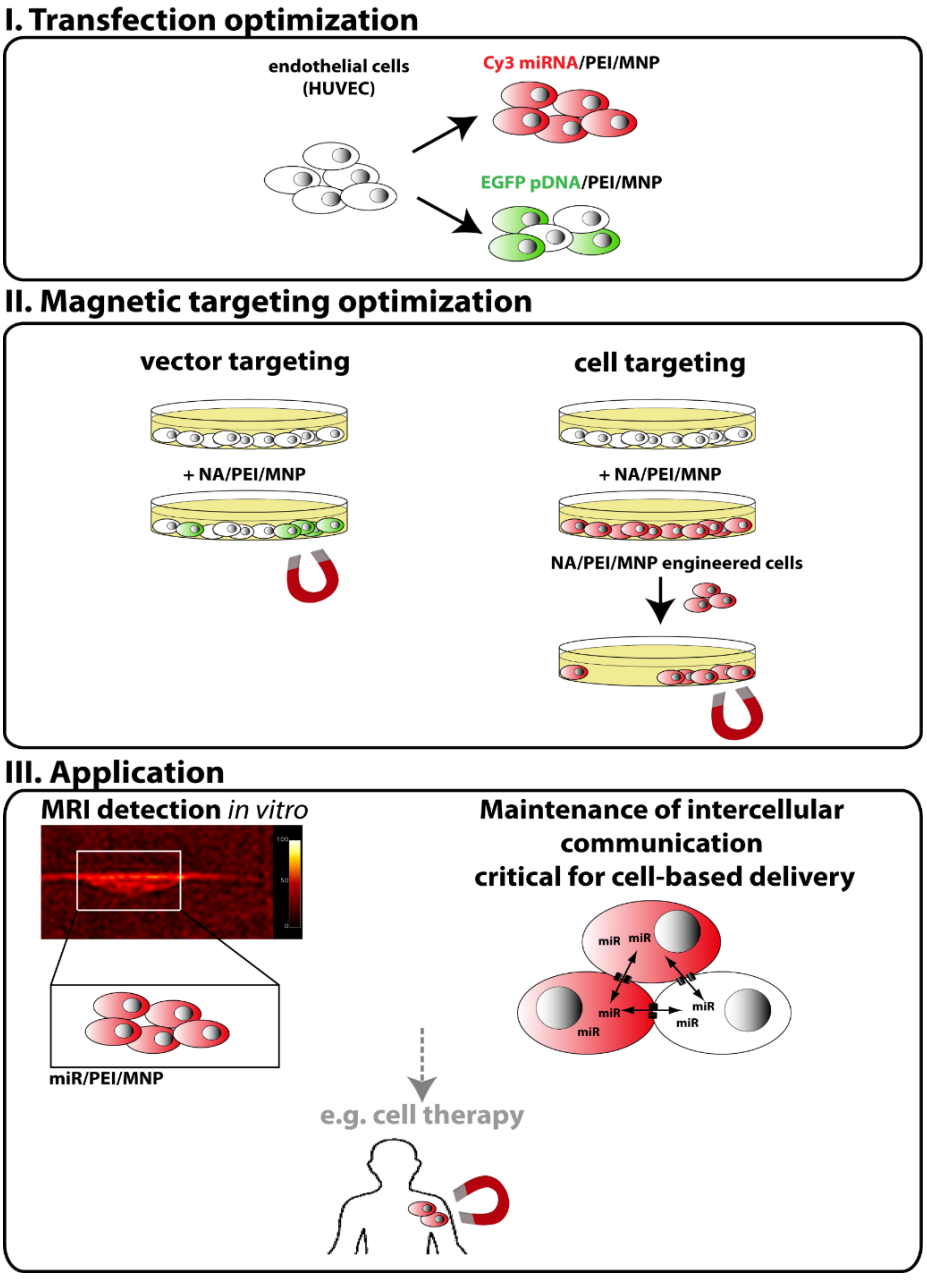

Figure 10. Schematic representation of experiments carried out with HUVEC. HUVECs were transfected with both, miR and pDNA, First, we have carried out transfection optimization in HUVEC **(I)** with both, miR and pDNA. Defined optimal conditions were further used for the selection of optimal targeting strategy **(II).** The direct NA/PEI/MNP vector targeting (left panel) was compared to cell targeting after their magnetic engineering with PEI/MNP (right panel). More promising setup from these – cell-based – was investigated in detail **(III)**, including intercellular communication of transfected cells and their possibility to be monitored using magnetic resonance imaging.

3.2.1 ENDOTHELIAL CELLS CAN BE SAFELY AND EFFICIENTLY MODIFIED USING NA/PEI/MNP

The identity of cells isolated from the umbilical cords was defined by the expression of the endothelial cell marker CD31 (platelet *endothelial* cell adhesion molecule, PECAM-1)[123] and an *in vitro* functional angiogenesis assay, tube formation[32] (Figure 11 A & B). Preliminary transfection optimization was carried out using polyplexes NA/PEI in order to define the optimal formulation for further experiments including MNP. The chosen setup revealed that under certain conditions extremely efficient miR uptake and unaffected cell survival were ensured. In particular, complexes built by 2.5 pmol/cm^2 miR and NP25 were taken up by 99% of HUVEC 24h after transfection (Figure 12A) and their viability did not differ from untreated cells (Figure 12B) as measured by flow cytometry.

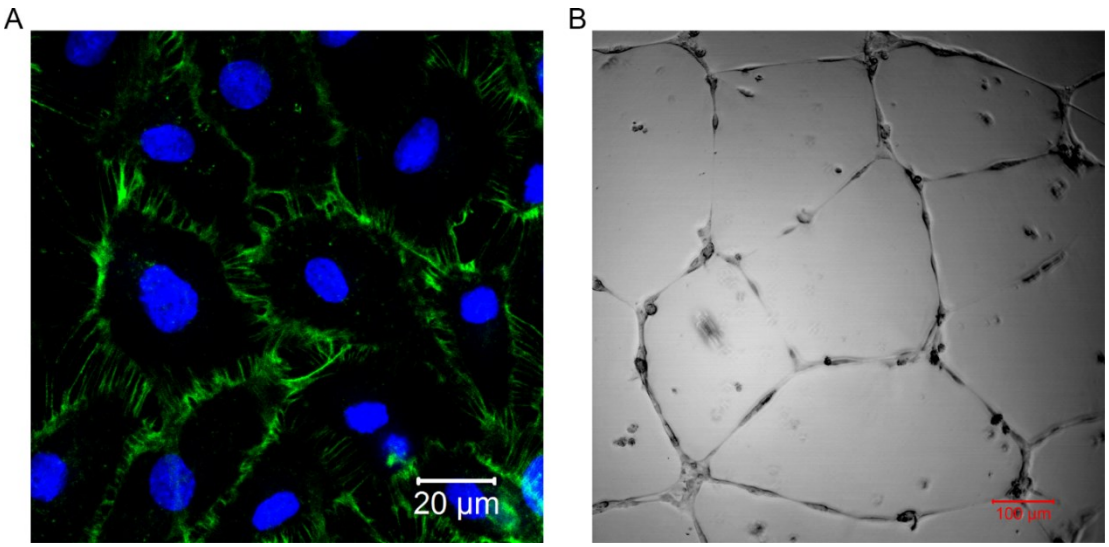

Figure 11. Characterization of HUVEC after isolation.
Isolated HUVECs were analyzed in terms of specific surface marker CD31 (PECAM-1) expression **(A)**. Representative image was obtained as a result of immunofluorescent staining (green) and nuclei staining with DAPI (blue). Functional activity of cells was evaluated in a standard tube-formation assay (differential interference contrast image **(B)**).

Microscopy confirmed these observations and the fact that cell morphology remained normal. Several tested complex formulations led to similar results. However, when the total amount of added PEI was taken into account and pilot experiments with MNPs were conducted, the above mentioned miR/PEI composition was selected for following trials.

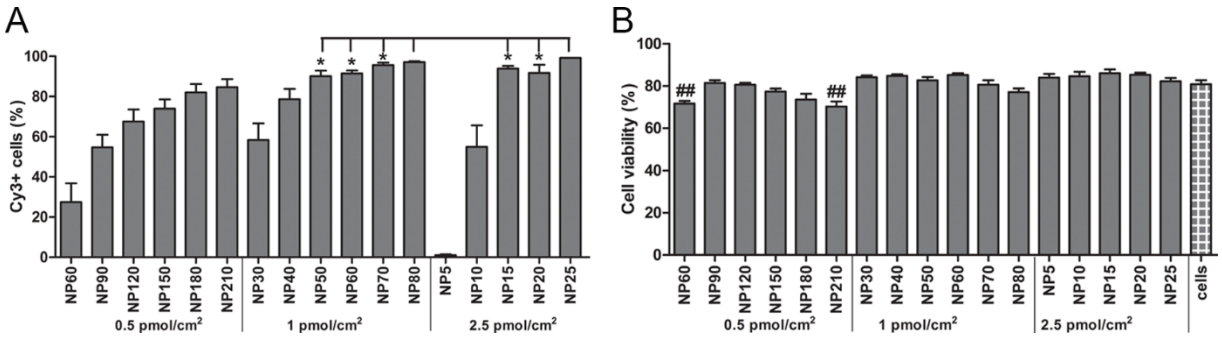

Figure 12. Optimization of transfection in HUVECs using tagged miR and biotinylated PEI. For miR, delivery efficiency **(A)** and cell viability **(B)** were evaluated 24h after transfection using Cy™3 labeled nucleic acid. Cells were treated with different amounts of miR (0.5, 1, 2.5 and 5 pmol/cm^2) and NP ratios (from 2.5 to 210) and subsequently analyzed using flow cytometry. The average number of Cy3+ viable cells **(A)** or viable cells **(B)**, relative to the whole cell population, was plotted (error bars: SEM, n=6).
* Indicates a significantly enhanced Cy3-miR uptake as compared between marked groups.
# Significant difference (decrease) in cell survival was determined in comparison with untreated cells serving as negative controls. * and # indicates $p < 0,05$.

Finding an optimal complex formulation for pDNA delivery turned out to be a more complicated issue. The highest level of transfection efficiency (~50-52%) was achieved

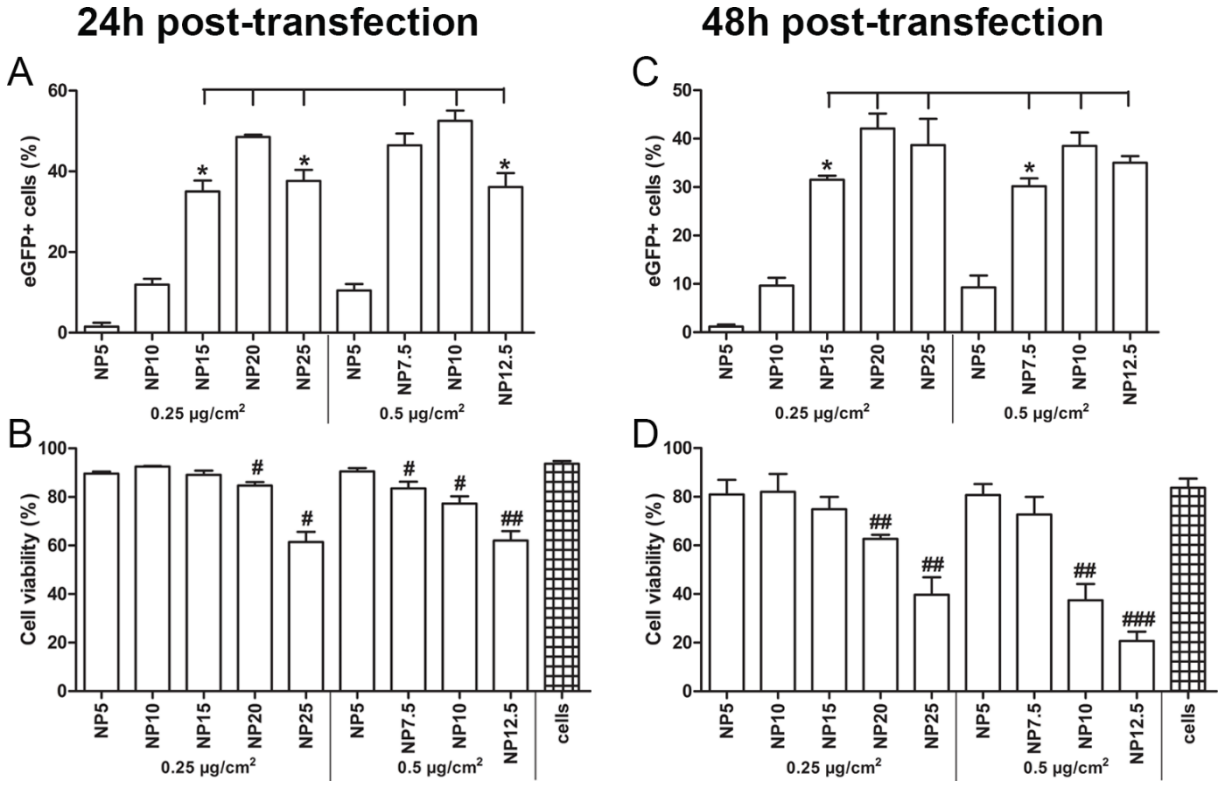

Figure 13. Optimization of transfection in HUVECs using pDNA/PEI complexes. Evaluation of pDNA delivery with PEI was carried out 24h **(A, B)** and 48h **(C, D)** after transfection in terms of protein expression **(A, C)** and cell survival **(B, D)**. Cells were treated with polyplexes containing various amounts of EGFP-encoding pDNA (0.25 or 0.5 µg/cm^2) and PEI (NP from 5 to 25) and analyzed by flow cytometry. Bars represent the average percent of EGFP-positive viable cells **(A, C)** or viable cells **(B, D)** in the whole cell population (error bars: SEM, n=3).
* Significantly enhanced expression of EGFP between indicated complex formulations.
# Significant difference (decrease) in cell survival was determined in comparison with untreated cells serving as negative controls. * and # indicates $p < 0,05$.

for 0.25 µg/cm² of pDNA and NP ratio 20, 0.5 µg/cm² of pDNA and NP 10 (Figure 13A). These conditions were also characterized by an acceptable decrease of cell viability by 10% compared to untransfected cells (Figure 13B). However, when cells were treated with respective complex formulations and examined 48h thereafter, a dramatic decline in cell survival down to ~60 and ~38% was discovered (Figure 13 C&D). This result was not compatible with the ultimate goal of developing a vector for clinical use. Therefore, balanced vector compositions of 0.25 µg/cm² NP15 and 0.5 µg/cm² NP 7.5 were chosen, which were characterized by moderate efficiency (average 35 and 46% EGFP-positive cells, respectively), and excellent HUVEC tolerance 24 and 48h after transfection.

The presence of magnetic nanoparticles in the vector changed the transfection pattern significantly (Figures 14, 15). In case of miR delivery (Figure 14A), its uptake level declined by 5 to 10% at 20 & 25 µg/ml of MNPs (µg of iron per ml of prepared NA/PEI).

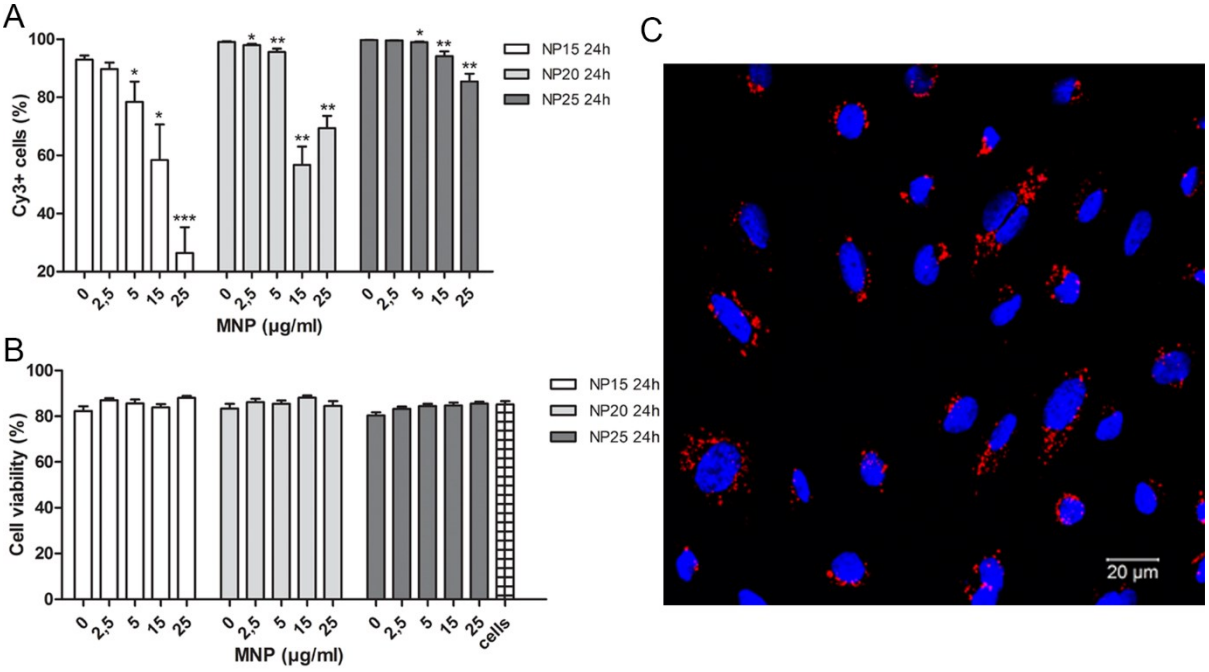

Figure 14. Optimization of HUVEC transfection with miR/PEI/MNP complexes. The efficiency of miR uptake and cell viability after transfection were assessed using different complex compositions: 2.5 pmol/cm² of Cy3-miR, NP ratios 15, 20 or 25 complemented with 2.5 to 25 µg/ml MNPs. Bars are depicting the ratio between the average number of either Cy3-positive viable **(A)** or viable cells **(B)** and the whole cell population (n=6; error bars: SEM). **(C)** Representative image illustrates the active uptake of Cy3-miR (red) by every cell (treated by 2.5 pmol/cm² of Cy3-miR, NP ratio 25 with 5 µg/ml MNPs), which were fixed 24h after transfection with their nuclei counterstained with DAPI (blue). Scale bar = 20 µm.
*Significant changes in the EGFP expression due to MNPs added as compared within different NP ratios (*p<0.05, **p<0.01, ***p<0.001).

This observation can be explained by interference of excessive MNP amounts with the PEI activity during transfection[124,125]. Since the targeting potential directly depends on

the magnetic component and the miR uptake was decreased only by 5 & 10% we decided to carry out all further targeting experiments with miR using the full range of tested MNP amounts: 2.5 pmol/cm^2 NP ratio 25 and MNP 5, 10, 15, 20 & 25 µg/ml.

In contrast, the amount of EGFP-expressing cells was not changing significantly as a result of pDNA transfection with MNP-containing vector (Figure 15A). The decrease in efficiency of 7 & 12% caused by nanoparticles was observed only with two formulations: 0.5 µg/cm^2 NP 7.5 MNP 3 & 4, respectively. However, in all experiments involving 0.5 µg/cm^2 pDNA and NP 7.5, the presence of MNP in delivery complexes resulted in greatly declined cell survival 24h and 48h after transfection (Figure 15B). At low iron concentrations of 0.5 µg/ml 48h after transfection, 65% of cells remained viable, while 1-4 µg/ml iron caused substantial cell death up to 42-68%. At the same time, the influence of MNP on cell viability was much lower in case of 0.25 µg/cm^2 NP 15 composition: this decrease was statistically significant, but it did not exceed 10% at all tested iron concentrations. Due to these findings, the formulations 0.25 µg/cm^2 pDNA NP ratio 15 with MNP 0.5, 1, 2, 3 & 4 µg/ml were selected for further studies involving pDNA.

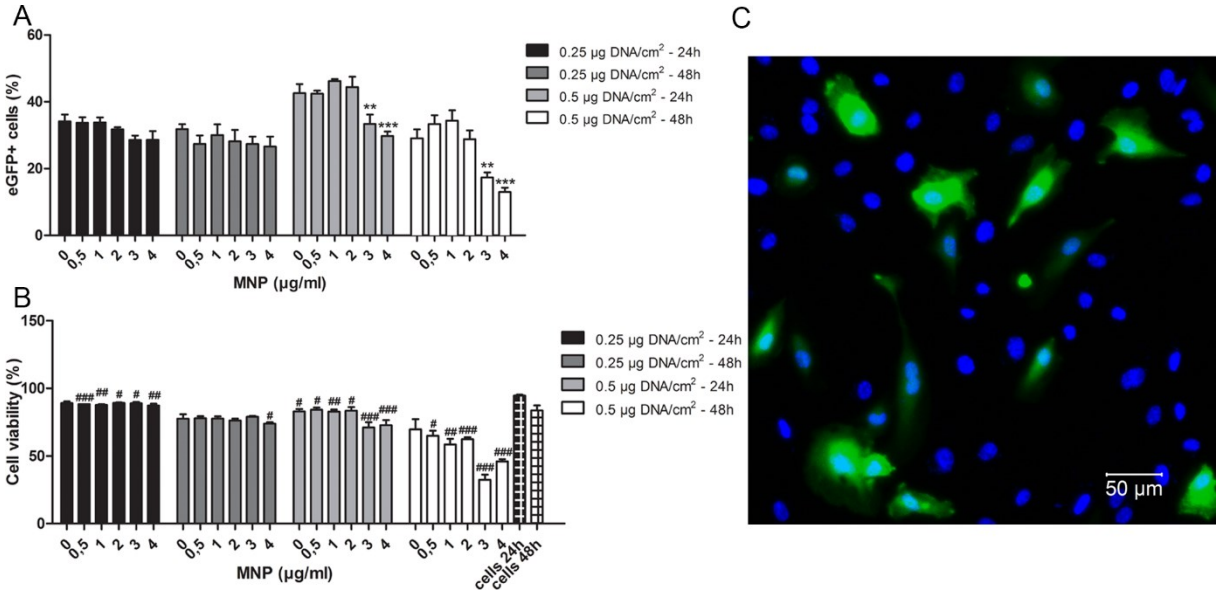

Figure 15. Optimization of HUVEC transfection with pDNA/PEI/MNP. Plasmid transfection was evaluated 24h and 48h after cell treatment with 0.25 or 0.5 µg/cm^2 of EGFP-encoding pDNA, complexed by PEI at NP ratios 15 or 7.5 and complemented with 0.5 to 4 µg/ml of MNP iron. As a result, the rate of EGFP-expressing cells within whole population **(A)** was measured by flow cytometry along with the rate of living cells **(B)** (values are presented as mean ± SEM, n=6). **(C)** Representative fluorescence microscopy image (EGFP - green, nuclei stained with DAPI - blue) depicts EGFP-expressing HUVECs 24-h post-transfection (0.25 µg/cm^2 of pEGFP, NP ratio 15 and 1 µg/ml MNPs). Scale bar = 50 µm. *Significant changes in the EGFP between EGFP/PEI/MNP vs EGFP/PEI within different NP ratios (*p<0.05, **p<0.01, ***p<0.001).
Significantly decreased cell viability vs untreated cells ($^{\#}$p<0.05, $^{\#\#}$p<0.01, $^{\#\#\#}$p<0.001).

It can be assumed that the difference in cell behavior after miR or pDNA transfection with PEI/MNP complexes is based on the total amount of PEI contained within the complex. For all cases plotted in Figures 12-15, the necessary amount of PEI for miR delivery was significantly lower than was required for pDNA delivery. Therefore, the toxicity of miR/PEI was substantially lower at baseline. Thus, for targeted delivery considerably higher amounts of iron (2.5-25 μg/ml) could be added to miR/PEI without causing cell damage, whereas only relatively low MNP concentrations of 0.5-4 μg/ml were tolerated by cells in case of pDNA/PEI transfection. At the same time, these iron levels of 15-25 μg/ml started to influence the delivery efficiency due to their excess versus PEI.

3.2.2 MAGNETIC TARGETING OF PEI/MNP VECTOR IS LIMITED

Next, the direct vector targeting approach was tested for selected optimal transfection conditions. The main purpose behind guided and localized delivery of therapeutics is to avoid off-target effects and reduce the dosage. Therefore, we carried out testing of possible transfection localization in parallel with attempts to gradually reduce the necessary amount of transfection complexes down to 50% from initial values (Figures 16 & 17).

For pDNA/PEI/MNP targeting evaluation, at first the most promising formulations were defined by LSM (0.25 μg/cm^2 pDNA NP 15 combined with MNP2). For this complex composition, after transfection with pDNA and magnet application the EGFP expression was localized to a certain degree, which increased at lower EGFP/PEI/MNP dosages of 50-80 % (Figure 16). At the same time, the lower the complex dosage was, the lower dropped the levels of transfection efficiency. For the dosages of 80 & 90% this shift was not very dramatic and the amount of EGFP-positive cells remained at 26-27% (Figure 16 B & C). Notable, these values are comparable with the results obtained during the transfection optimization steps by flow cytometry, which was employed to validate the cell counting from microscope images (Figure 16 C). With lower amounts of complexes added, the transfection efficiency reached 18, 16 & 9% minimums for 70, 60 and 50% dosages, respectively.

Similarly, in case of guided Cy3-miR uptake, at the lowest dosage (50% from initial) a substantial amount of cells was Cy3-positive in the off-magnet area (Figure 17 A-C), except for at high MNP concentrations, where transfection efficiency was insufficient

(below 30%) even above the magnet (Figure 17D). No difference in fluorescence intensity of transfected cells was observed over the magnet and without the magnet (Figure 17E).

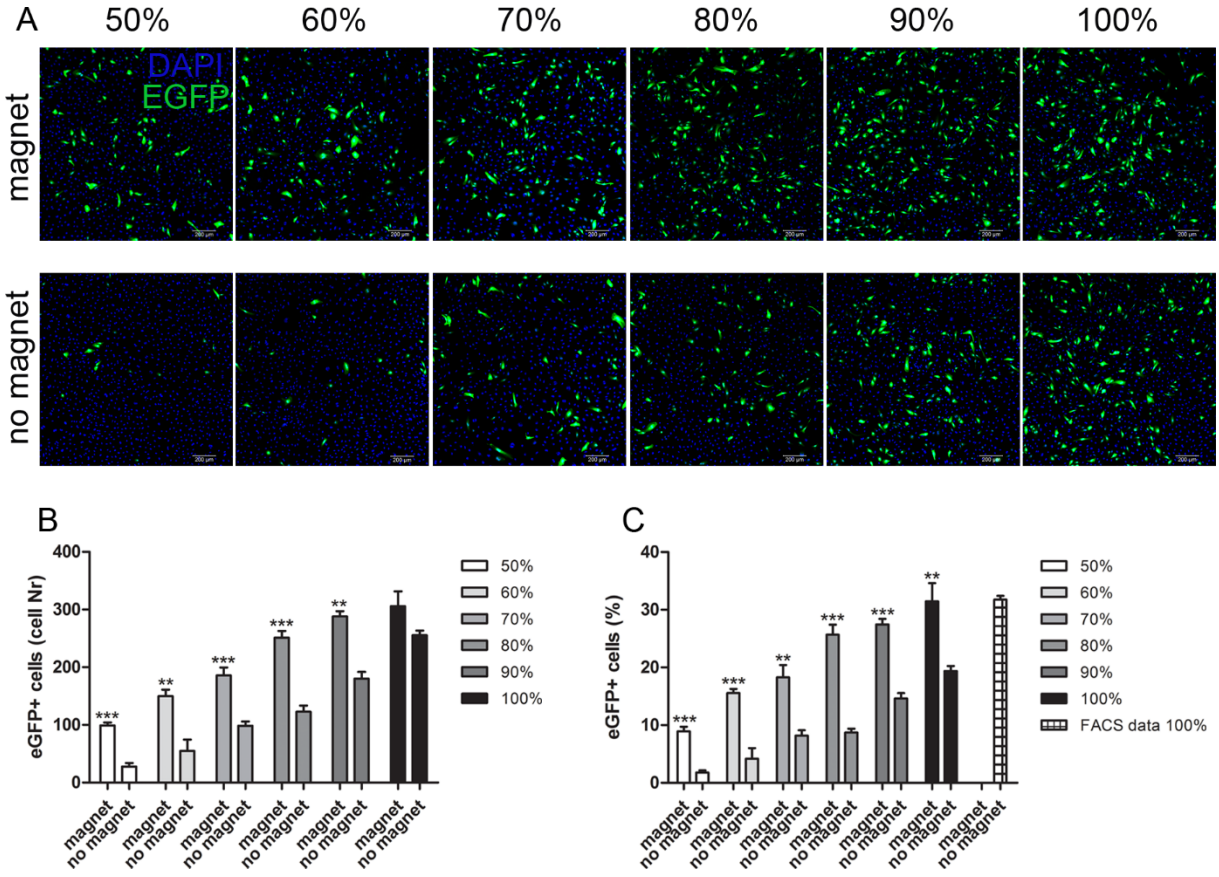

Figure 16. Magnetic guidance of DNA/PEI/MNP transfection in HUVEC. Pre-selected complex formulation (0.25 μg/cm^2 of EGFP-pDNA, NP ratio 15 & 2 μg/ml of MNP) was applied on HUVEC **in different dosages from original**: from 50 to 100%. Immediately after transfection the magnet was applied locally under the culture well and cells were incubated in this manner for 24h. Obtained samples were fixed, stained with DAPI and analyzed for possible magnetic guidance of EGFP expression due to PEI/MNP vector targeting. Representative images illustrate obtained results **(A)**: EGFP channel is green, DAPI – blue. Scale bar = 200 μm. Presented plots were created out of such images: they depict calculated ratio between the area with and without magnet application in terms of Nr of EGFP+ cells **(B)** and transfection efficiency **(C).** Values are presented as mean ± SEM (n=3). Results, previously obtained by flow cytometry and indicated as "FACS 100%" on the plot, were used to validate the counting method applied to define transfection efficiency.
*Significant difference between areas with and without magnet are defined for every dosage by comparing respective values pairwise (**p<0.01, ***p<0.001).

These findings indicate that direct vector targeting was significant, but never complete and a certain number of off-target transfected cells was always observed. Acceptable targeting selectivity can be achieved for the pDNA/PEI/MNP vector only by reducing the dosage dramatically and, therefore, compromising transfection efficiency.

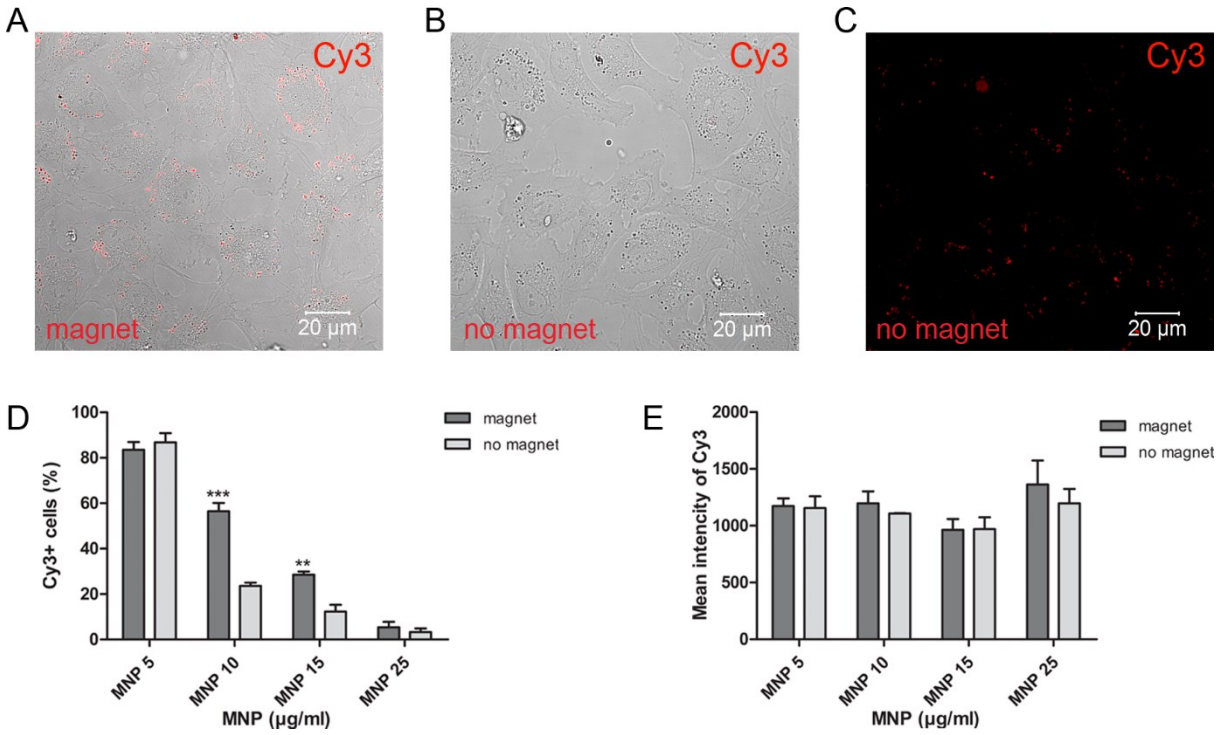

Figure 17. Magnetic guidance of miR/PEI/MNP uptake by HUVEC. Localized by a magnetic force uptake of Cy3-labelled miR was examined 24h post-transfection by confocal laser scanning microscopy. Representative images **(A-C)** were obtained for cells treated with 50% of the original complex amount (2.5 pmol/cm^2 Cy3-miR, NP ratio 25 & 5 µg/ml of MNP). Different acquisition and processing settings were applied in cases A & B vs C: in the latter, the laser power was 5 times higher and resulting z-stacks were compressed to detect significantly weaker Cy3 signal in the cytoplasm. Scale bars: 20 µm. To compare the areas with and without a magnet, cell from these regions were selectively collected and analyzed separately using flow cytometry in terms of uptake efficiency **(D)** and mean fluorescence intensity of Cy3+ cells **(E)**. Bars represent the rate of Cy3+ cells in the total cell population (D) and fluorescence intensities of these cells (E) in the areas over and without a magnet (n=4, error bars: SEM).
* Significantly higher level of Cy3-positive cells mag+ versus mag- as defined for each complex formulation after pairwise comparison (**p<0.01, ***p<0.001).

3.2.3 MAGNETICALLY ENGINEERED CELLS REPRESENT AN OPTIMAL TARGETING APPROACH

Another targeting opportunity offered by PEI/MNP vector is the generation of magnetically responsive NA-modified cells as tools for their subsequent targeting, which we investigated further.

For this purpose, HUVEC were treated with various complex formulations defined previously as optimal (5 pmol/cm^2 miR NP ratio 25 complemented by 2.5-25 µg/ml of MNP or 0.25 µg/cm^2 pDNA NP ratio 15 combined with 0.5-4 2.5 µg/ml MNP), incubated for 24h, collected and seeded again with the magnet attached locally under the culture well-plate. Resulting cell growth in the areas with and without applied magnet was recorded and is illustrated by Figure 18. Magnetically guided cell migration was observed for both, miR- (Figure 18A) and pDNA- (Figure 18B) modified cells, except for

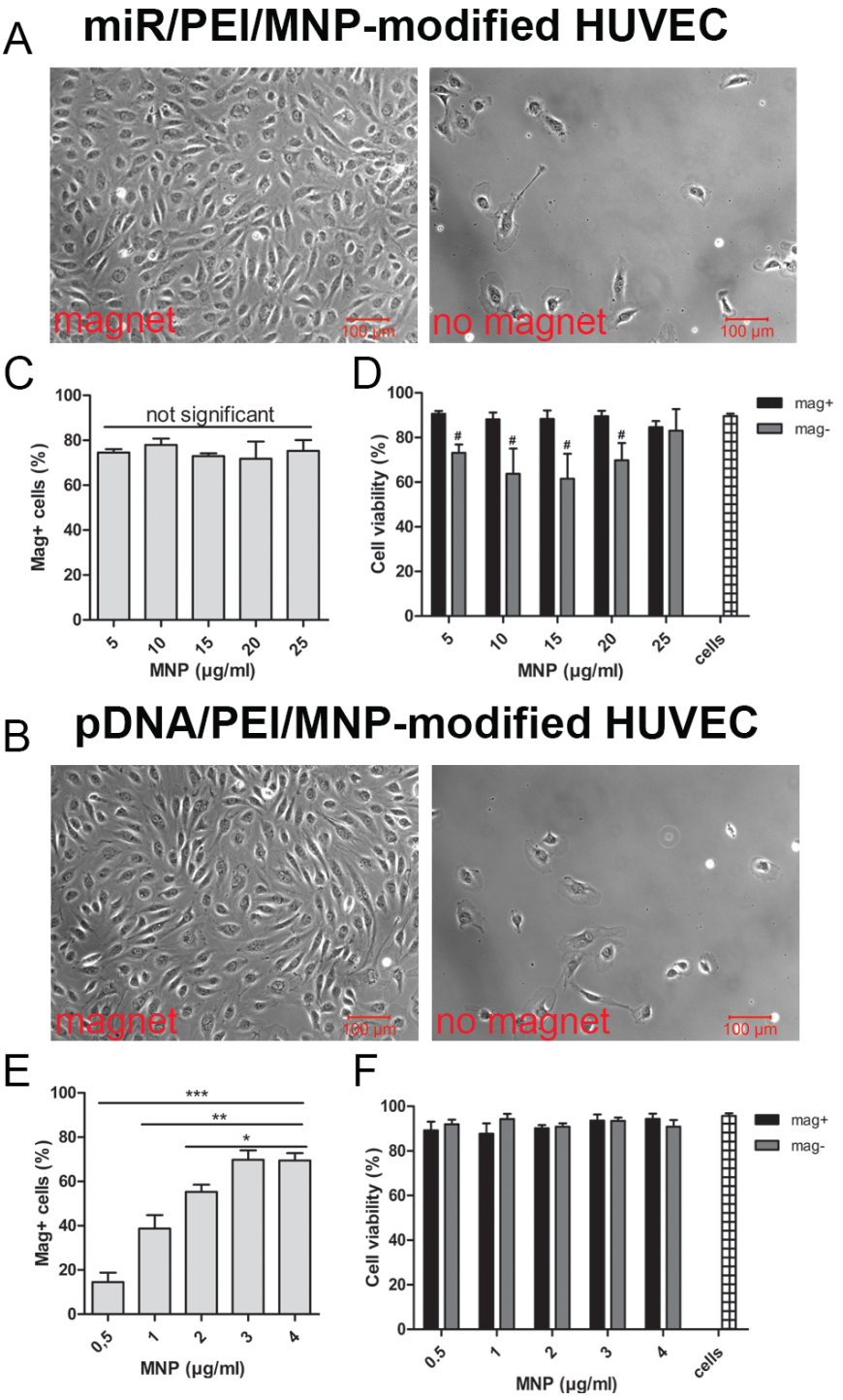

Figure 18. Magnetic targeting of NA/PEI/MNP-HUVECs in static conditions. Representative images of cell targeting **(A, B)** depict the growth of HUVECs, which were collected 24h after transfection, seeded with the magnet applied locally under the well-plate and analyzed 24h thereafter. NA/PEI/MNP formulations used for transfection were the following: 2.5 pmol/cm^2 miR, NP 25 & 25 µg/ml MNP **(A)** and 2.5 µg/cm^2 pDNA NP 15 & 4 µg/ml MNP **(B)**. Scale bars: 100 µm. Quantitative analysis of targeting for transfected cells was also carried out 24h after their treatment with various magnetopolyplex compositions: 2.5 pmol/cm^2 miR, NP 25 with 5 - 25 µg/ml MNP and 2.5 µg/cm^2 pDNA NP 15 with 1- 4 µg/ml MNP. To separate transfected cells into magnetically positive (mag+) and negative (mag-) fractions, MACS columns were applied. Subsequently, cells numbers in both fractions were recorded (C, E) and their viability was assessed via Trypan blue exclusion assay (D, F). Bars represent either percentage of magnetically-responsive cells or rate of living cells in the whole cell population, respectively (n=3; error bars: SEM).

* Significant differences in the amount of magnetically responsive cells for different MNP concentrations (*p<0.05, **p<0.01, ***p<0.001).

the low iron concentrations of 2.5 µg/ml of MNP used for miR delivery and 0.5, 1 & 2 µg/ml applied for plasmid.

To quantify the amount of magnetically responsive (mag+) and non-responsive (mag-) cells, these fractions were separated using MACS© columns. Moreover, this allowed to carry out independent analyses of mag+ and mag- cell fractions and to identify a possible toxic influence of static magnetic field on MNP-loaded cells. Subsequent cell counting revealed that on average 70-83% of miR/PEI/MNP-modified cells were responding to the magnetic field (Figure 18C). In case of pDNA transfection, similarly high values of 66-71% mag+ cells were achieved only with the highest iron concentrations of 3 & 4 µg/ml. With all other MNP amounts in pDNA/PEI/MNP, the number of cells remaining in the column varied from 11 to 55% (Figure 18E).

Viability evaluation using Trypan blue exclusion assay of both, mag+ and mag- fractions, showed no significant cell death (Figure 18D & F), except for the magnetically non-responsive miR-modified cells. Interestingly, their survival was 10 to 20% lower as compared to untreated control (Figure 18D), whereas the survival of magnetically responsive cells did not differ from untransfected HUVECs. This observation corresponds with the previously published observation that MNP can improve vector safety[94].

Next, a more challenging set-up was used for cell targeting evaluation – simulation of dynamic conditions *in vitro.* Here, miR-modified cells were examined as containing higher amounts of iron vs pDNA. For this purpose, HUVEC treated with 2.5 pmol/cm^2 miR NP 25 with MNP 5 & 25 µg/ml were collected 24h after transfection and transferred into the wells of a well-plate attached to a shaker rotating at 150 RPM.

After 12h, the guidance of these cells by a magnet placed locally on the side of each well was studied. As illustrated in Figure 19, the majority of magnetically modified HUVEC were growing in the area of magnet application and the lowest cell density was recorded in the non-magnetic area. At the same time, a conspicuous difference between static and dynamic set-up was observed: in the latter case, liquid flow was concentrating some cells in the middle of the well. However, their amount was still significantly lower than near the magnet, thereby confirming that even active movement of the liquid is not interfering with efficient cell targeting.

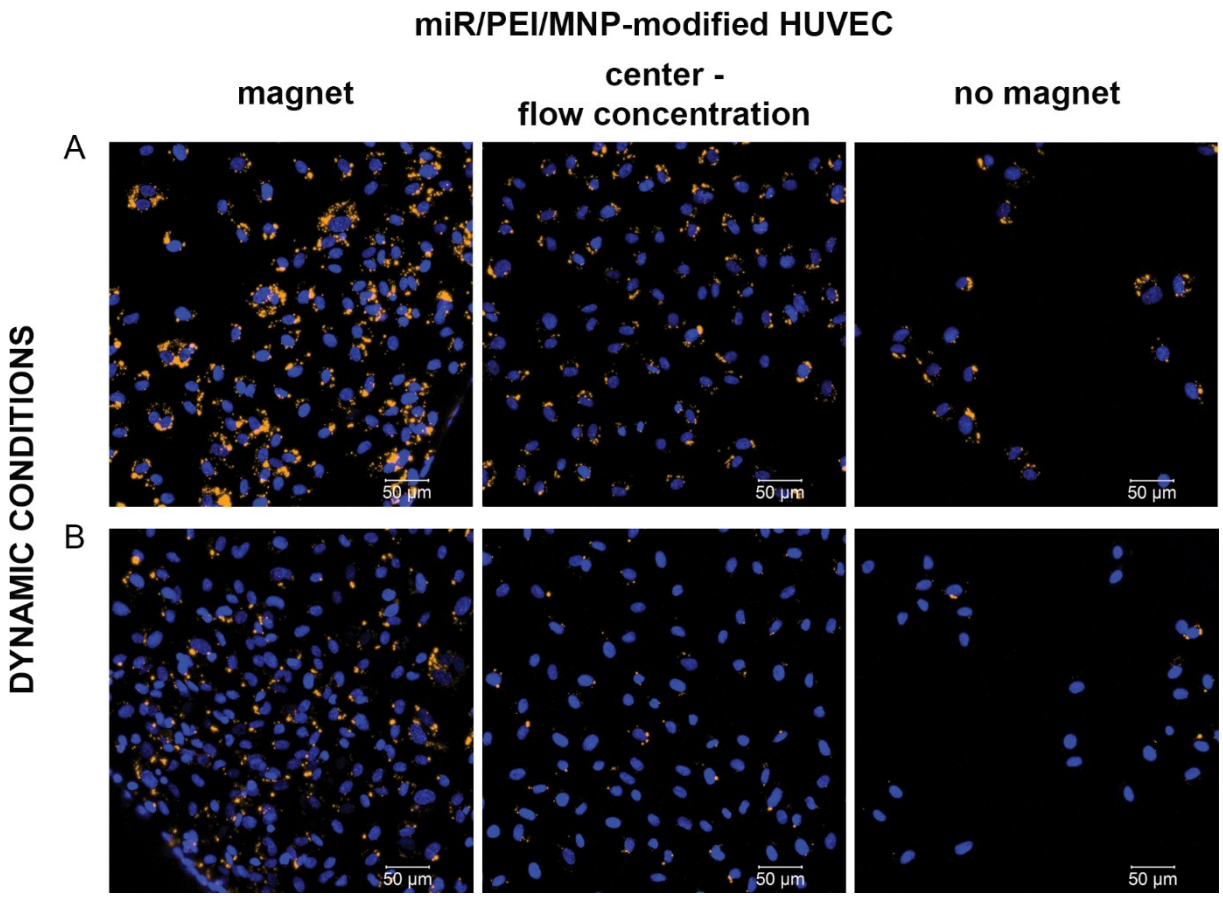

Figure 19. Magnetic targeting of HUVEC modified with miR in simulated dynamic conditions *in vitro*. Cells were transfected with optimized complex formulations (2.5 pmol/cm^2 of Cy3-tagged miR, NP 25 complemented with MNPs 5 **(A)** & 25 **(B)**), collected after 24h of incubation, seeded in the wells of a plate attached to a rotating shaker, whereas on the sides of wells a magnet was applied locally. Resulting cell growth was recorded on PFA fixed and stained with DAPI cells 12h thereafter. Scale bars: 50 µm.

3.2.4 DEFINING IRON LOADING OF CELLS SUFFICIENT FOR THEIR MAGNETIC GUIDANCE

Further, in order to identify the amount of MNP loading of cells sufficient for their magnetic targeting, magnetic particle spectroscopy measurements were carried out. These revealed that 0.16 pg of iron per cell is enough for massive migration of cells to the area of local magnet application (Table 2). This required level of MNPs in cells was reached when the following compositions of transfection complexes were used: 0.25 µg/cm^2 pDNA NP 15 with MNP 3 & 4 µg/ml and 2.5 pmol/cm^2 miR NP 25 with MNP 5, 15, & 25 µg/ml. For all formulations which did not ensure efficient cell guidance the intracellular iron concentration was below the detection limit.

To summarize, the detailed investigation of both targeting approaches – direct vector guidance and magnetic modification of cells for their further targeting – clearly

demonstrated substantial advantages of the latter. Therefore, the further investigation was focused on magnetic cell engineering.

Table 2. Intracellular iron content of transfected cells measured by MPS.

Delivered NA, NA/PEI composition	MNP content in NA/PEI/MNP, µg/ml of NA/PEI	Intracellular iron, pg/cell (Mean ± SEM, n=3)
miR, 2.5 pmol/cm² NP ratio 25	0	0.02 ± 0.002
	2.5	0.11 ± 0.033
	5	**0.37 ± 0.079**
	15	**0.62 ± 0.204**
	25	**0.7 ± 0.150**
pDNA, 0.25 µg/cm² NP ratio 15	0	0.05 ± 0.023
	0.5	0.03 ± 0.009
	1	0.03 ± 0.012
	2	0.05 ± 0.026
	3	**0.16 ± 0.038**
	4	**0.34 ± 0.147**

The MPS examination of transfected cells was carried out by F. Wiekhorst[131].

3.3 DETAILED EXAMINATION OF MAGNETICALLY ENGINEERED ENDOTHELIAL CELLS

3.3.1 TIME DEPENDENT ANALYSIS OF MAGNETICALLY RESPONSIVE AND NON-RESPONSIVE TRANSFECTED HUVEC

In this study, the vector NA/PEI/MNP is proposed for magnetic cell engineering prior to transplantation. Therefore, monitoring of cell characteristics is of great importance, including their behavior after the exposure to a strong magnetic field.

The examination of transfected HUVECs was carried out after the separation of mag+ and mag- fractions with a MACS column (Figures 20 & 21). In particular, cells were analyzed by flow cytometry either immediately after magnetic separation (0h) or after culturing them for 24h, which was equal to 24, 48 and 96 hours after transfection, respectively.

The viability assessment showed that cell survival remained very high during the entire time of observation, up to 96h after transfection. For both, miR and pDNA, it did not differ significantly from untransfected controls, independently of the iron concentration (Figure 20D & F; 21B, D & F). The only notable exception was observed directly after

isolation during the analysis of magnetically non-responsive cells transfected with miR/PEI/MNP (Figure 21B). Their survival was significantly decreased as reported above.

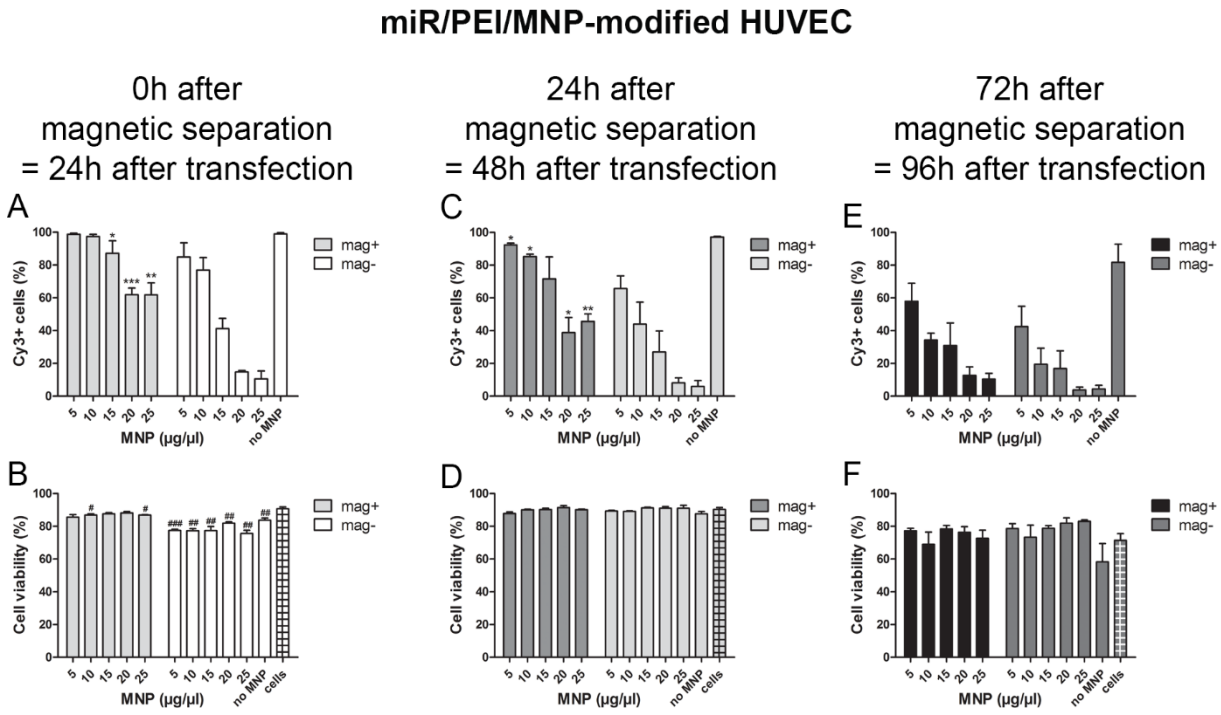

Figure 20. Long-term characterization of magnetically responsive and non-responsive miR/PEI/MNP-HUVEC. HUVEC were transfected at optimal conditions with Cy3-miR/PEI/MNP (2.5 pmol/cm^2 of miR, NP ratio 25 & 5-25 µg/ml of MNP), incubated for 24h and collected. In order to differentiate between magnetically-responsive (mag+) and non-responsive (mag-) cells within total volume of transfected HUVEC, they were applied on MACS separation columns. Resulting mag+ and mag- fractions were split in 3 parts: for immediate analysis with flow cytometry (A, B) or for seeding and further analysis, after 24h (C, D) or 48h (E, F) in culture. Both, amount of Cy3-positive cells (A, C, E) and viability (B, D, F) were assessed and are presented on the plots as ratio between the average amount of viable Cy3-positive cells (A, C, E) or viable cells (B, D, F) and total cell number (n=3; error bars: SEM).
* Significant increase in the amount of Cy3-positive cells in mag+ vs mag- defined for each complex formulation (*p<0.05, **p<0.01, ***p<0.001).
# Statistically significant decrease in cell viability compared to untransfected cells ($^{\#}$p<0.05, $^{\#\#}$p<0.01, $^{\#\#\#}$p<0.001).

The overall amount of Cy3-positive cells in the magnetically-responsive fraction declined over time with all iron concentrations used to form miR/PEI/MNP complexes (Figure 20A, C & E). For the MNP amount of 5 µg/ml, the Cy3-HUVEC number remained constant at first, after 24h of incubation (98%), but was decreased nearly by half at 72h time-point (96h after transfection). With growing concentration of iron, the tendency became more pronounced. The following decrease in the amount of Cy3-positive cells was observed for 10 & 15 µg/ml of MNP: from 98 and 90% in the beginning through 88% and 82% 24h after separation down to 35% and 32% after 72h in culture. The amount of Cy3-positive cells at 20 & 25 MNP declined in the same manner, ie in the first

probe, in average, 60% of HUVEC were positive for Cy3, 40% of them were detected 24h after and only 10% - 72h after.

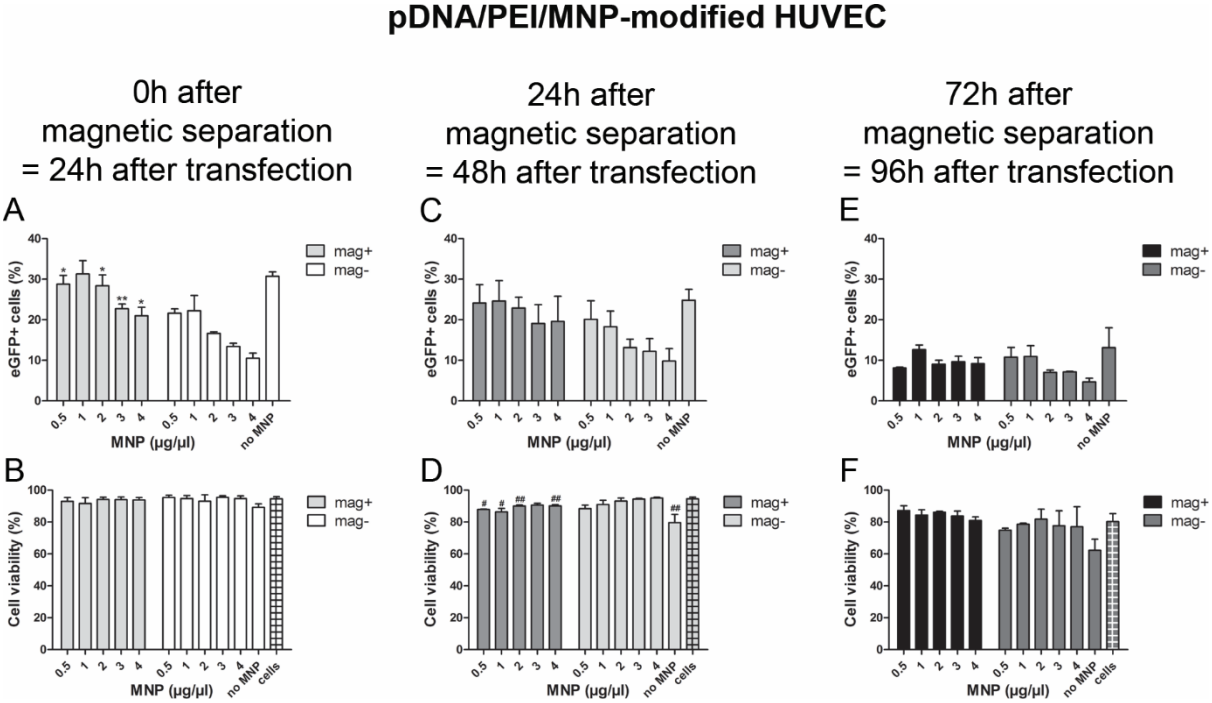

Figure 21. Long-term characterization of magnetically responsive and non-responsive pDNA/PEI/MNP-HUVEC. Magnetically responsive (mag+) and non-responsive (mag-) transfected HUVECs were analyzed independently. For this purpose, they were transfected (2.5 µg/cm^2 of EGFP-encoding pDNA, NP ratio 15 & 0.5-4 µg/ml of MNP) 3-miR/PEI/MNP (optimal 2.5 pmol/cm^2 of miR, NP ratio 25 & 5-25 µg/ml of MNP), incubated for 24h, collected and separated using MACS columns. Obtained mag+ and mag- fractions were analyzed by flow cytometry for viability and amount of Cy3-positive cells at 3 time-points: directly after separation (A, B) or after 24h (C, D) and 72 (E, F) hours in culture. Bars represent the ratio between the average amount of viable EGFP-positive cells (A, C, E) or viable cells (B, D, F) and total cell number (n=3; error bars: SEM).
*Significantly higher eGFP expression in mag+ vs mag- as defined within each complex formulation (*p<0.05, **p<0.01).
Statistically significant decrease in cell viability as compared to untreated HUVECs ($^{\#}$p<0.05, $^{\#\#}$p<0.01).

Cells treated with miR/PEI/MNP and collected in the negative fraction behaved similarly in terms of gradual decrease. The only difference was observed in the total numbers of Cy3-positive cells: they were significantly higher for magnetically-responsive cells compared to non-responsive cells of respective complex formulations directly after separation and 24h after culturing.

The same tendency was observed during the analysis of cells transfected using pDNA/PEI/MNP (Figure 21A, C & E). Numbers of EGFP-positive HUVEC collected in the positive fraction slowly declined from 21-32% as measured immediately after isolation to 13-21% after 24h of incubation and down to 8-13% after 72h in culture. At all iron concentrations, the amount of EGFP expressing cells in the positive fraction was

significantly higher (versus respective complex formulations in negative fraction) on average when recorded right after cell separation.

Transfection with miR/PEI complexes was used as a control and resulted in a very slow decrease of Cy3-positive cell amount over time. Even 72h after isolation (96h after transfection) its rate remained at an average level of 80%. Interestingly, the level of EGFP expressing cells obtained as a result of pDNA/PEI transfection was declining in the same manner as for HUVEC modified with pDNA/PEI/MNP-containing complexes. This observation can be explained by the differences in these complex formulations, ie by the higher amount of iron added in case of miR vs pDNA and its influence on PEI intracellular processing.

Notably, in case of pDNA delivery, safe magnetic loading of cells with iron was limited to a certain degree because of the higher overall amounts of PEI required for efficient transfection compared to miR. Due to this fact and several others, which are described in detail in the Discussion section, further investigation focused on miR modification of cells.

3.3.2 ANTI-MIR DELIVERY WITH PEI/MNP RESULTS IN EFFICIENT KNOCKDOWN OF ENDOGENOUS MIR

Previously, efficient and safe intracellular delivery of tagged Cy3-miR was demonstrated and intense Cy3 signal was detected in the cytoplasm (3.2.1). However, this does not necessarily correlate with subsequent intracellular miR release and its adequate functional activity, especially when endosomal escape is considered as one of the major barriers for non-viral miR delivery[126]. Moreover, even if transfection complexes are released from endosomes, miR can be overly tightly condensed by PEI/MNP, which might prevent its intracellular processing.

In order to prove proper miR functioning after its delivery with PEI/MNP, functional studies were carried out based on an anti-miR directed against miR-92a which is expressed in HUVEC[32]. As a result of qRT-PCR measurement, the efficient silencing of miR-92a was recorded (Figure 22A). Further investigation of target gene expression (integrin subunit α5, ITGA5 – directly suppressed by miR-92a[32]) revealed that it was significantly upregulated as a result of efficient miR-92a knockdown (Figure 22B). Interestingly, whereas miR-92a expression was reduced to negligible levels, ITGA5 gene expression was enhanced only to a certain degree (1.5-fold). This observation can be

explained by the fact that gene expression is most often regulated by several miR simultaneously.

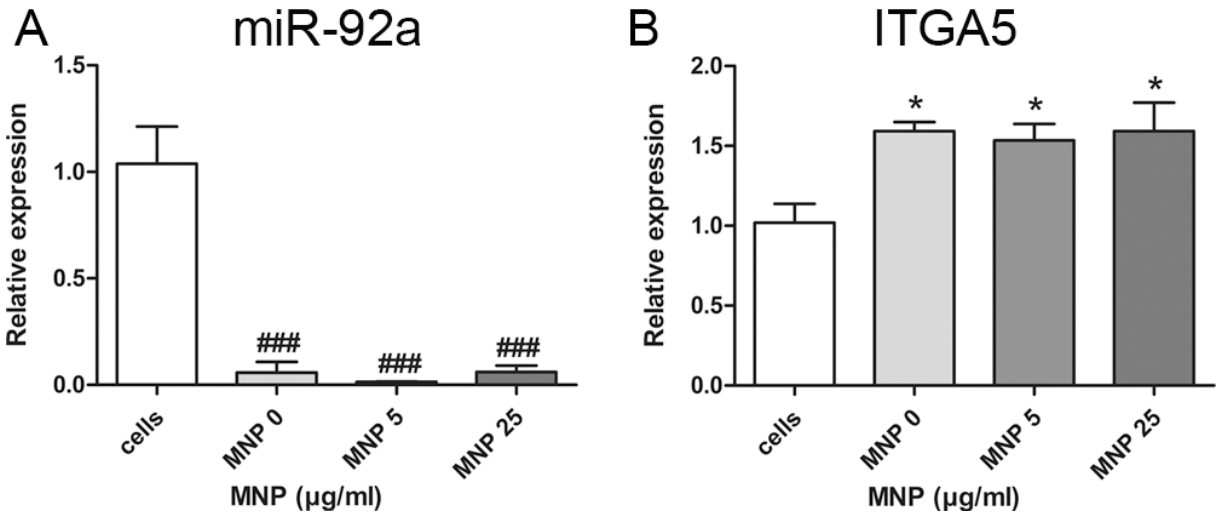

Figure 22. Functionality of delivered by PEI/MNP anti-miR in HUVECs. Proper processing and functioning of delivered miR was assessed by qRT-PCR 48h after transfection. Anti-miR targeted against HUVEC's endogenous miR-92a was delivered with PEI/MNP (2.5 pmol/cm^2 of miR, NP ratio 25, 5 & 25 µg/ml of MNP). Resulting silencing was observed in terms of miR-92a suppression **(A)** and enhanced expression of its target gene **(B)**: ITGA5 is known to be downregulated by miR-92a.
Bars represent relative expression either of miR-92a **(A)** or ITGA5 **(B)**, normalized to RNU6B or 18s expression, respectively (n=3, error bars: SEM).
* Significant up-regulation of gene expression as compared to untreated HUVECs (*$p<0.05$)
# Significantly decreased expression of miR-92a vs untreated cells (###$p<0.001$).
The PCR analysis of transfected cells was carried out by Dr. C. Rimmbach[131].

3.3.3 CELLS TRANSFECTED WITH MIR/PEI/MNP MAINTAIN THEIR KEY FUNCTIONAL PROPERTIES

Furthermore, extended studies of vector safety were carried out since PEI toxicity remains its main limitation. In particular, the functional capacities of miR/PEI/MNP-modified cells were examined in terms of proliferation and tube formation, which are commonly used for HUVEC characterization[32]. Both assays have confirmed the negative influence of PEI alone, which decreased the functionality of cells dramatically: ~20-50% decrease in tube formation parameters (Figure 23A, B) and 60% lower proliferation rate compared to untreated cells (Figure 23C, D). Notably, the presence of MNPs in the vector restored tube formation by HUVECs and improved their proliferative capacity.

However, in the latter case all complex formulations decreased the proliferation to a certain extent vs untransfected cells (~35%).

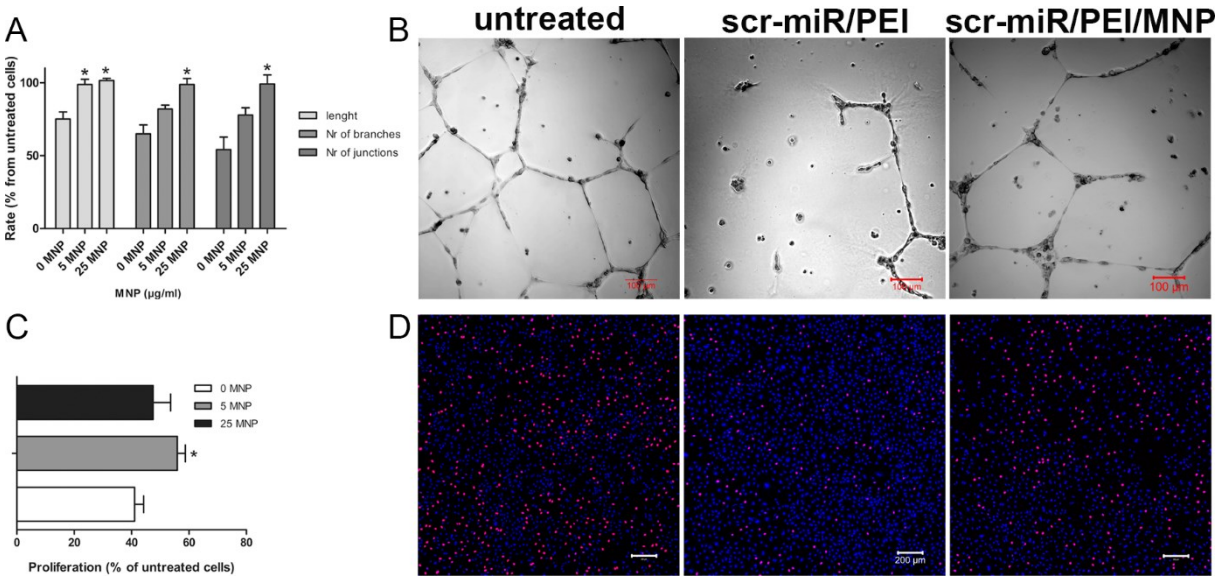

Figure 23. Functional capacities of miR/PEI/MNP-modified HUVECs.
(A) Standard for endothelial cells functional assay – tube formation – was performed to evaluate safety of transfection using 2.5 pmol/cm^2 of scrambled miR, NP ratio 25, 5 & 25 µg/ml of MNPs. Modified cells were collected 48h post-transfection, seeded on Matrigel and incubated for 18h before evaluation. Bars depict the ratio between transfected HUVEC and untreated control in % for several parameters: tube length, number of branches and junctions (n=3, error bars: SEM). **(B)** Representative images of tubes for different complex formulations were taken using confocal microscope in differential interference contrast. Scale bar = 100 nm. **(C)** Another key functional parameter, proliferative capacity, is presented as the ratio between proliferating cells in transfected samples vs untreated HUVECs (n=3, error bars: SEM). **(D)** To obtain representative images, cells were transfected as described above and stained for EdU, whereas nuclei were counterstained with DAPI (blue). Scale bar = 200 nm.
* Significantly improved functional capacity of transfected HUVEC in miR/PEI/MNP vs miR/PEI (*p<0.05).

3.3.4 VECTOR INTERNALIZATION STUDIES

Endocytosis is a fundamental determinant for the efficiency of non-viral vectors and the activity of the delivered cargo. Therefore, understanding of the uptake route and improved control over it are of crucial importance for every new vehicle which is introduced as a therapeutic agent. Many reports have been published on cellular entry and subcellular trafficking of PEI[98,99]. However, MNP presence in the vector might change its pattern dramatically[100]. Moreover, it could shed light on how MNPs decrease PEI toxicity since endosomal escape (i.e. disruption) is one of the key points in PEI-mediated transfection and its toxicity[14,127]. Therefore, the investigation of PEI/MNP uptake mechanism was carried out.

Using Dynasore – an inhibitor of Dynamin and, hence, of clathrin-based and caveolar endocytosis[98] – the predominant way of vector internalization was defined as active uptake. By application of low dosages of Dynasore[111], it was possible to avoid its toxic influence and to discriminate the difference between PEI and PEI/MNP (MNP 5 & 25

μg/ml): the activity of Dynasore in the suppression of uptake was stronger with higher amounts of iron in the vector composition (Figure 24B).

In order to understand the underlying mechanisms, the colocalization between transfection complexes and endocytosis-related organelles was examined, i.e. between labelled PEI of transfection complexes and immunofluorescently stained early endosomes (EEA1 marker), lysosomes (LAMP1) or endoplasmic reticulum (Calnexin). Different time-points – 30 min, 1h and 4h – during the uptake were investigated for different complex formulations (2.5 pmol/cm^2 miR NP 25 with MNP 5 & 25 μg/ml). In general, iron-containing complexes were taken up slower than miR/PEI. In addition, after 30 min and 1h the overall amount of vesicles for PEI/MNP vector was lower than that for PEI only. Massive colocalization of delivery vector with early endosomes was detected 30 min after transfection (Figure 24C), which later significantly decreased and 4h after transfection only single events of colocalization could be recorded. At the same time, the most pronounced overlap between PEI and LAMP1 signal was observed at 1h and 4h time-points. On the contrary, no significant colocalization was observed with the endoplasmic reticulum. Taken together, the obtained data suggest that subcellular vector processing involves mainly acidifying pathways.

Next, a protocol for 3-color fluorescent labelling of miR/PEI/MNP complexes previously developed in our group[94] was employed and applied for superresolution imaging. The tagging procedure does not affect transfection efficiency or viability and allows to study the intracellular vector distribution. In case of transfected HUVECs, transfection vector and delivered cargo formed round structures of 50-500 nm in diameter (rarely up to 1 μm) located in the cytoplasm (Figure 24A). The signal of PEI in these structures was colocalized either with the signal of MNP or with both, miR and MNP. Interestingly, the miR signal was colocalized with the other two only in X-Y dimension, whereas in Z they were laying apart. This can be explained by the fact that lateral SIM resolution is significantly higher than axial.

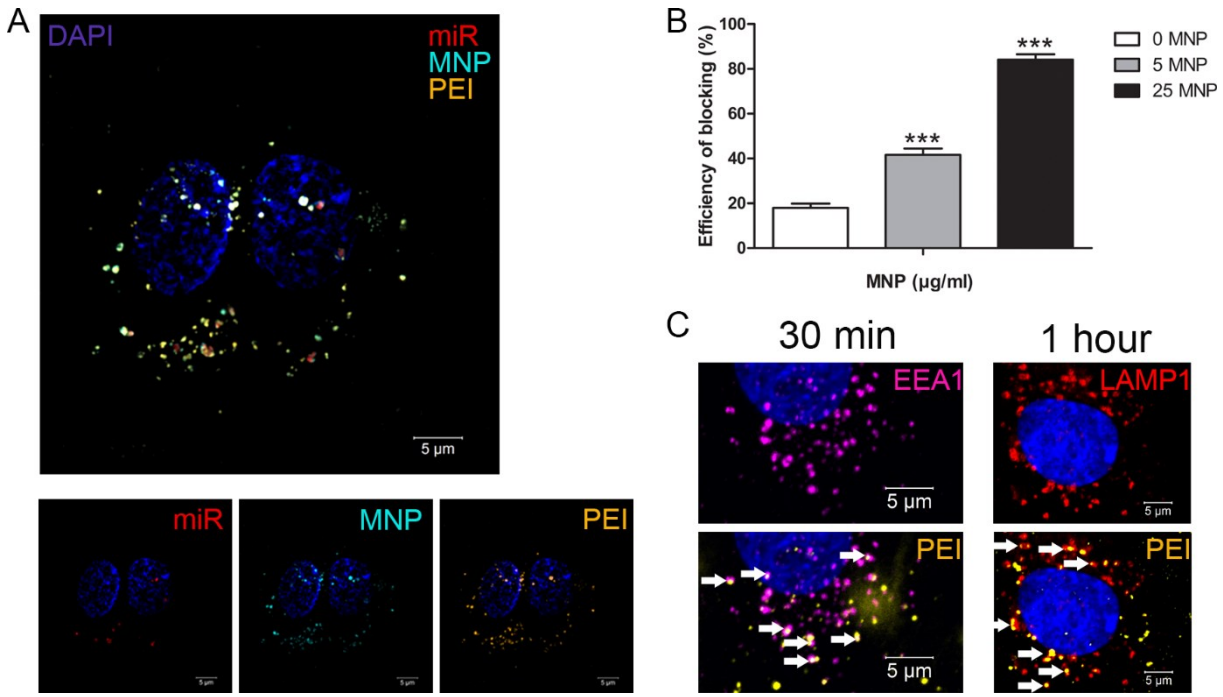

Figure 24. Vector internalization and intracellular localization. (A) Intracellular localization of 3-color labelled transfection complexes was studied 24h after transfection using structured illumination microscopy. Nuclei were counterstained with DAPI. Scale bars: 5µm. **(B)** Activity of endocytosis inhibitor Dynasore was studied using flow cytometry. Dynasore pre-treated cells were transfected with Cy3-miR using PEI or PEI/MNP (2.5 pmol/cm^2 of miR, NP ratio 25, 5 & 25 µg/ml of MNP). The resulting uptake of miR was measured 4h after transfection and respective efficiency of Dynasore (%) in blocking endocytosis was calculated (n=4; error bars: SEM). **(C)** Representative images illustrate the colocalization of transfection complexes, miR/PEI/MNP, with early endosomes (EEA1, magenta) or lysosomes (LAMP1, red) at different time-points during the internalization and intracellular processing. To obtain them cells were fixed, stained using appropriate antibodies and DAPI and visualized using confocal miscoscopy. Scale bar = 5µm.
* Significantly higher inhibiting activity of Dynasore in miR/PEI/MNP treated cells compared to miR/PEI transfection (***p<0.001).
The experimental work on organelle staining and subsequent image acquisition during co-localization studies was shared with Dr. H. Lemcke[131].

3.3.5 IMPACT OF TRANSFECTION ON GJIC

NA of interest used for cell modification can be applied to improve the properties of transplanted cells or to influence cells in the injured organ. In the latter case, modified cells can serve as carrier, i.e. for miR, and bring them to the site of interest. Therefore, it is important to evaluate if normal intercellular communication pathways and molecular transfer mechanics are affected by the proposed transfection vector.

Several mechanisms have been described to mediate the intercellular exchange of miR, including exosomes or GJs (reviewed in [128]). The gap-junctional pathway was selected as GJs connect the cytoplasm of two adjacent cells, allowing for a more directed/targeted shuttling of miR molecules. Moreover, speed and efficiency of miR transfer are increased due to the lack of dilution effects caused by the intercellular space. In order to evaluate

GJ-intercellular communication (GJIC), FRAP technique was used since it allows for non-invasive dynamic monitoring of cells with high temporal resolution[112], whereby the applied 3D-setup is superior to 2D as it is more sensitive for subtle alterations of fluorescence intensity.

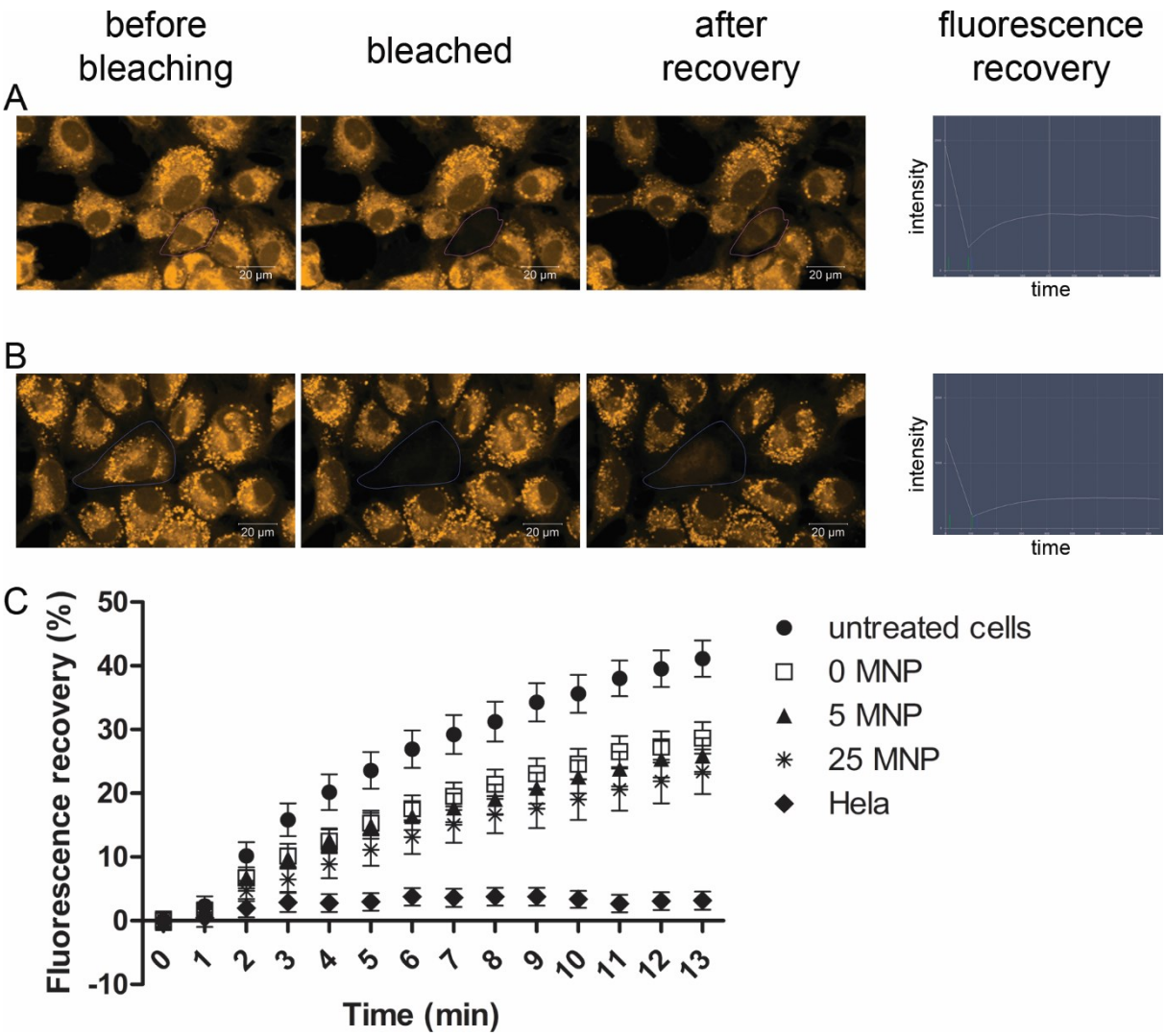

Figure 25. Intercellular communication of miR/PEI/MNP-HUVEC via gap-junctions. Transfected with miR/PEI **(A)** or miR/PEI/MNP **(B)** HUVECs (2.5 pmol/cm^2 of miR, NP ratio 25 combined with 5 (A) & 25 (B) µg/ml of MNP) were loaded with gap-junction permeable fluorescent dye (orange). Selected cells were bleached and recovery of their fluorescence was measured. Representative images reflect the recovery process **(A, B)** Scale bars: 20 µm. Quantitative measurements were also carried out **(C)** using untreated HUVECs and HeLa cells as controls. The extent of gap-junctional communication expressed in % of initial fluorescence is reflected in plotted values (n≥50 cells, error bars: SEM).

In order to exclude unspecific dye transfer and exosomal molecular exchange, the FRAP data for HeLA cells (which do not establish GJs[113]) was collected. As expected, the amplitude of the recovery was negligible compared to that of HUVECs (Figure 25C). In

addition, chosen setup of the FRAP experiment, with its short recording time of 15 minutes, allowed to include mainly fast ways of molecular exchange like GJIC, whereas slower exosomal transfer was not accounted[129]. Together these factors mean that when using 3D-FRAP to study molecular exchange in endothelial cells, mainly GJIC was assessed. As a result, in magnetically modified HUVEC the intercellular transfer of the GJ-permeable dye calcein was recorded: the fluorescence was partly recovered in the bleached cells already after 15 minutes (Figure 25). Yet, the efficiency of recovery was slightly lower for transfected cells, with both, miR/PEI and miR/PEI/MNP, compared to untreated.

This indicates that modified cells maintain their machinery to exchange molecules including miR. Therefore, they do have a significant potential to serve as miR vehicles in addition to their intrinsic therapeutic properties.

3.3.6 DETECTION LIMITS OF MRI VISUALIZATION FOR MIR/PEI/MNP-MODIFIED CELLS

Further, another possible PEI/MNP benefit was explored, offered by the presence of a magnetic component – non-invasive MRI tracking. For this purpose, *in vitro* agarose phantoms mimicking susceptibiity of murine tissues[130] were prepared with different numbers of magnetically modified cells embedded inside (Figure 26A).

First, preliminary tests were carried out with the highest cell number of 5,5 x 10^5, transfected with complexes containing 25 µg/ml of iron 24h prior to phantom preparation. These cells were clearly visible with MRI (Figure 26B). Notably, hypo-intensities were detected in the samples which contained untreated cells or miR/PEI-modified cells and no MNPs. These negative controls, therefore, were used to set a baseline and exclude possible false-positive results. Relying on this, MRI detection limits were defined using various amounts of cells modified with different miR/PEI/MNP formulations: 2.5 pmol/cm^2 miR NP 25 with MNP 5, 15 & 25 µg/ml (Figure 26B). As few as 10 000 cells could be visualized when their iron loading exceeds 0.37 pg iron/cell (Table 2). This is achieved by transfection with 2.5 pmol/cm^2 miR NP 25 complemented by at least MNP 5 µg/ml.

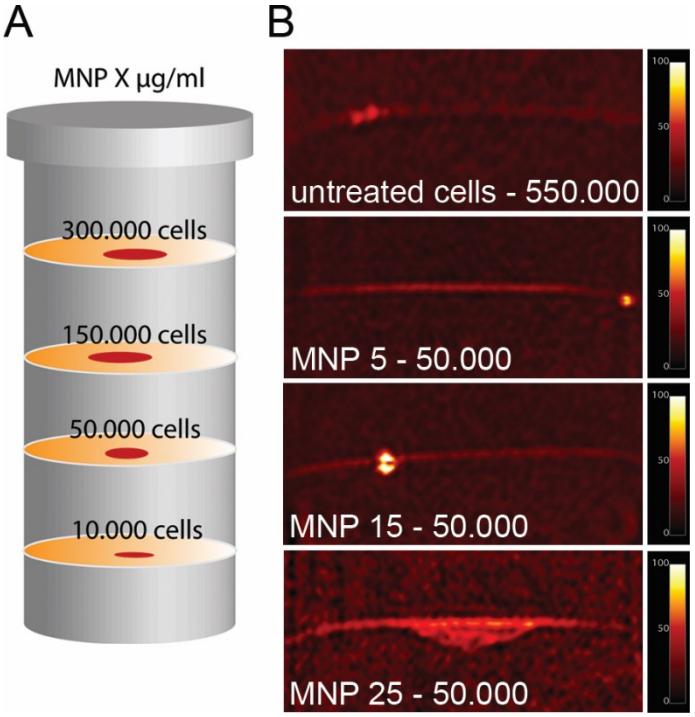

Figure 26. Detection limits of miR/PEI/MNP-modified HUVEC in magnetic resonance imaging.
(A) Agarose gel phantoms were prepared for *in vitro* MRI experiments with different numbers of transfected cells (2.5 pmol/cm² of miR, NP ratio 25 complemented by 5, 15 & 25 µg/ml of MNP). **(B)** Representative images illustrate obtained results for various iron concentrations and cell numbers.
The MR imaging and data acquisition of agarose phantoms was performed by Dr. J.-P. Kühn[131].

To conclude, PEI/MNP vector is highly suitable – in terms of safety and efficiency – for the delivery of plasmid DNA as well as microRNA into human endothelial cells. Importantly, the possibility of MNP to reduce the cytotoxicity caused by the cationic polymer was shown. Moreover, an optimal targeting strategy for PEI/MNP was defined – production of magnetic miR-engineered cells which are suitable for further targeting or retention at the site of interest. The possibility of these cells to be efficiently guided magnetically and visualized non-invasively with MRI has been proven *in vitro*.

3.4 APPLICATION OF THE DEVELOPED ENGINEERING APPROACH FOR A PRODUCTION OF MODIFIED HEMATOPOIETIC STEM CELLS

Further, the developed strategy was transferred to a cell type with even higher therapeutic potential, namely, CD133+ hematopoietic stem cells.

3.4.1 CD133+ CELLS WELL TOLERATE TRANSFECTION WITH MIR/PEI/MNP RESULTING IN EFFICIENT MIR UPTAKE

The purity of cells isolated from bone marrow was defined using their specific surface marker expression measured by flow cytometry (Figure 5). This value varied between patients, however, for all experiments only samples with a purity of ≥80% CD133+ cells were used. In addition, functional hematopoietic capacities of these cells was analyzed in a standard CFU assay.

Transfection optimization was carried out similarly to HUVECs (3.2.1). First, different compositions of miR/PEI were tested (10; 20; 30 and 40 pmol of tagged Cy3-miR per $5x10^4$ cells combined with PEI at NP ratios 2.5, 5 or 7.5) in order to select the most appropriate ones for testing of MNP.

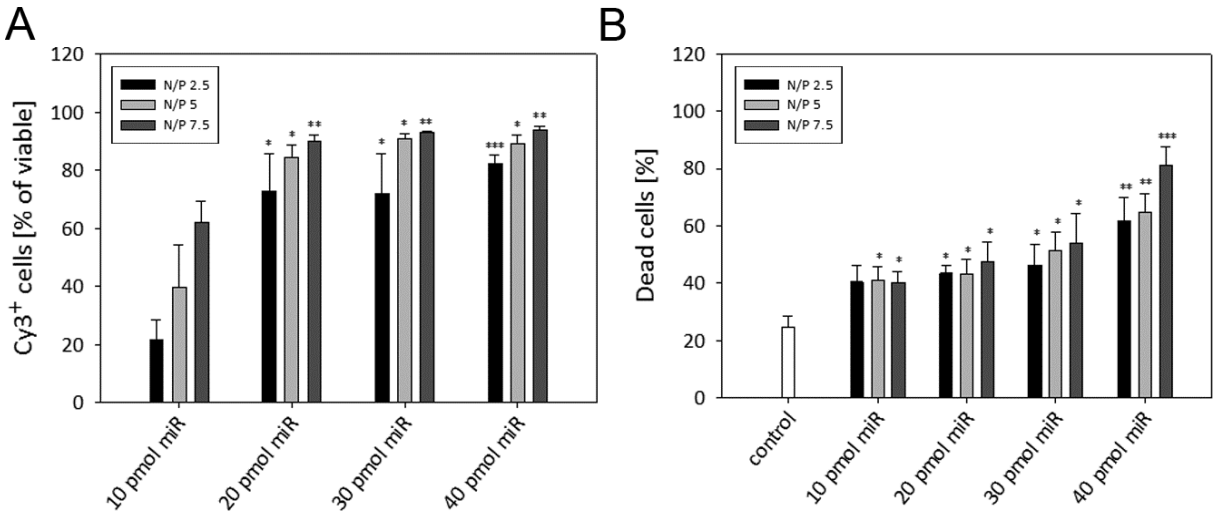

Figure 27. Optimization of transfection in CD133+ cells using miR/PEI polyplexes. CD133+ cells were transfected with different amounts of Cy3-miR (10; 20; 30; and 40 pmol). These were combined with PEI at different NP ratios: 2.5, 5 & 7.5. Uptake efficiency of miR **(A)** and cytotoxicity **(B)** were evaluated by flow cytometry 18 h post-transfection. Bars represent the % of either viable Cy3+ **(A)** or dead **(B)** cells in total CD133+ population (mean ± SEM; n = 4).
(A) * Significantly increased miR uptake vs lowest miR concentration 10pmol. **(B)** * Statistically significant decrease of cell viability vs untransfected control. (*p ≤ 0.05, **p ≤ 0.01, ***p ≤ 0.001)
The experimental data presented in this figure was obtained as a result of equally shared contribution of N. Voronina, P. Müller & F. Hausburg[132].

In CD133+, starting from 20 pmol of miR high uptake rates could be reached, which varied from 70 to 95% depending on NP ratio and miR amount (Figure 27A). In particular, the higher NP ratio and miR amount was, the more efficiently complexes were taken up. However, a significant decrease in cell viability was observed for all transfected samples: on average 40% of cells were dead at all NP combinations with 10 & 20 pmol; 45-55% at 30 pmol; 60-80% at 40 pmol (Figure 27B). At the same time, untreated cells also showed significantly decreased survival rate (down to ~80%) after 18h in culture, whereas directly after isolation this value was 95%.

Taking this into account, the actual toxicity of transfection complexes with 10 and 20 pmol of miR did not exceed 20%, which can be considered acceptable to carry out further investigations. Therefore, complexes built by 20 pmol miR and PEI at NP ratios 2.5, 5 and 7.5 were selected for the following tests with MNPs.

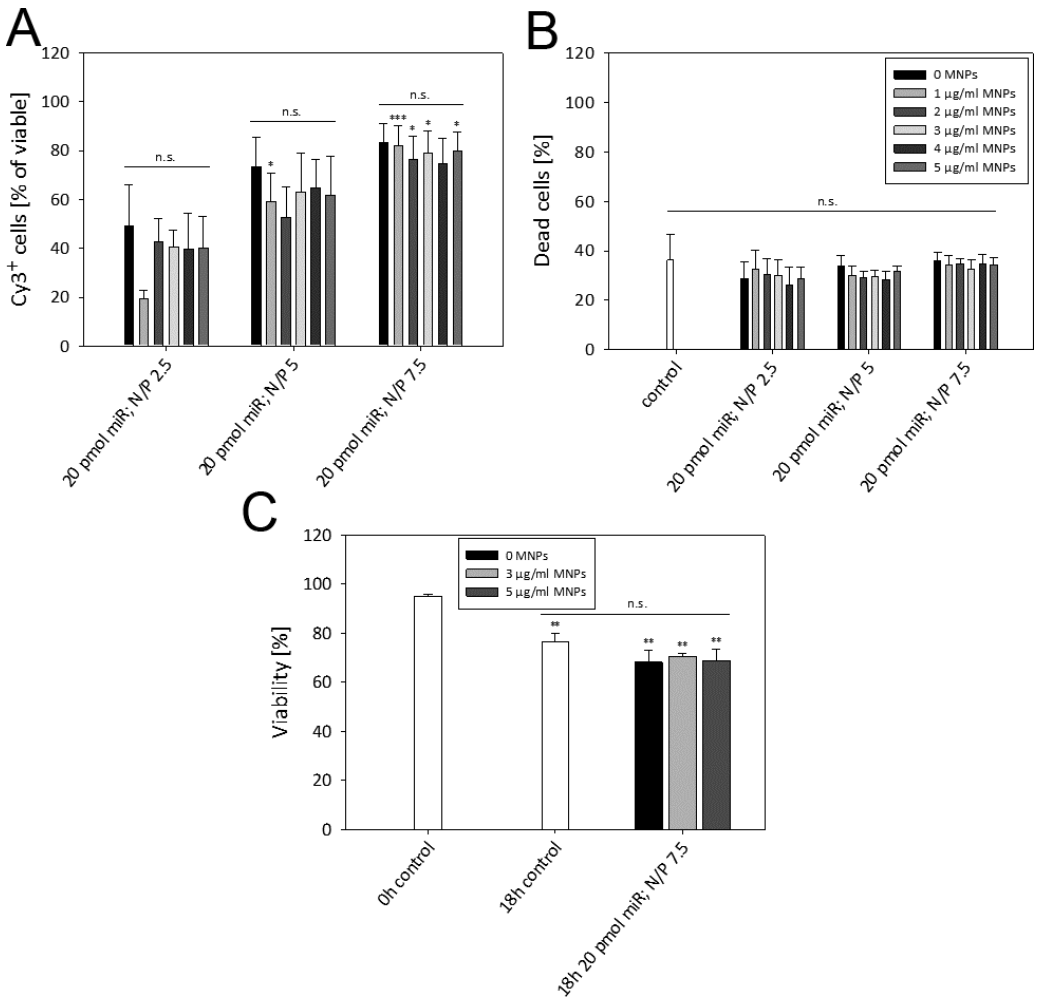

Figure 28. Optimization of transfection in CD133+ cells using miR/PEI/MNP magnetopolyplexes. CD133+ cells were transfected at pre-optimized conditions – 20 pmol of miR with NP ratios 2.5, 5 & 7.5 – complemented by different amount of iron (0, 1, 2, 3, 4 & 5 µg/ml MNP). Uptake efficiency **(A)** and cell viability **(B)** were assessed by flow cytometry 18 h after transfection. Bars depict the % of viable Cy3+ cells **(A)** or dead cells **(B)** in total CD133+ cells. Values are presented as mean ± SEM (n = 4). During the extended analysis of cell viability **(C)**, CD133+ cells from more patients were transfected with pre-selected optimal complex formulations (20 pmol miR with NP ratio 7.5 and 0, 3 or 5 µg/ml MNPs). Untreated freshly isolated cells and untreated cells after 18h in culture were used for comparison. The plot depicts the % of viable cells in whole cell population are presented as mean ± SEM; n = 3.
* Significantly changed miR uptake **(A)** or cell viability **(B)** compared to either uptake at 20 pmol miR NP 2.5 & respective MNP **(A)** or untreated control **(B)**. (*p ≤ 0.05; **p ≤ 0.01; ***p ≤ 0.001)
The experimental data presented in this figure was obtained as a result of equally shared contribution of N. Voronina, P. Müller & F. Hausburg[132].

Different amounts of iron were included in transfection complexes: 1, 2, 3, 4, and 5 µg MNPs per ml of ready miR/PEI. As a result, no significant difference was observed in the Cy3-miR uptake between PEI and PEI/MNP within certain NP ratio (Figure 28A). The amount of Cy3-positive cells varied from ~40 to 80 % and this value was increasing with higher NP ratio and miR amount. (Fig. 28B). Notably, observed result differs from the data obtained for HUVECs, where presence of MNPs decreased the efficiency of miR uptake (Figure 14A).

The amount of dead cells ranged between ~25 – 35% for all applied complex compositions and similar numbers were obtained for the untreated control (Figure 28B). Based on these data, complexes composed by 20 pmol miR NP ratio 7.5 complemented by 3 and 5 µg/ml MNPs were selected for further tests with respect to their high uptake rates and acceptable cytotoxicity vs untreated cells.

Since the experiments on transfection optimization had shown a variability in cell survival from patient to patient, cell viability was examined for several more patients. The obtained average value differed from that in the transfection optimization setup, but the tendency was similar: no significant difference in viability was recorded between untreated and transfected cells (20 pmol miR, N/P 7.5 and 0, 3 and 5 µg/ml MNPs). Notably, a significant decrease in CD133+ viability in the untransfected control was observed during culture: from ~95% viability directly after isolation down to 77% after 18 h in culture (Figure 28C). Such cell death most likely resulted from suboptimal content of culture medium – serum-supplemented DMEM – selected for the establishment of transfection system. Thus, obviously, the transfection setup optimal for targeting does not affect CD133+ cell survival itself, whereas culture conditions decrease cell viability.

Next, the intracellular localization of transfection complexes (including delivered miR) was confirmed, z-stack imaging of transfected cells was performed using laser scanning confocal microscopy. Representative images (Figure 29A) of CD133+ transfected with 20 pmol Cy3-miR NP 7.5 & MNP 3 correlate with flow cytometry data in terms of high uptake rates and illustrate the intracellular localization of the Cy3 signal. Moreover, the intracellular localization of transfection complexes was studied in greater details using a previously described technique for 3-colour labelling of miR/PEI/MNP[94]. It was adapted here for suspension cells and used for confocal and superresolution imaging of prepared cells. As a result, both, miR/PEI and miR/PEI/MNP complexes, were mainly detected in the cytoplasm. The signal of polyethyleneimine was always colocalized with MNP and miR and formed complexes were located in the perinuclear region (Figure 29B). Formed structures of 100-400 nm in size were located in a different focal plane than the nucleus, as a recording of z-stacks demonstrated.

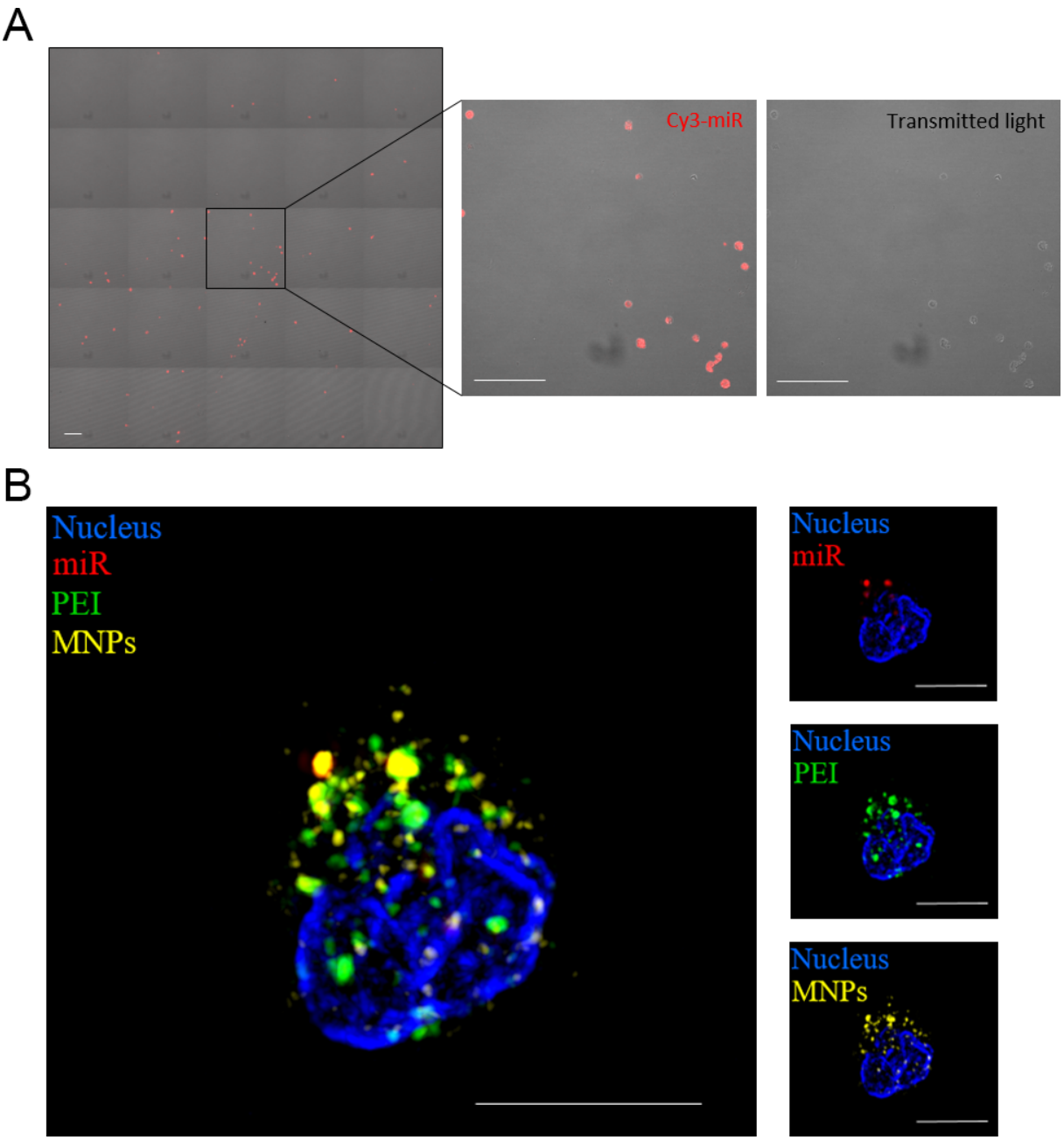

Figure 29. Intracellular localization of transfection complexes in CD133+ cells. (A) CD133+ cells were transfected with Cy3-labeled miR (20 pmol) using different NP ratios (2.5, 5 and 7.5) and MNP amounts (0, 1, 2, 3, 4 and 5 µg/ml). Representative images illustrating intracellular localization of Cy3 signal were taken 18 h post-transfection using laser scanning confocal microscopy. **(B)** The detailed localization of miR, PEI and MNP in cells was defined using structured illumination microscopy. Representative images were obtained 18h after transfection with 3-color labelled complexes (Cy5-miR (red), Atto488-PEI (green) and Atto565-MNPs (yellow)) at optimal conditions: 20 pmol miR, NP ratio 7.5, 3 µg/ml MNPs. Nuclei were counterstained with DAPI (blue). Scale bar = 5 µm.
The experimental data presented in this figure was obtained as a result of equally shared contribution of N. Voronina, P. Müller & F. Hausburg[132].

3.4.2 MAGNETICALLY MODIFIED CD133+ ARE EFFICIENTLY GUIDED IN VITRO

Next, the targeting potential of magnetically modified cells was investigated under static conditions *in vitro*. For this purpose, transfected cells (18h) were transferred into wells with a magnet applied locally under the plate and incubated for 24h (illustrated by

Figure 30A). Similar numbers of untransfected cells were detected in both areas, with and without magnet (Figure 30B). This confirms that magnetic MACS CD133 MicroBeads used for isolation are not sufficient for targeting of cells. On the contrary, cells magnetically modified with miR/PEI/MNP (20 pmol miR, NP 5 and 7.5 combined with MNP 3 and 5 µg/ml) were efficiently targeted.

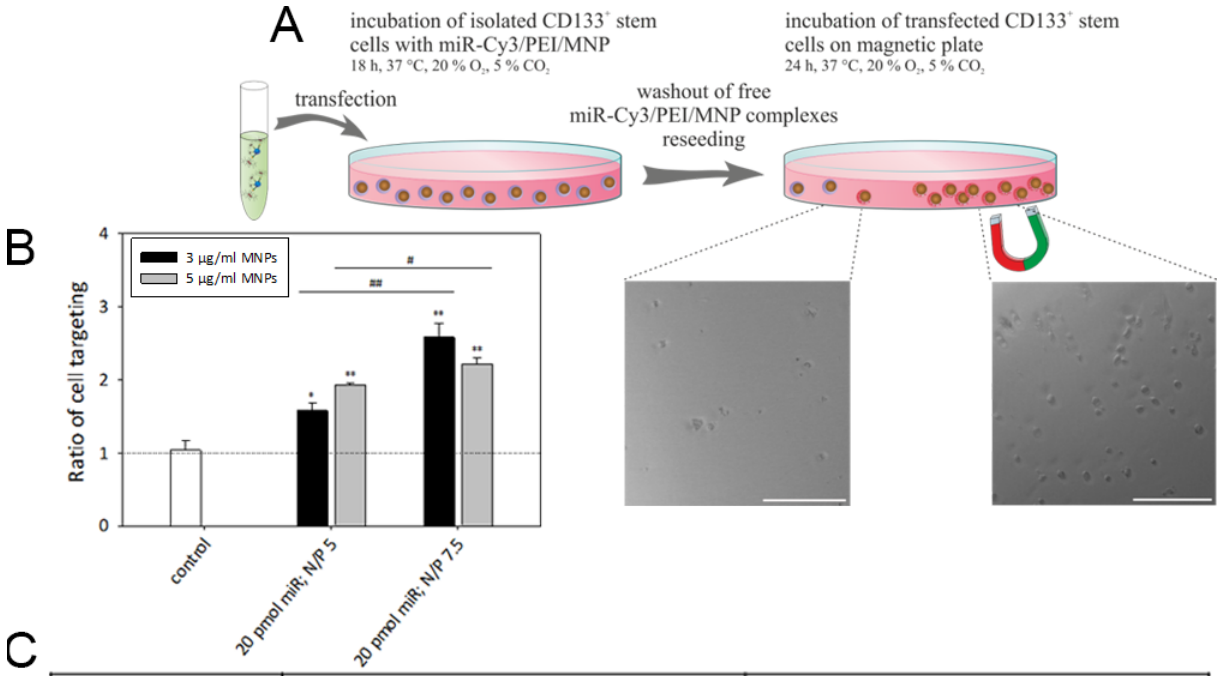

C

control		20 pmol miR; N/P 5				20 pmol; N/P 7.5			
		3 µg/ml MNPs		5 µg/ml MNPs		3 µg/ml MNPs		5 µg/ml MNPs	
+ magnet	- magnet	+ magnet	- magnet	+ magnet	- magnet	+ magnet	- magnet	+ magnet	- magnet
29	22	56	32	55	28	62	25	53	23
31	32	49	31	45	23	57	24	69	34
33	40	41	29	51	28	46	16	54	24

Figure 30. Magnetic targeting of miR/PEI/MNP-CD133+ cells in static conditions.
Representative images of magnetically guided cell migration **(A)** were taken for CD133+ cells modified in pre-selected conditions: 20 pmol Cy3-miR, NP ratios 5 and 7.5 complemented by MNPs 3 & 5 µg/ml. For this purpose, cells collected 18h post-transfection were seeded with the magnet applied locally under the well-plate and analyzed 24h thereafter with laser scanning confocal microscopy. Scale bars = 100 µm. In addition, cell numbers in the areas with and without magnet application were counted **(C)** and correlated magnetic targeting ratios were calculated **(B)**. Values are presented as mean ± SEM (n = 3).
* Significant magnetic targeting as compare to untransfected cells (*p ≤ 0.05, **p ≤ 0.01, ***p ≤ 0.001).
The experimental data presented in this figure was obtained as a result of equally shared contribution of N. Voronina, P. Müller & F. Hausburg[132].

In particular, in untransfected samples the ratio between magnetically guided and non-guided cells was 1 ± 0.12 (Mean ± SEM). For transfected cells this value varied: 1.6 ± 0.09; 1.9 ± 0.02; 2.6 ± 0.17 and 2.2 ± 0.08 for complexes formed at NP 5 with MNP 3 & 5 µg/ml and for complexes with NP 7.5 with 3 & 5 µg/ml MNPs, respectively (Figure 30C). These numbers - ~70% of modified cells are targeted – obtained for CD133+ cells (20

pmol miR, NP ratio 7.5 and 3 or 5 µg/ml MNP) are corresponding to the targeting efficiency demonstrated for HUVECs.

Next, for this optimal targeting complex formulation the amount of intracellular iron in CD133+ was defined by MPS. It reached 0.155 ± 0.0419 pg iron per cell, which also corresponded with data obtained for HUVECs.

Importantly, in case of CD133+ where magnetic MicroBeads were used for cell isolation, the MPS technique allowed to distinguish between these MicroBeads and internalized MNPs to avoid false positive signals. This discrimination was possible due to the fact that miR/PEI/MNP-cells were characterized by A_5/A_3 values in the range 20.5 ± 3.1 %, whereas A_5/A_3 values in the range 27 to 30 % were attributed exclusively to CD133 MicroBeads used for cell isolation.

3.4.3 TRANSFECTION WITH MIR/PEI/MNP HAS NO NEGATIVE INFLUENCE ON CD133+ SURFACE MARKER EXPRESSION AND DIFFERENTIATION

Since the proposed transfection method is intended for cell modification prior to their transplantation, maintenance of intrinsic therapeutic cell properties is crucial. Therefore, the retention of specific surface markers and maintenance of hematopoietic differentiation potential by CD133+ was evaluated using flow cytometry.

As a result, 18h after cell transfection at conditions optimal for targeting (20 pmol miR, NP 7.5 complemented by 0, 3, and 5 µg/ml MNPs), no significant changes in the expression of surface markers were observed (Figure 31A). In particular, for CD133+ it remained 89-92% for all vector compositions vs 87% for untreated cells. Interestingly, CD133+ expression did not change over time: as the examination of the untreated cells showed, it was 93% at 0h and remained at 87% after 18h. Thus, in case of CD133+ culturing for 18h negatively influenced only cell survival (3.4.1), but not stem cell marker expression.

Furthermore, the multipotency of miR/PEI/MNP-modified CD133+ cells was examined in terms of hematopoietic differentiation capacity by application of CFU assays. No significant difference between transfected (20 pmol NP 7.5 and MNP 0, 3, or 5 µl/ml) and untreated cells was observed in the numbers of formed CFU-granulocyte, erythroid, macrophage, megakaryocyte (CFU-GEMM), CFU-granulocyte, macrophage (CFU-GM), burst-forming unit-erythroid (BFU-E), and CFU-erythroid (CFU-E) (Figure 31B & C). In

addition, no morphological abnormalities were detected during visual examination of the CFUs.

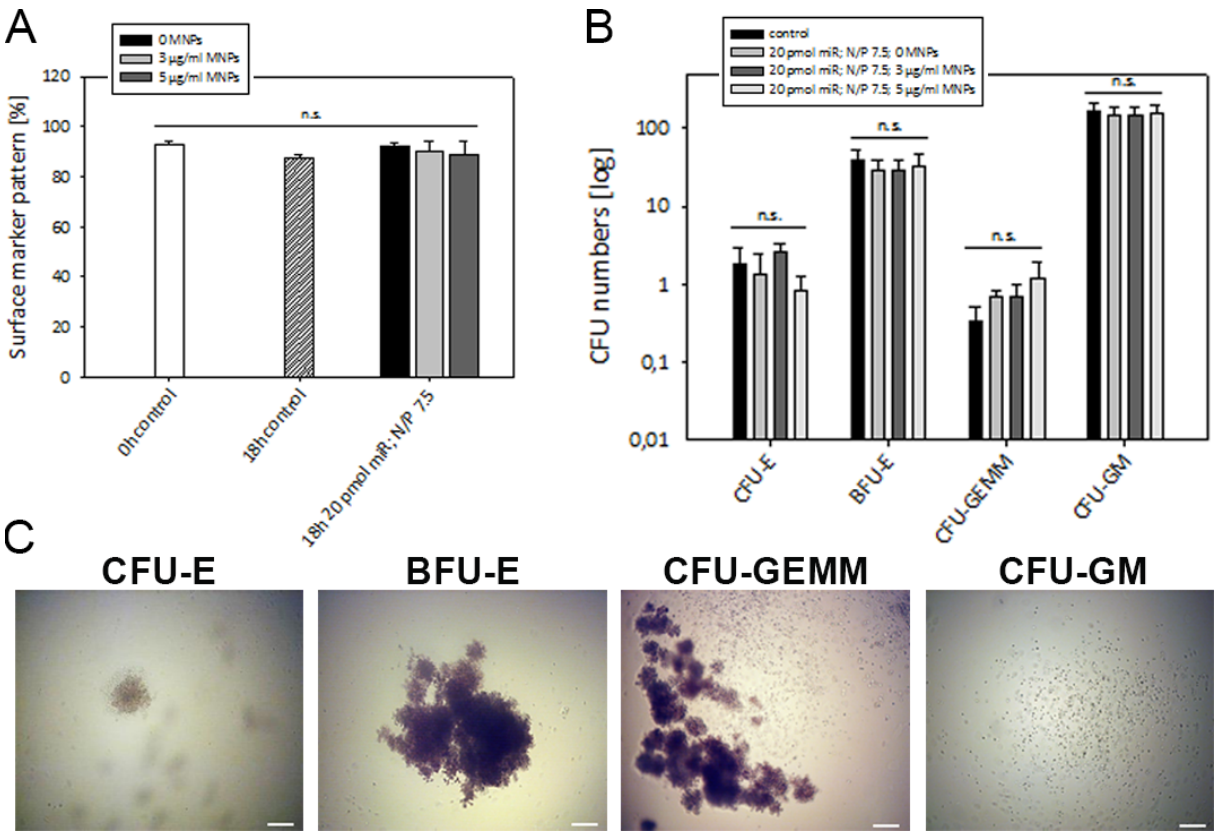

Figure 31. Surface marker pattern and differentiation capacity of CD133+ after transfection. The safety of transfection in terms of cell functional activity was defined by surface marker expression and hematopoietic differentiation potential. Optimized miR/PEI (20 pmol miR, NP ratio 7.5) and miR/PEI/MNP (20 pmol miR, NP ratio 7.5; 3 and 5 µg/ml MNPs) were applied during transfection with following 18h of incubation. **(A)** Surface marker expression was examined by flow cytometry; untreated CD133+ cells were used for comparison. Values are presented as mean ± SEM (n = 3). **(B)** Hematopoietic differentiation potential of transfected cells was assessed in colony-forming unit (CFU) assay (14d incubation). Resulting numbers of CFU-erythroid (CFU-E), Burst-forming unit-erythroid (BFU-E), CFU-granulocyte, erythroid, macrophage, megakaryocyte (CFU-GEMM) and CFU-granulocyte, macrophage (CFU-GM) were counted and compared to respective numbers obtained for untreated cells. **(C)** Representative images reflect the appearance of the colonies. Values are presented as mean ± SEM (n=3). n.s. no significant difference.
The experimental data presented in this figure was obtained as a result of equally shared contribution of N. Voronina, P. Müller & F. Hausburg[132].

3.4.4 PEI/MNP VECTOR IS EFFICIENT IN SUPPORTIVE CYTOKINE-SUPPLEMENTED MEDIUM OPTIMAL FOR CD133+ CELLS

The establishment of transfection and targeting was carried out in DMEM culture medium, simple and easily controlled. In this case, 18 h of incubation were sufficient for miR/PEI/MNP delivery but cell viability was strongly affected (~25 % dead cells). In order to improve culture conditions, StemSpan™ supplemented with StemSpan CC100

was tested as highly suitable for hematopoietic stem cells. This medium is more complex in terms of its molecular content, however, this factor did not prevent efficient transfection with PEI and PEI/MNP. In particular, after the transfection with 20 pmol miR, NP 7.5 combined with 3 and 5 µg/ml MNPs uptake efficiencies in StemSpan were of 87 ± 2 % and 82 ± 5 %, respectively, whereas in DMEM corresponding values were 79 ± 9% and 80 ± 8 % (Figures 32A, 28A).

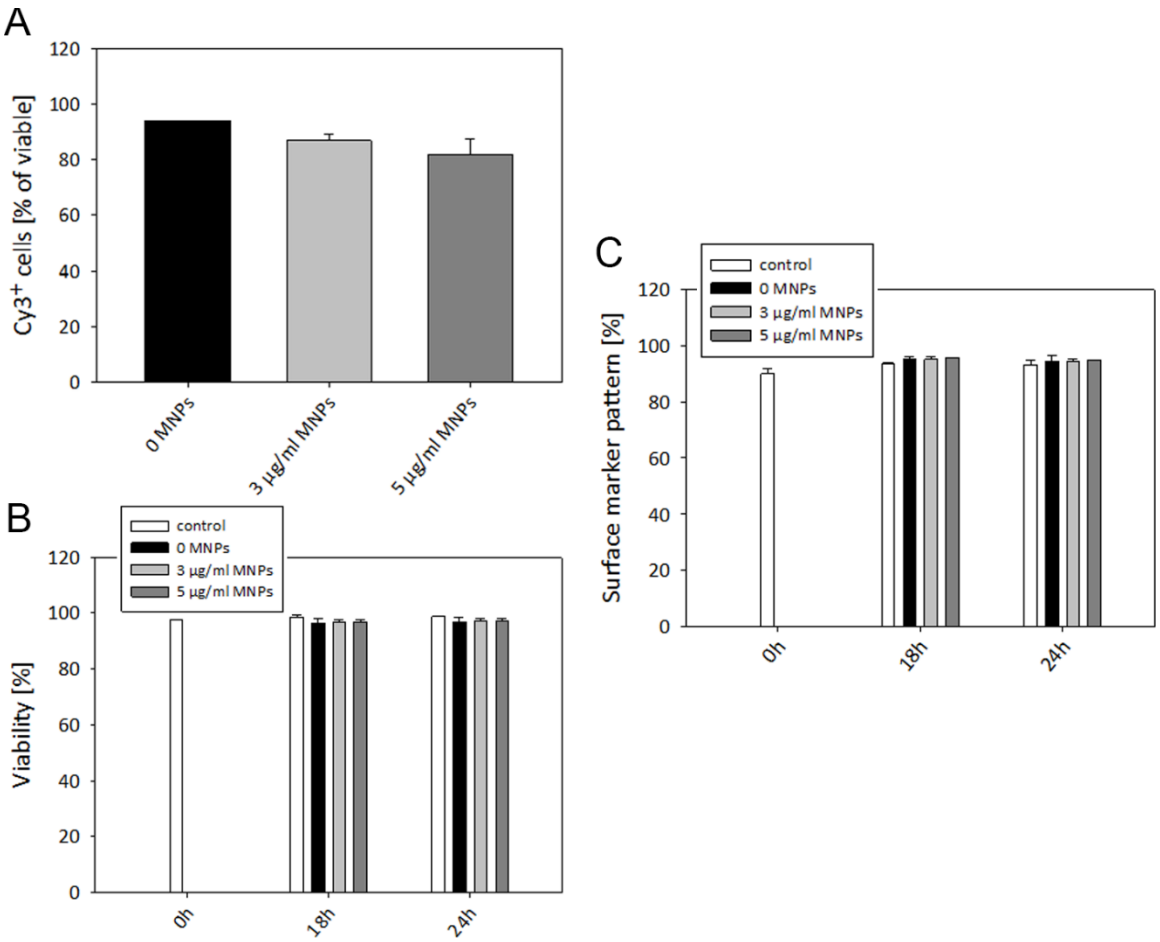

Figure 32: miR uptake, cell viability and surface marker expression of transfected CD133+ in supportive cytokine-supplemented culture medium. Formulations optimized for transfection and targeting (20 pmol miR; NP ratio 7.5; 0, 3 and 5 µg/ml MNPs) were added to CD133+ cells cultured in StemSpan™ H3000 supplemented with StemSpan™ CC100. Cy3-miR uptake efficiency **(A)** and cell viability **(B)** were measured 18- and 24h post-transfection by flow cytometry, along with the expression of CD45, CD34 and CD133+ **(C)**. Untransfected cells (freshly isolated and cultured) were used for comparison. Values are presented as mean ± SEM; n = 2.
The experimental data presented in this figure was obtained as a result of equally shared contribution of N. Voronina, P. Müller & F. Hausburg[132].

Importantly, in StemSpan™ transfected and untransfected CD133+ cells retained their viability after 18 and 24 h in culture: cell survival did not differ from freshly isolated cells (Figure 32B). In addition, no changes in stem cell surface marker expression were observed after an incubation of 18 h and 24 h vs 0h (Figure 32C).

These results clearly demonstrate that efficient transfection of $CD133^+$ cells with PEI/MNP can be performed under optimized cell culture conditions with no resulting negative influence on cell survival and surface marker expression.

To conclude, for CD133+ hematopoietic stem cells, the key findings demonstrated for endothelial cells were confirmed in terms of vector efficiency, safety and targeting potential of modified cells.

3.5 SUMMARY

First, this work provides evidence that a vector previously designed in our group based on PEI/MNP is suitable for such susceptible and difficult to transfect cells types as endothelial cells and hematopoietic stem cells.
In endothelial cells, the uptake of non-functional tagged miR of ~98% was achieved, the delivery of functional anti-miR was followed by almost complete silencing of respective target miR and pDNA transfection resulted in ~40-55% of gene expression. At these optimal transfection conditions cell viability and functionality remained unaffected. Importantly, MNPs were demonstrated to dramatically reduce the known toxicity of PEI. In this study, no mechanistic influence of MNPs on the transfection process which could lead to this positive impact was observed.
In CD133+ hematopoietic stem cells, 80% of miR uptake level was reached with cell survival unaffected and intrinsic differentiation potential fully maintained. Notably, cell culture conditions required optimization even for such a short time of post-transfection incubation as 18h.

Next, magnetic cell engineering for their further guidance was proven to be a superior targeting approach for a PEI/MNP vector compared to direct vector targeting. In particular, direct guidance of NA/PEI/MNP on cells was restricted – presumably by PEI action during transfection. This is possibly explaining why previous *in vivo* studies of our group had limited success. In contrast, over 70% of miR-modified cells, both HUVECs and CD133+, responded to the influence of a static magnetic field. For HUVECs, this was additionally confirmed in dynamic conditions simulated *in vitro*. Modified cells were proven to maintain their intrinsic functional properties. Moreover, the capability of miR/PEI/MNP-modified cells to realize GJ-associated intercellular communication was proven for HUVECs.

Furthermore, for miRNA/PEI/MNP-modified cells loaded with 0.37 pg iron/cell, the MRI detection limit is not less than 10^4 cells as experiments on HUVECs demonstrated.

4 DISCUSSION

To date, conventional surgical and pharmaceutical treatment of CVDs is limited and they remain a major cause of mortality worldwide (1.1.2). In order to solve this problem, alternative therapeutic strategies are being actively developed, whereby cell therapy, gene therapy and their combination are the most promising approaches (1.1.3). Genetic cell engineering is a complex answer to currently existing drawbacks in both fields. There are various methods that enable delivery of genetic material, however, the development of adequate vectors for its delivery of genetic material remains one of the major engineering challenges.

In our group, a non-viral PEI/MNP vector was designed as a potential tool for gene therapy of CVD, either by direct vector application or by vector-assisted genetic engineering of cell therapeutics. In addition to the delivery of genetic material, the proposed NA/PEI/MNP construct has a considerable potential for magnetic guidance and non-invasive MRI monitoring post-application due to its superparamagnetic nanoparticle based part (MNP)[86,95,133].

First, these potential benefits were examined in endothelial cells – HUVECs (parts 4.1-4.3). These cells were selected as a test model since they are relatively easy to isolate and represent a well described, widely accepted *in vitro* model of angiogenesis[32], which is in turn one of the key targets in CVD treatment[16,44]. Extensive optimization of transfection conditions, selection of the most appropriate magnetic targeting strategy and its detailed characterization were performed *in vitro* (4.1-4.3). Further, the optimized concept and protocols were translated into a more clinically relevant cell type – bone-marrow derived CD133+ hematopoietic stem cells[134–138] (4.4).

4.1 PEI/MNP EFFICIENTLY DELIVERS FUNCTIONAL MIR AND DNA TO ENDOTHELIAL CELLS AND ENSURES THEIR LOADING WITH IRON

Transfection optimization experiments have demonstrated that a PEI/MNP vector can be applied for the efficient delivery of both, miR and pDNA, into HUVEC (3.2.1, Figures 12-15). HUVECs are known as cells difficult to transfect and susceptible for toxic influence. In particular, the levels of EGFP expression resulting from pDNA delivery are reported to range from 12-20 to 33-50% on average [120–122,139]. Thus, protein expression levels of ~35-46% obtained safely with EGFP/PEI/MNP are among the highest reported in the literature. The level of Cy3-miR uptake over 95% reached in HUVECs using

PEI/MNP is typically obtained by PEI-based delivery vectors and Lipofectamine™ (commonly used cationic lipid-based transfection reagent)[140].

Interestingly, the selected optimal concentrations of plasmid and miR – 0.25 μg/cm^2 and 2.5pmol/cm^2, respectively (Figures 12, 13) – differ dramatically from those previously reported for PEI/MNP. In particular, 1-3 μg/cm^2 for pDNA[94] and 5pmol/ cm^2 for miR[97] were defined as optimal in earlier work of our group for hMSCs and obtained in the course of this study for cos7 fibroblasts. At the same time, the here defined optimal NP ratios (25 for miR and 7.5-15 for pDNA) correspond with previously published numbers of NP 20-40 for miR and 10-20 for DNA[97,141]. This observation illustrates the known fact about the dependence of transfection efficiency and toxicity on the respective cell type[142].

Importantly, such low required amounts of miR resulted in overall low amounts of PEI necessary for its delivery. Therefore, the baseline toxicity of miR/PEI was low before adding MNPs, which allowed avoiding synergistic toxicity between PEI and MNPs using high iron oxide loading. In particular, up to 25 μg/ml MNPs could be introduced without affecting cell survival (Figure 14), whereas previously in our group MNP concentrations up to maximum 6 μg/ml were applied[94,97]. The situation was different for pDNA: PEI amounts required for efficient gene expression were on average much higher, which is easily explained by the size and charge density of DNA molecule vs miR[141]. In this case, the amounts of iron oxide nanoparticles introduced without cell damage did not exceed 4 μg/ml (Figure 15).

Interestingly, the increase in the amount of iron in NA/PEI/MNP – potentially beneficial for targeting and MRI detection – was negatively influencing transfection efficiency (~5-10% of miR uptake and ~7-12% of EGFP expression; Figures 14A, 15A). This can be explained by the extensively demonstrated fact that the presence of free PEI is necessary for efficient transfection when using complex delivery vectors on its basis[125,143]. Moreover, the importance of the polymer end-group structure has been proven[124]. These are required for efficient NA condensation, internalization of transfection complexes and, for pDNA, its delivery to the nucleus[125]. In case of high iron concentrations in PEI/MNP, excessive nanoparticles could bind all PEI diminishing its activity[125].

In this project, this hypothesis was confirmed directly by tests with the same amount of miR and lower amounts of PEI, at NP ratios 15 & 20. The resulting decrease of miR

uptake was more intensive with a higher iron to PEI ratio and the amount of Cy3-positive HUVEC gradually declined to averages of 90, 70, 60 and 25% (Figure 14A).
Indirectly, it was supported by the examination of uptake mechanism of miR/PEI and miR/PEI/MNP with endocytosis inhibitors and colocalization studies with endosomes at different time points post-transfection (3.3.4). In particular, the internalization of the delivery vector was slower in case of MNP-containing complexes and the number of formed vesicles was lower, too. In addition, the low dosages of endocytosis inhibitor Dynasore were much more efficient in preventing miR/PEI/MNP uptake compared to miR/PEI (Figure 24B). This observation is easily explained when the decreased uptake efficiency of particle-containing complexes is taken into account.

The highly efficient uptake of Cy3-tagged non-functional miR applied during optimization, does not necessarily guarantee proper miR processing and function[144]. In case of PEI, with its tight electrostatic condensation of NA, the release from endosomes and further biological processing is a critical step in delivery (1.4.2). Previous investigation of miR/PEI/MNP by our group demonstrated that once the transfection is optimized with Cy3-miR – these conditions are successful with functional miR[97]. In addition, the intracellular localization of tagged miR in HUVECs has been proven by z-stacks of confocal LSM (Figure 14C). However, in this project, the resulting functional capacity of delivered miR was tested, too. In particular, a functional miR endogenously expressed in HUVEC – miR-92a[32] – was selected and anti-miR against it was delivered using PEI and PEI/MNP. As a result, almost complete knock-down of target miR-92a (Figure 22A) proved the efficient release of the anti-miR from transfection complexes. Moreover, while the highest tested MNP amounts negatively influenced the Cy3-miR cellular uptake, the transfection efficiency of delivered anti-92a did not differ from PEI only. Interestingly, the examined effect of anti-92a on its target gene ITGA5 was very pronounced, yet limited to a certain degree (Figure 22B). This might be explained by multiple miR involved in the regulation of the same gene simultaneously[21]. In addition, in the reported setup HUVECs were treated in normal conditions, whereas a disease can alter gene expression patterns significantly and miR activity can change dramatically, too[21].

To summarize, during the optimization a transfection setup suitable for HUVECs was selected: it allowed to retain cell viability unaffected up to 48 h, while pDNA and miR were successfully delivered and simultaneous cell loading with iron was achieved.

4.2 SELECTION OF OPTIMAL TARGETING APPROACH – MIR/PEI/MNP-MODIFIED CELLS

4.2.1 MAGNETICALLY ENGINEERED CELLS REPRESENT A SUPERIOR TARGETING APPROACH COMPARED TO DIRECT PEI/MNP TARGETING

When successful, localized delivery of therapeutics will ensure target organ selectivity, maximal avoidance of off-target activity and, as a result, reduction of their dosage. This has a great potential in solving such problems of gene therapeutics as insufficient accumulation at the site of interest and off-target toxicity (1.2.2, 1.2.4). This is particularly important for the delivery to highly perfused organs like heart.

The observed outcome of the direct NA/PEI/MNP magnetic guidance on seeded cells clearly demonstrated that targeting was notable, but never complete (3.2.2; Figures 16, 17). When the applied dosages of transfection complexes were reduced by half (in % from initial amount used in transfection optimization), the rate of vector targeting was higher. However, it was accompanied by inefficient transfection, below 30% of uptake for Cy3-miR and 9-18% of eGFP-positive cells for pDNA. Here, the necessity of free PEI for efficient transfection (4.1.)[100,125] explains the limitations of PEI/MNP vector magnetic targeting, which was also observed in a previous *in vivo* proof-of principle study of our group[96]. In particular, free PEI ensuring efficient transfection is not controlled by a magnetic field and can bring NA to off-target cells. Therefore, acceptable targeting conditions can be obtained by application of suboptimal transfection conditions and thereby compromising the efficiency. Another negative factor which must be taken into account in the direct vector targeting approach is a lack of control over the amount of iron loaded into cells.

Magnetic engineering of cell therapeutics for their further magnetically controlled guidance is another targeting approach, which was investigated (3.2.3). Successful application of this strategy would allow to overcome such difficulties of cell therapy as low retention and poor engraftment in the injured area (1.3.2)[49–51] by providing magnetically guided cell products for transplantation. Moreover, simultaneous

introduction of genetic material could promote cell properties and thus increase functional benefits (1.3.3)[62].

For both, with miR and pDNA, ~0.11-0.16 pg of iron loading per cell was sufficient to obtain magnetic responsiveness and cell guidance *in vitro* (3.2.4, Figure 18, Table 2). This iron content was achieved and exceeded with MNP amounts of 3-25 µg/ml without affecting cell viability. Notably, in case of magnetic cell engineering, the necessity of free PEI does not put limitations on targeting as the magnetic field is applied after successful transfection. Moreover, magnetically responsive cells can be sorted: MACS separation, applied in the current study, has not compromised the viability of NA/PEI/MNP-cells (Figures 17, 19, 20). Interestingly, in case of miR/PEI/MNP modification magnetically sorted cells were more viable than non-responsive cells. This can be explained by lower toxicity of PEI/MNP transfection complexes compared to PEI alone (magnetically non-responsive), which corresponds with previously obtained data for hMSCs[94].

To summarize, for PEI/MNP vector, the option with magnetic cell engineering is preferable compared to direct vector targeting.

4.2.2 MIR DELIVERY USING PEI/MNP IS BENEFICIAL AND OPTIMAL VS DNA

In this study, safe and efficient delivery of pDNA and miR to endothelial cells has been achieved with PEI/MNP. However, the maximally achievable iron loading of cells under conditions free from cytotoxic effects – beneficial for magnetic targeting and further MRI detection – was significantly higher using miR. In addition, miR-based therapeutics possess significant benefits *per se* compared to DNA (reviewed in [145]). In particular, plasmid DNA transfection requires its delivery to the nucleus by overcoming the nuclear membrane, limiting thereby its wide application in non-proliferating cell types[145]. Moreover, low transfection efficiencies are restricting pDNA application for stem and precursor cells in a clinical setup: cell modification is usually performed directly prior transplantation and sorting of positive cells may compromise the procedure[146]. In addition, use of pDNA-based therapeutics is associated with the risk of insertional mutagenesis, including abnormal cell functioning and latent oncogenesis[146]. Furthermore, since miR recognition involves only partial complementarity, a single miR can influence expression of multiple targets[147]. Thus, properly selected miR for delivery can regulate complex disease-associated networks of gene expression[28,148,149].

As a result, further investigation was focused on the miR/PEI/MNP-modified cells.

Long-term observation of miR/PEI/MNP-transfected cells (3.3.1; Figure 20A, C & E) has demonstrated that the level of Cy3-positive cells was dramatically reduced by the end of the observation period (96 h). This fact characterizes the proposed system as predictable and controlled. Regulation of such events as angiogenesis in CVDs requires transient genetic modification. However, the protein expression and miR presence might not last long enough to ensure a time-frame sufficient for therapeutic angiogenesis, which is usually described as several weeks[150,151]. Although vector safety clearly supports the possibility of repeated administration, the selected cell-based strategy does not. Thus, for future pre-clinical studies the application of therapeutic miR aimed to improve the properties of transplanted cells should be considered, rather than focusing on pro-angiogenic miRs or genes. In particular, survival and engraftment of transplanted cells (e.g. miR-133a, miR-126, miR-34a, combination of 3 miRNAs, namely miR-21, miR-24, and miR-221) or their homing to target sites (miR-150, miR-146, miR-15a/16)[152,153] could be modified. As a recent report on the clinical trial CELLWAVE indicated, an increase in cell homing to the target area (in this case caused by shock wave) can enhance the outcome of cell therapy[154]. Moreover, the functionality of transplanted cells can be improved, e.g. by application of protective miR-214 or by enhancing their differentiation (e.g. miR-1, miR-499)[153]. This approach is supported by the C-CURE clinical trial, where priming of hMSCs was performed in order to obtain cardiopoietic lineage-specified cells[155]. This study did not involve genetic engineering of these cells, however it has proven the safety of such a modification and its feasibility, which resulted in initiation of similar trials CHART-1 and CHART-2[4]. Moreover, attempts could be made to correct the negative effect of aging on the regenerative capacity of transplanted cells, which was demonstrated in several recent trials[41,47,48] (e.g. miR-10a*, miR-21[153], and miR-34a[28]). In addition, internalized miRs could be employed to influence endogenous cells in the injured tissues[156] (1.2.3).

4.3 DETAILED CHARACTERIZATION OF MIR/PEI/MNP-MODIFIED CELLS

4.3.1 MNP PRESENCE RESTORE FUNCTIONAL CAPACITY OF HUVEC INITIALLY COMPROMISED BY PEI

Polyethyleneimine (PEI) and its derivatives are commonly used for virus-free delivery of nucleic acids (NA) due to their high efficiency and flexibility for modifications[71,157]. In addition, PEI is often incorporated into different types of hybrid nanoparticles as a NA binding and endosome escape agent[147]. To date, PEI has been included in clinical trials testing local gene therapy of various cancers (phases 1 and 2) and multiple successful multi-purpose *in vivo* trials have been published[71,157]. Nevertheless, safety concerns keep the PEI-based vectors from being widely integrated in clinical trials and practice[71,147,157]. Therefore, multiple approaches have been proposed to reduce its toxicity which are mainly intending either to increase biocompatibility or to exclude possible off-target effects by specific guidance[71,100,157,158].

Previously, the decrease of PEI toxicity by the MNPs (in terms of cell survival) was reported by our group for hMSCs[94]. In HUVECs, this positive influence has not been observed in such viability assays as Trypan blue exclusion or LIVE/DEAD® staining with following flow cytometry (Figures 14, 15, 18). The only exception was the higher viability of miR/PEI/MNP-modified Mag+ cells versus Mag- cells shown 24h after transfection and directly after their magnetic separation (Figure 18D). This can be explained by the fact that during the optimization step only such compositions of NA/PEI and NA/PEI/MNP were pre-selected which did not affect cell viability (3.2.1).

In order to address possible PEI toxicity and MNP influence in greater detail, functional studies have been carried out. Tube formation and proliferation are among the most commonly accepted and illustrative assays used to study HUVECs *in vitro*[32]. While extremely high toxicity of miR/PEI was observed in both tests (~60% proliferation inhibition and ~20-50% decrease in tube formation parameters vs untreated), the presence of MNPs improved the vector properties dramatically (3.3.3; Figure 22). In particular, in the presence of iron, the tube formation capacity of cells was fully restored and proliferation activity was improved (up to ~35% proliferation inhibition).

The mechanism of this improvement is unclear. It has been previously hypothesized by our group[94] and others[125] that MNPs prevent PEI from aggressive interaction with nuclear DNA, which has been reported as one of the cytotoxic mechanisms[127,147]. This

hypothesis was partially confirmed by laser confocal[125] and structured illumination microscopy (SIM) imaging[94]. In particular, the lower degree of PEI co-localization with nucleus was demonstrated in the presence of MNPs compared to PEI only. However, even SIM superresolution technique does not allow to detect single molecules of PEI, which might be still detectable in the nucleus by other methods[159].

In this study, another mechanism was investigated – possible influence of MNPs on endocytosis since endosomal/lysosomal disruption is a proposed point in PEI toxicity, too[127]. As studies of vector colocalization with early endosomes, lysosomes and endoplasmic reticulum have demonstrated, PEI/MNP vector follows the same acidifying pathway within cells as PEI does and there is no shift to transport via endoplasmic reticulum (avoiding lysosomes) (3.3.4).

Notably, in the particular case of HUVECs the significant improvement of tube formation might occur due to transient production of ROS which is a known property of iron oxide nanoparticles[160]. A strong correlation exists between the levels of ROS and angiogenic growth factors[161]. Moreover, simultaneous increase in ROS, VEGF and FGF has been reported for endothelial progenitor cells as a result of their loading with superparamagnetic iron oxide nanoparticles[162]. Similar processes could occur in HUVECs[163] after transfection with PEI/MNPs influencing thereby functional activity of cells.

The majority of MNP-associated toxicity is dose-dependent and related to ROS formation and cytoskeleton [160]. Specific investigation of these two possible side-effects was not conducted, however, indirect evidence strongly suggests the safety of applied amounts of MNPs. First, the production of ROS-related to iron oxide particles is transient and peaks 24 h post-treatment – a suitable time point to study possible resulting toxicity (apoptosis) is 72 h[160,164]. During this study, the HUVECs survival was monitored up to 96 h and no decrease in cell viability was observed. Second, the toxic cytoskeletal damage in HUVECs results in their inability to form tubes[165]. Here, the functional activity of MNP-treated HUVECs on the Matrigel® was very active and did not differ from untreated cells (Figure 23A & B).

To conclude, it is remarkable that decrease of PEI toxicity, one of the biggest concerns on its way to clinical trials, was achieved by the introduction of low levels of iron oxide,

biocompatible and routinely used as a contrast reagent in human subjects[160,166]. Moreover, in the current project, no MNP-related toxicity has been observed within the range of selected optimal conditions.

4.3.2 APPLICATION OF STATIC MAGNETIC FIELD IS SAFE FOR MIR/PEI/MNP-MODIFIED CELLS

Characterization of MNPs magnetic properties has demonstrated that the average size of a single iron oxide core within nanoparticles is 4.3(3) nm and this data corresponded with TEM images (Figure 6). Thus, MNPs have demonstrated typical superparamagnetic behaviour, beneficial for biomedical purposes: such small core size results in no remnant magnetization remaining in the absence of an external magnetic field, whereas the magnetic susceptibility for such materials is comparable to that of ferromagnetic bulk material[133,160]. At the same time, superparamagnetic nanoparticles are magnetized in the presence of static magnetic field (SMF). Therefore, it is reasonable to examine the behavior and cytotoxicity of MNP-containing agent in combination with SMF since its application is implied and can possibly cause additional unidentified adverse effects[167]. The recent work of Bae *et al*. has demonstrated that SMF (field strength 0.4 T for 1 h) can enhance the acute toxicity of MNPs (liver-selective MRI contrast agent) in hepatocytes due to resulting formation of bigger aggregates[167]. At the same time, Shaw *et al*. demonstrated that damaging effect of combination of SMF and iron oxide nanoparticles on DNA integrity and membrane potential can be reversible and cell-type dependent[168]. In particular, cancer cells were much more susceptible to genotoxicity than “normal” peripheral blood mononuclear cells. This was attributed by the authors to certain flexibility of “normal” cells in terms of depolarization[168]. To date, very few studies have been carried on the topic[160].

Thus, in the current study, the properties of magnetically-modified cells (transfected without a magnetic field influence) were studied after the application of SMF in the magnetic cell separation columns MACS© (field strength 0.4-1T, gradient up to 10^4 T/m)[107]. This allowed quantifying the amount of magnetically-responsive cells, to characterize them separately from magnetically non-responsive cells and to define the influence of strong SMF on MNP-loaded cells (3.3.1; Figures 18D & F; 20B, D & F; 21B, D & F). The examination of NA/PEI/MNP-HUVECs` properties up to 72 h after magnetic separation (96 h post-transfection) demonstrated no negative influence on cell viability of either magnetic field itself (untransfected cells control) or its combination with MNPs.

Importantly, the reported toxicity of SMF in previous works was dose dependent[167] and in case of miR/PEI/MNP with highest obtained intracellular MNP loading, no toxicity was observed. Moreover, during the targeting of modified cells (Figures 18, 19) a magnet was applied for at least 12 h. Even after such lasting exposure to a strong SMF (1.3 T), no adverse effects on cell survival or morphology were observed.

The obtained results indicate that intracellular iron loading achieved with miR/PEI/MNP is safe even in the presence of a SMF.

4.3.3 TARGETING PERSPECTIVES OF MIR/PEI/MNP-CELLS IN VIVO

The proposed *in vitro* approach with magnetic targeting of transfected cells is clearly sophisticated in terms of successful future *in vivo* application. To date, multiple studies have reported successful *in vivo* magnetic guidance of magnetized stem and progenitor cells for the purposes of regenerative medicine[162,169–174], including CVD treatment[169,170,173,175]. In those studies, where iron oxide nanoparticles were internalized and the amount of iron loading was identified, it varied between ~4 and 30 pg/cell[162,169–171]. These numbers significantly exceed the values ~0.16-0.7 pg/cell, which were sufficient for *in vitro* targeting of NA/PEI/MNP-HUVECs in static conditions.

Such low iron amounts are beneficial in terms of safety and functional capacity of modified cells. For example, a commonly known mechanism of iron oxide nanoparticle-associated toxicity – production of reactive oxygen species (ROS) – is known to be directly associated with the amount of internalized nanoparticles[160]. In addition, several studies have demonstrated that high intracellular levels of iron oxide nanoparticles can lead to dose-dependent cytoskeletal disorganization and damage[165,176].

However, too low MNP loading might be not sufficient for magnetic targeting in a turbulent environment with blood flow. In order to come closer to the challenging *in vivo* situation, dynamic conditions were simulated *in vitro* (3.2.3) by placing culture plates with targetable miR/PEI/MNP-HUVECs suspension on the rotating shaker[114]. While this experiment clearly cannot cover all the interactions within a living organism, it leads to better understanding of targeting potential and *in vivo* usability of PEI/MNP-modified cells. As a result, the highly efficient cell targeting was demonstrated and even active shaking of the culture medium did not interfere with cell movement towards the magnet (Figure 19).

Notably, the majority of mentioned *in vivo* studies[169,171] (including the most successful ones with significant magnetic cell targeting followed by beneficial therapeutic effect[170,173,174,177,178]) practiced cell retention strategy after local administration over the cell guidance after i.v. injection. In one study, where successful cell targeting and positive therapeutic outcome were achieved after i.v. administration, magnetic and antibody-based targeting were combined[179]. At the same time, in the clinical trials of gene therapy for CVD – which is an ultimate aim for PEI/MNP – local injections are well established and the most preferred type of intervention[4,16]. Taken together, the above mentioned factors indicate that PEI/MNP-modified cells will be well suited for magnet based retention at the site of injection *in vivo*.

4.3.4 MODIFIED CELLS MAINTAIN GJIC CRITICAL IN CELL ENGINEERING

The therapeutic effects of SKMs transplanted to patients with CVD were seriously compromised by their arrhythmogenic potential. This was mainly accounted to SKM's lack of Cx43 leading to inability of GJ-mediated intercellular communication and resulting inability of electromechanical integration after transplantation[1,38,180]. Moreover, some studies have shown that transplantation of cells overexpressing of Cx43 significantly decreases the risk of ventricular arrhythmias after MI[180].

Furthermore, modified cell therapeutics can serve as a vehicle for therapeutic miR and bring it to the injured tissues – having thereby gene regulatory effects in the recipient cells[27]. In this case, their capacity to exchange miR with surrounding tissues defines their success as a carrier. Therefore, it is of great importance to investigate the influence of delivery vectors to intercellular communication capacities of modified cells.

In case of miR/PEI/MNP-modified HUVECs, cells were capable to establish GJ, although in a slightly decreased rate as compared with untreated HUVECs (3.3.5; Figure 25). This indicates that potentially, when modified cells are transplanted, they can maintain intercellular communication, miR transfer and integration.

4.3.5 MIR/PEI/MNP-TRANSFECTED CELLS CAN BE SUFFICIENTLY VISUALIZED USING MRI

In case of magnetic nanoparticle-based vectors, therapy can be associated with imaging[81,133].

To date, 2 major non-invasive visualization strategies are proposed for iron oxide-containing vectors: MRI and tracking and a novel sensitive imaging modality magnetic

particle imaging (MPI)[81,95]. HUVECs transfected with miR/PEI/MNP were tested *in vitro* for their potential in non-invasive monitoring by MRI. As a result, 10^4 cells with iron loading 0.37 pg/cell (embedded in *in vitro* agarose phantoms) were detectable using 7.1 Tesla animal MRI system. This result corresponds with detection limits reported by other groups for such levels of intracellular iron[181]. Detected cell numbers are not among the lowest described: from single-cells to hundreds were visualized using various MRI configurations[90,182,183]. However, in these cases the intracellular iron amounts were also incomparably higher, 5-60 pg/cell. Such loading is often applied in cancer research, but not compatible with the transfection approach proposed in this study (discussed in 4.2.2). At the same time, the amount of cells used for transplantation in patients with CVD typically reaches several millions and billions[4]. Therefore, detection limits defined for miR/PEI/MNP-HUVECs could be sufficient to evaluate cell retention and targeting efficiency after cell transplantation.

4.3.6 THERAPEUTIC VALUE OF MODIFIED HUVEC

The perspective of HUVECs transplantation in CVD treatment is very questionable and they mainly serve as a model to study angiogenesis and endothelial cell development[184]. At the same time, *in vivo* HUVECs were investigated as an alternative cell source for cardiac regeneration since they are easily isolated, have strong proliferative activity, and do not possess ethical issues[184]. When transplanted to rats after MI, HUVECs caused significant functional improvement in terms of neovascularization, LVEF and ventricular remodeling[184,185]. Importantly, such mechanism as endothelial-to-mesenchymal transition has been proven to contribute to heart development and regeneration[186]. Thus, efforts which are made to develop HUVECs cell banks are justified[187], especially since the allogenic transplantation has been proven safe in clinical trials for hMSCs[1,4].

In addition, magnetically modified endothelial cells (BAEC) were proposed as a guided coating for steel stents as an alternative solution for the lack of reendothelization after stent angioplasty[188]. Interestingly, the targeting of cells towards the stent is ensured by the application of a uniform magnetic field and by using 304-grade stainless steel as a material for the stent (more magnetically responsive than commonly applied medical-grade 316L). In this situation, the short-range, high-gradient magnetic fields are produced by the magnetizable wires of a stent and, therefore, the regional magnetic force on magnetically engineered endothelial cells is maximized[188].

More importantly, in co-culture HUVECs were proven to positively affect the differentiation and proliferation rates of other cell types[184]. Furthermore, they participate in the regulation of the activity of hematopoietic stem and progenitor cells[189,190]. In addition, when used as a feeder for HSC, HUVECs provide a marker for cell sorting of target HSCs cells after co-culture (by not expressing CD34 and CD45)[191]. Thus, they are successfully applied in platforms for HSC culture and expansion[192,193], which is crucial in HSC-based therapies[194]. Genetic engineering of HUVECs could facilitate their properties. To summarize, having a readily established tool for safe and efficient genetic modification of endothelial cells and their simultaneous magnetization could provide a great benefit for all applications mentioned above.

4.4 APPLICATION OF THE DEVELOPED STRATEGY TO HIGHLY CLINICALLY RELEVANT CD133+ HEMATOPOIETIC STEM CELLS

4.4.1 PEI/MNP IS SUITABLE FOR MIR DELIVERY TO CD133+ AND THEIR MAGNETIZATION

Using HUVEC as a model, the PEI/MNP vector has been proven efficient for transient transfection and magnetic engineering of proliferating cells. Next, it would be of great importance to investigate the suitability of PEI/MNP for non-proliferating cells with higher clinical relevance. In this project, bone-marrow derived CD133+ (highly conserved transmembrane antigen prominin-1[195]) hematopoietic stem and progenitor cells were investigated.

Apart from safety of transplantation proven in multiple clinical trials[44,196], CD133+ bear significant regenerative potential in cardiovascular field[135]. These cells were proven to participate in angiogenesis and stimulate healing due to endothelial differentiation, activation of Wnt-signalling and paracrine mechanisms[134,197,198]. In addition, they have also been described to differentiate into haematopoietic[197] and myogenic lineages[199] (interestingly, the myogenic potential of muscle-derived CD133+ was reportedly higher than for myoblasts[200]). Moreover, as compared to cells isolated on CD34 expression (also actively applied in clinical trials, 1.3.1), the CD133 marker is correlated with a higher content of long-term culture initiating cells and increased proliferative capacity *in vitro*[201]. Based on these properties, more than 30 clinical trials have been initiated based on application of $CD133^+$ stem cells for the treatment of various degenerative diseases (clinicaltrials.gov). Among these, the increase in LVEF of ~6-7%

was demonstrated for the patients with chronic ischemic heart disease after intramyocardial CD133+ cell injection[202]; ~3-4% of LVEF improvement and ~5-6% of decrease in myocardial perfusion were reported after intracoronary cell administration for patients with MI[203].

Hence, CD133+ hematopoietic stem cells are among the strongest cell type candidates for CVD regeneration (1.3.3). At the same time, they share such major difficulties of cellular therapeutics as inconsistent therapeutic outcomes and limited efficacy, partly explained by rapid washout from damaged myocardium and initial cell death post-transplantation (1.3.2)[22,44,204]. Therefore, production of miR-modified magnetically guided CD133+ would be beneficial since it could custom-improve their properties and ensure retention after transplantation.

Despite the fact, that HSC are extremely difficult to transfect and electroporation is the methods of choice for their modification among non-viral delivery techniques[144,205], PEI/MNP has successfully delivered Cy3-tagged miR into cells (~80%) with no significant cytotoxic effects as compared to untreated cells (3.4.1; Figure 28). Moreover, the introduction of miR/PEI/MNP has not affected stem cell marker expression and the hematopoietic differentiation capacity of CD133+ cells, indicating thereby preservation of their intrinsic properties (3.4.3, Figure 31).

Interestingly, it has been reported recently that PEI was unable to sufficiently deliver labelled miR into CD133+ cells and transfection complexes were mainly accumulated on the cell surface[144]. However, in our case both, LSM and superresolution SIM confirmed that delivery vector and miR were located inside the cells (Figures 29). This dramatic difference can be explained by the difference in the PEI used: in the published study low molecular weight branched PEI (2 kDa) has been applied[144], whereas PEI/MNP vector is built on branched 25 kDa PEI. The molecular weight and structure (branching) of PEI are major factors defining PEI efficiency in transfection (1.4.2) [72]. This is mostly explained by the respective growth of the net positive charge and the presence of primary, secondary, and tertiary amines in the branched PEI (vs primary and secondary in the linear)[72,206]. Together, these factors ensure better complexation and condensation properties and higher pH-buffering capacities of the branched PEIs with higher molecular weight. Partly, the choice of low molecular weight PEI is justified because

with the increasing molecular weight and efficiency, the toxicity increases, too[72,206]. At the same time, in the PEI/MNP vector, MNPs are successfully introduced in order to reduce toxicity and it is not compromising high efficiency of branched 25kDa PEI (3.2.3).

4.4.2 TARGETING POTENTIAL OF MIR/PEI/MNP-CD133+ IN VITRO IN STATIC CONDITIONS

Modified CD133+ were guided in static conditions *in vitro* by the locally applied magnet (~70% of cells, which corresponds to HUVECs) whereas MACS CD133 MicroBeads alone were not sufficient for magnetic targeting of cells (3.4.2; Figure 30). This observation contradicts the studies of Ochis' group, where CD133+ cells isolated from peripheral blood were successfully retained by a magnet either in the injured spine or skeletal muscle due to the presence of magnetic isolation beads[174,207]. Several points could lead to the difference in results: 1) in the reported papers the characteristics of beads are not specified and could differ from MACS CD133 MicroBeads; 2) distances used in the experiments could lead to different resulting magnetic field gradients – both, spine and muscle injuries were located on the surface; 3) in the setup applied here the migration of CD133+ was required, while in [174,207] mainly cell capture was involved; 4) a much more advanced setup of the magnet was applied by Fujioka *et al.* and Ohkawa *et al.* with higher field strength and the peak of the magnetic gradient adjusted to the target site[174,207]. This means that the presence of MACS CD133 MicroBeads remaining on the cell surface is beneficial and that a proper setup of the magnet can lead to the improved targeting.

4.4.3 OPTIMAL CULTURE CONDITIONS ENSURE HIGH CD133+ SURVIVAL WITHOUT AFFECTING TRANSFECTION EFFICIENCY OF MIR/PEI/MNP

Notably, culture conditions applied to establish the PEI/MNP transfection were dramatically decreasing CD133+ cell viability (by ~25 % after 18 h cultivation time vs freshly isolated cells).

Multiple independent studies have demonstrated that the fate of HSC in terms of self-renewal, differentiation and apoptosis is greatly affected by such extrinsic components as growth factors/interleukins and serum included in culture medium[33,208]. To date, to define optimal culture and expansion protocols, multiple cytokines and their cocktails have been studied including SCF, Tpo, Flt-3L, IL-11, IL-3, IL-6 and GM-CSF[208]. As a result, a combination of SCF, Flt-3L and IL-11 has been defined as efficiently supporting HSC

survival, proliferation and maintenance *in vitro*[33] and, thus, included in basic supplement in respective types of medium such as StemSpan™ CC100 supplement.
Since electroporation is a commonly applied transfection tool for HSCs, which is not affected by culture medium, very few information is available on suitability of complex supporting medium for transfection with chemical agents[209]. Therefore, for the optimization and establishment of PEI/MNP transfection, simple and controllable DMEM medium was applied. As a result, the suitability of delivery vector was demonstrated for miR delivery to CD133+ cells and their magnetic targeting. However, such culture conditions were proven to be suboptimal already after 18 h incubation time necessary for miR/PEI/MNP uptake (70-75% viable cells in both, treated and untreated samples). Thus, transfection with optimal complex formulations was carried out in StemSpan™ H3000 (xeno- and serum-free) supplemented with Stem Span™ CC100, more suitable for HSCs. Under these conditions, transfection efficiency remained as high as in DMEM (80-90% Cy3-miR positive cells) with preserved expression of stem cell markers, whereas cell viability was comparable to freshly isolated CD133+ cells (Figure 32).

To conclude, the established PEI/MNP vector was proven to be suitable for safe transfection of CD133+ hematopoietic stem cells in optimal culture condition. This resulted in the production of miR-modified magnetically targetable CD133+ cells with retained stem cell marker expression and hematopoietic differentiation capacity, suitable for further pre-clinical evaluation.

4.5 PERSPECTIVES

Such detailed and extensive *in vitro* research as was carried within this project maximizes the chances of the proposed concept in preclinical trials. Several factors should be considered during future investigation of magnetically guided miR/PEI/MNP cells.

Vector development. Current state of standardized vector production and characterization obtained during this study is satisfying for laboratory and *in vivo* tests. However, any level of clinical testing requires GLP standards of the applied procedures. Therefore, attempts should be made to produce PEI/MNP according to GLP guidelines.

Studies on modified CD133+ cell product. Further optimization in terms of CD133+ cell expansion prior to transfection is of great importance[33]. The progress in HSC

research would be greatly facilitated when such problems as lack of donor material and low cell numbers after isolation can be solved.

After selection of suitable therapeutic miRs for delivery, functional assays with modified CD133+ are needed. It has been clearly demonstrated in the previous work of our group[97] and in this study, that once Cy3-miR is internalized at optimal conditions its functional efficiency is also observed in the following gene expression analyses. This indicates that the obtained intracellular miR delivery into $CD133^+$ will also result in an efficient cell transfection. However, the precise details about the functional outcome of delivered miR are necessary for CD133+, too. In addition, the same functional tests with therapeutic miR should be performed in ischemic conditions *in vitro* to predict the response of modified cells *in vivo*.

The possible intracellular toxicity of miR/PEI/MNP modification has to be studied in greater detail. Notably, the recent study of Jin *et al*. has demonstrated a new aspect of miR mimics application: their transient supraphysiological increase in cells caused non-specific alterations in gene expression[210]. Moreover, it is known that the amounts of RNAi pathway components are limited[126]. Therefore, it would be interesting to understand to which degree exogenous miR might compete with endogenous for the intracellular processing machinery and whether this mechanism could cause cytotoxicity. Moreover, the potentially beneficial multi-targeting of miRs can cause unpredictable effects. Thus, the effects of selected therapeutic molecules must be studied in detail.

***In vivo* targeting experiments.** The setup and configuration of magnets should be most carefully considered since this is a crucial criterion of the targeting success. Interestingly, the absolute majority of successful pre-clinical targeting studies was performed in small animals (mainly mice[162,171] and rats[169,170,173,175]). From a technical perspective, the adaptation of these approaches to bigger animals is challenging. The main reason is the rapid decay of the magnetic field gradients which occurs with increasing distance from the magnet and results in the limited interventional depth of permanent magnets[211]. However, improved engineering setups have been developed to solve this question, including custom-made electromagnets, the use of an arrangement of permanent magnets, the implantation of a magnetizable material, or the design of special gradient coils for conventional MRI scanners[211]. Moreover, advanced strategies for noninvasive targeting of magnetized therapeutics are being actively investigated –

application of MR and MRI equipment is among them[212]. In particular, MRI has been successfully applied *in vivo* to image-guide gene therapy[213], to ensure delivery in difficult to access anatomic sites[214,215] and to directly target therapeutics[216]. In addition, the use of simulation models is highly suitable in the cardiovascular field since the variation in basic conditions (e.g. flow and vascular access to damaged myocardium) is relatively low, which potentially allows successful estimation of magnetic targeting efficiency[211].

***In vivo* MR imaging.** The possibility of HUVEC detection has been demonstrated using *in vitro* phantoms mimicking susceptibility of murine tissues. This setup is conclusive as proof-of-principle, however, further dynamic *in vivo* studies are required. In addition, the iron oxide loading of CD133 is several times lower compared to analyzed HUVECs and the detection limits for their MR imaging should be defined.

***In vivo* toxicity studies.** Next, the fate of PEI/MNP *in vivo* in terms of degradation and exocytosis has not been studied and should be subject to examination. It is unlikely that introduced MNPs would have adverse effects[164] since the applied MNP loading is very low (~0.155-0.7 pg per cell) and did not have any negative influence on modified endothelial and hematopoietic stem cells *in vitro*. In general, moderate amounts of iron oxide nanoparticles are proven to be non-toxic: they remain detectable in serum more than 3 weeks (the concentration starts to decrease after 1 week), accumulate mostly in liver and spleen and lead to transient non-pathological increase in ALT, AST and AKP[217]. As published studies suggest, nanoparticles would likely be rapidly cleared by the reticuloendothelial system[147,218]. On the other hand, PEI has a very low biocompatibility and its possible accumulation in different organs, interaction with serum proteins and circulation half-life should be closely monitored[206]. Here, established 3-colour labeling of transfection complexes could be tested and applied to obtain histological information of vector distribution[133]. Importantly, the absence of immune stimulation which might be produced by PEI needs to be determined by appropriate tests *in vivo*.

Intracellular processing investigation. The intracellular trafficking of PEI/MNP vector has been described partly in previous works of our group[94] as well as in the current report. However, these studies lack resolution, whereas such microscopic techniques as PALM and STED allow much higher resolution and single-molecule detection[159]. Their application is challenging and requires the development of complex protocols[219], but will bring the mechanistic descriptions of PEI/MNP transfection to a different level. For

example, the understanding of the degree and dynamics of remaining PEI binding to nucleus will define possible means to protect from its toxicity.

REFERENCES

1. Chen, C.-H., Sereti, K.-I., Wu, B. M. & Ardehali, R. Translational aspects of cardiac cell therapy. *J. Cell. Mol. Med.* **19,** 1757–72 (2015).
2. Mozaffarian, D. *et al. Heart disease and stroke statistics-2015 update : A report from the American Heart Association*. *Circulation* **131,** (2015).
3. Mason, D., Chen, Y.-Z., Krishnan, H. V. & Sant, S. Cardiac gene therapy: Recent advances and future directions. *J. Control. Release* **215,** 101–111 (2015).
4. Behfar, A., Crespo-Diaz, R., Terzic, A. & Gersh, B. J. Cell therapy for cardiac repair—lessons from clinical trials. *Nat. Rev. Cardiol.* **11,** 232–246 (2014).
5. Kostis, J. B. The Importance of Managing Hypertension and Dyslipidemia to Decrease Cardiovascular Disease. *Cardiovasc. Drugs Ther.* **21,** 297–309 (2007).
6. Eurotransplant. at <https://www.eurotransplant.org>
7. Mirotsou, M., Jayawardena, T. M., Schmeckpeper, J., Gnecchi, M. & Dzau, V. J. Paracrine mechanisms of stem cell reparative and regenerative actions in the heart. *J. Mol. Cell. Cardiol.* **50,** 280–9 (2011).
8. Wang, D. & Gao, G. State-of-the-art human gene therapy: part II. Gene therapy strategies and clinical applications. *Discov. Med.* **18,** 151–61 (2014).
9. Bongianino, R. & Priori, S. G. Gene therapy to treat cardiac arrhythmias. *Nat. Rev. Cardiol.* **12,** 531–46 (2015).
10. Cox, D. B. T., Platt, R. J. & Zhang, F. Therapeutic genome editing: prospects and challenges. *Nat. Med.* **21,** 121–131 (2015).
11. Naldini, L. Gene therapy returns to centre stage. *Nature* **526,** 351–360 (2015).
12. Booth, C., Gaspar, H. B. & Thrasher, A. J. Treating Immunodeficiency through HSC Gene Therapy. *Trends Mol. Med.* **22,** 317–327 (2016).
13. Kumar, S. R. *et al.* Clinical development of gene therapy: results and lessons from recent successes. *Mol. Ther. — Methods Clin. Dev.* **3,** 16034 (2016).
14. Villate-Beitia, I. *et al.* in *Gene Therapy - Principles and Challenges* (InTech, 2015). doi:10.5772/61060
15. The Journal of Gene Medicine, Database of Gene Therapy Clinical Trials. at <http://www.abedia.com/>
16. Wolfram, J. A. & Donahue, J. K. Gene therapy to treat cardiovascular disease. *J. Am. Heart Assoc.* **2,** e000119 (2013).
17. Rincon, M. Y. *et al.* Gene therapy for cardiovascular disease: advances in vector development, targeting, and delivery for clinical translation. *Cardiovasc. Res.* **108,** 4–20 (2015).
18. Hedman, M., Hartikainen, J. & Ylä-Herttuala, S. Progress and prospects: hurdles to cardiovascular gene therapy clinical trials. *Gene Ther.* **18,** 743–749 (2011).
19. Bishop, T. & Ratcliffe, P. J. HIF hydroxylase pathways in cardiovascular physiology and medicine. *Circ. Res.* **117,** 65–79 (2015).
20. Wang, D. & Gao, G. State-Of-The-Art Human Gene Therapy: Part II. Gene Therapy

Strategies and Clinical Applications. *Discov. Med.* **18,** 151–161

21. Braunwald, E. The war against heart failure: the Lancet lecture. *Lancet* **385,** 812–824 (2015).
22. Tongers, J., Losordo, D. W. & Landmesser, U. Stem and progenitor cell-based therapy in ischaemic heart disease: promise, uncertainties, and challenges. *Eur. Heart J.* **32,** 1197–206 (2011).
23. Kolwicz, S. C. *et al.* AAV6-mediated Cardiac-specific Overexpression of Ribonucleotide Reductase Enhances Myocardial Contractility. *Mol. Ther.* **24,** 240–250 (2016).
24. Sabatel, C. *et al.* MicroRNA-21 Exhibits Antiangiogenic Function by Targeting RhoB Expression in Endothelial Cells. *PLoS One* **6,** 126–139 (2011).
25. Fish, J. E. *et al.* miR-126 regulates angiogenic signaling and vascular integrity. *Dev. Cell* **15,** 272–84 (2008).
26. Zhou, Q. *et al.* Regulation of angiogenesis and choroidal neovascularization by members of microRNA-23~27~24 clusters. *Proc. Natl. Acad. Sci. U. S. A.* **108,** 8287–92 (2011).
27. Alaiti, M. A. *et al.* Up-regulation of miR-210 by vascular endothelial growth factor in ex vivo expanded CD34+ cells enhances cell-mediated angiogenesis. *J. Cell. Mol. Med.* **16,** 2413–21 (2012).
28. Boon, R. A. *et al.* MicroRNA-34a regulates cardiac ageing and function. *Nature* **495,** 107–10 (2013).
29. Jakob, P. *et al.* Loss of angiomiR-126 and 130a in angiogenic early outgrowth cells from patients with chronic heart failure: role for impaired in vivo neovascularization and cardiac repair capacity. *Circulation* **126,** 2962–75 (2012).
30. Caporali, A. *et al.* Deregulation of microRNA-503 contributes to diabetes mellitus-induced impairment of endothelial function and reparative angiogenesis after limb ischemia. *Circulation* **123,** 282–91 (2011).
31. Chamorro-Jorganes, A. *et al.* MicroRNA-16 and microRNA-424 regulate cell-autonomous angiogenic functions in endothelial cells via targeting vascular endothelial growth factor receptor-2 and fibroblast growth factor receptor-1. *Arterioscler. Thromb. Vasc. Biol.* **31,** 2595–606 (2011).
32. Bonauer, A. *et al.* MicroRNA-92a controls angiogenesis and functional recovery of ischemic tissues in mice. *Science* **324,** 1710–3 (2009).
33. Walasek, M. A., van Os, R. & de Haan, G. Hematopoietic stem cell expansion: challenges and opportunities. *Ann. N. Y. Acad. Sci.* **1266,** 138–150 (2012).
34. Schulte, C. & Zeller, T. microRNA-based diagnostics and therapy in cardiovascular disease-Summing up the facts. *Cardiovasc. Diagn. Ther.* **5,** 17–36 (2015).
35. Hill, A. B. *et al.* Overcoming Gene-Delivery Hurdles: Physiological Considerations for Nonviral Vectors. *Trends Biotechnol.* **34,** 91–105 (2016).
36. Menasché, P. *et al.* Human embryonic stem cell-derived cardiac progenitors for severe heart failure treatment: first clinical case report. *Eur. Heart J.* **36,** 2011–7 (2015).

37. Povsic, T. J. *et al.* A double-blind, randomized, controlled, multicenter study to assess the safety and cardiovascular effects of skeletal myoblast implantation by catheter delivery in patients with chronic heart failure after myocardial infarction. *Am. Heart J.* **162,** (2011).

38. Leeper, N. J., Hunter, A. L. & Cooke, J. P. Stem Cell Therapy for Vascular Regeneration: Adult, Embryonic, and Induced Pluripotent Stem Cells. *Circulation* **122,** 517–526 (2010).

39. Fuster, V. Top 10 cardiovascular therapies and interventions for the next decade. *Nat. Rev. Cardiol.* **11,** 671–683 (2014).

40. Lalit, P. A., Hei, D. J., Raval, A. N. & Kamp, T. J. Induced pluripotent stem cells for post-myocardial infarction repair: remarkable opportunities and challenges. *Circ. Res.* **114,** 1328–45 (2014).

41. Rosen, M. R., Myerburg, R. J., Francis, D. P., Cole, G. D. & Marbán, E. Translating Stem Cell Research to Cardiac Disease Therapies: Pitfalls and Prospects for Improvement. *J. Am. Coll. Cardiol.* **64,** 922–937 (2014).

42. Hou, L. *et al.* Stem cell-based therapies to promote angiogenesis in ischemic cardiovascular disease. *Am. J. Physiol. Heart Circ. Physiol.* **310,** H455-65 (2016).

43. Grimaldi, V. *et al.* Potential benefits of cell therapy in coronary heart disease. *J. Cardiol.* **62,** 267–276 (2013).

44. Ni, N. C. *et al.* The promise and challenges of cardiac stem cell therapy. *Semin. Thorac. Cardiovasc. Surg.* **26,** 44–52 (2014).

45. Karantalis, V. *et al.* Autologous mesenchymal stem cells produce concordant improvements in regional function, tissue perfusion, and fibrotic burden when administered to patients undergoing coronary artery bypass grafting: The Prospective Randomized Study of Mesenchymal Stem Ce. *Circ. Res.* **114,** 1302–10 (2014).

46. Perin, E. C. *et al.* Adipose-derived regenerative cells in patients with ischemic cardiomyopathy: The PRECISE Trial. *Am. Heart J.* **168,** 88–95.e2 (2014).

47. Kim, H. *et al.* Aging disrupts cell subpopulation dynamics and diminishes the function of mesenchymal stem cells. *Arch. Med. Res.* **223,** 158–167 (2015).

48. Golpanian, S. *et al.* Effect of aging on human mesenchymal stem cell therapy in ischemic cardiomyopathy patients. *J. Am. Coll. Cardiol.* **65,** 125–132 (2015).

49. Zeng, L. *et al.* Bioenergetic and functional consequences of bone marrow-derived multipotent progenitor cell transplantation in hearts with postinfarction left ventricular remodeling. *Circulation* **115,** 1866–75 (2007).

50. Dib, N., Khawaja, H., Varner, S., McCarthy, M. & Campbell, A. Cell therapy for cardiovascular disease: a comparison of methods of delivery. *J. Cardiovasc. Transl. Res.* **4,** 177–81 (2011).

51. Terrovitis, J. *et al.* Noninvasive Quantification and Optimization of Acute Cell Retention by In Vivo Positron Emission Tomography After Intramyocardial Cardiac-Derived Stem Cell Delivery. *J. Am. Coll. Cardiol.* **54,** 1619–1626 (2009).

52. Robey, T. E., Saiget, M. K., Reinecke, H. & Murry, C. E. Systems approaches to

preventing transplanted cell death in cardiac repair. *J. Mol. Cell. Cardiol.* **45,** 567–581 (2008).

53. Zhang, M. *et al.* Cardiomyocyte grafting for cardiac repair: graft cell death and anti-death strategies. *J. Mol. Cell. Cardiol.* **33,** 907–21 (2001).

54. Zhu, K. *et al.* Intramyocardial Autologous Bone Marrow-derived Stem Cells Injection for Ischemic Heart Disease Ineligible for Revascularization: A Systematic Review and Meta-analysis. *Arch. Med. Res.* **46,** 286–295 (2015).

55. Shafiq, M., Jung, Y. & Kim, S. H. Insight on stem cell preconditioning and instructive biomaterials to enhance cell adhesion, retention, and engraftment for tissue repair. *Biomaterials* **90,** 85–115 (2016).

56. Sart, S., Ma, T. & Li, Y. Preconditioning Stem Cells for In Vivo Delivery. *Biores. Open Access* **0,** 140702124007003 (2014).

57. Li, X., Tamama, K., Xie, X. & Guan, J. Improving Cell Engraftment in Cardiac Stem Cell Therapy. *Stem Cells Int.* **2016,** 7168797 (2016).

58. Chavakis, E., Koyanagi, M. & Dimmeler, S. Enhancing the Outcome of Cell Therapy for Cardiac Repair: Progress From Bench to Bedside and Back. *Circulation* **121,** 325–335 (2010).

59. Russo, V., Young, S., Hamilton, A., Amsden, B. G. & Flynn, L. E. Mesenchymal stem cell delivery strategies to promote cardiac regeneration following ischemic injury. *Biomaterials* **35,** 3956–74 (2014).

60. Traverse, J. H. Using biomaterials to improve the efficacy of cell therapy following acute myocardial infarction. *J. Cardiovasc. Transl. Res.* **5,** 67–72 (2012).

61. Park, J. S., Suryaprakash, S., Lao, Y.-H. & Leong, K. W. Engineering mesenchymal stem cells for regenerative medicine and drug delivery. *Methods* **84,** 3–16 (2015).

62. Robert D. Kirkton, N. B. Genetic Engineering and Stem Cells: Combinatorial Approaches for Cardiac Cell Therapy. *IEEE Eng. Med. Biol. Mag.* **27,** 85 (2008).

63. Huber, I. *et al.* Identification and selection of cardiomyocytes during human embryonic stem cell differentiation. *FASEB J.* **21,** 2551–63 (2007).

64. Krishnan, M. *et al.* Effects of epigenetic modulation on reporter gene expression: implications for stem cell imaging. *FASEB J.* **20,** 106–8 (2006).

65. Grauss, R. W. *et al.* Forced myocardin expression enhances the therapeutic effect of human mesenchymal stem cells after transplantation in ischemic mouse hearts. *Stem Cells* **26,** 1083–93 (2008).

66. Cheng, Z. *et al.* Targeted migration of mesenchymal stem cells modified with CXCR4 gene to infarcted myocardium improves cardiac performance. *Mol. Ther.* **16,** 571–9 (2008).

67. Song, H. *et al.* Tissue transglutaminase is essential for integrin-mediated survival of bone marrow-derived mesenchymal stem cells. *Stem Cells* **25,** 1431–8 (2007).

68. Pan, A., Weintraub, N. L. & Tang, Y. Enhancing stem cell survival in an ischemic heart by CRISPR-dCas9-based gene regulation. *Med. Hypotheses* **83,** 702–705 (2014).

69. Dai, Y. *et al.* HIF-1alpha induced-VEGF overexpression in bone marrow stem cells

protects cardiomyocytes against ischemia. *J. Mol. Cell. Cardiol.* **42,** 1036–44 (2007).

70. Joladarashi, D. *et al.* Enhanced Cardiac Regenerative Ability of Stem Cells After Ischemia-Reperfusion Injury. *J. Am. Coll. Cardiol.* **66,** 2214–2226 (2015).

71. Yin, H. *et al.* Non-viral vectors for gene-based therapy. *Nat. Rev. Genet.* **15,** 541–555 (2014).

72. Nayerossadat, N., Maedeh, T. & Ali, P. A. Viral and nonviral delivery systems for gene delivery. *Adv. Biomed. Res.* **1,** 27 (2012).

73. Anjos-Afonso, F., Siapati, E. K. & Bonnet, D. In vivo contribution of murine mesenchymal stem cells into multiple cell-types under minimal damage conditions. *J. Cell Sci.* **117,** 5655–64 (2004).

74. Boura, J. S. *et al.* Evaluation of gene delivery strategies to efficiently overexpress functional HLA-G on human bone marrow stromal cells. *Mol. Ther. — Methods Clin. Dev.* **1,** 14041 (2014).

75. Olmedillas López, S., Garcia-Arranz, M., Garcia-Olmo, D. & Liras, A. Preliminary study on non-viral transfection of F9 (factor IX) gene by nucleofection in human adipose-derived mesenchymal stem cells. *PeerJ* **4,** e1907 (2016).

76. Xue, X. *et al.* Stable gene transfer and expression in cord blood-derived CD34+ hematopoietic stem and progenitor cells by a hyperactive Sleeping Beauty transposon system. *Blood* **114,** 1319–30 (2009).

77. Nasimuzzaman, M. *et al.* High-titer foamy virus vector transduction and integration sites of human CD34+ cell–derived SCID-repopulating cells. *Mol. Ther. — Methods Clin. Dev.* **1,** 14020 (2014).

78. Chira, S. *et al.* Progresses towards safe and efficient gene therapy vectors. *Oncotarget* **6,** 30675–30703 (2015).

79. Voronina, N., Delyagina, E., David, R. & Steinhoff, G. in *Advances and Challenges in the Delivery of Nucleic Acid Therapeutics (Volume 1)* 108–123 (Future MEdicine, 2015). doi:doi: 10.4155/fseb2013.13.106

80. Tian, H., Chen, J. & Chen, X. Nanoparticles for Gene Delivery. *Small* **9,** 2034–2044 (2013).

81. Almstätter, I. *et al.* Characterization of magnetic viral complexes for targeted delivery in oncology. *Theranostics* **5,** 667–85 (2015).

82. Yamashita, S. *et al.* Controlled-release system of single-stranded DNA triggered by the photothermal effect of gold nanorods and its in vivo application. *Bioorg. Med. Chem.* **19,** 2130–2135 (2011).

83. Ma, X. *et al.* Redox-responsive mesoporous silica nanoparticles: a physiologically sensitive codelivery vehicle for siRNA and doxorubicin. *Antioxid. Redox Signal.* **21,** 707–22 (2014).

84. Mannell, H. *et al.* Site directed vascular gene delivery in vivo by ultrasonic destruction of magnetic nanoparticle coated microbubbles. *Nanomedicine* **8,** 1309–18 (2012).

85. Namiki, Y. *et al.* A novel magnetic crystal-lipid nanostructure for magnetically

guided in vivo gene delivery. *Nat. Nanotechnol.* **4,** 598–606 (2009).

86. Sokolova, V. & Epple, M. Inorganic nanoparticles as carriers of nucleic acids into cells. *Angew. Chem. Int. Ed. Engl.* **47,** 1382–95 (2008).

87. Paul, A., Shao, W., Shum-Tim, D. & Prakash, S. The attenuation of restenosis following arterial gene transfer using carbon nanotube coated stent incorporating TAT/DNA(Ang1+Vegf) nanoparticles. *Biomaterials* **33,** 7655–64 (2012).

88. Meng, H. *et al.* Codelivery of an optimal drug/siRNA combination using mesoporous silica nanoparticles to overcome drug resistance in breast cancer in vitro and in vivo. *ACS Nano* **7,** 994–1005 (2013).

89. Muroski, M. E., Kogot, J. M. & Strouse, G. F. Bimodal gold nanoparticle therapeutics for manipulating exogenous and endogenous protein levels in mammalian cells. *J. Am. Chem. Soc.* **134,** 19722–30 (2012).

90. Rad, A. M., Arbab, A. S., Iskander, A. S. M., Jiang, Q. & Soltanian-Zadeh, H. Quantification of superparamagnetic iron oxide (SPIO)-labeled cells using MRI. *J. Magn. Reson. Imaging* **26,** 366–74 (2007).

91. Park, J. *et al.* Quantum Dots in an Amphiphilic Polyethyleneimine Derivative Platform for Cellular Labeling, Targeting, Gene Delivery, and Ratiometric Oxygen Sensing. *ACS Nano* **9,** 6511–21 (2015).

92. Namiki, Y. *et al.* A novel magnetic crystal–lipid nanostructure for magnetically guided in vivo gene delivery. *Nat. Nanotechnol.* **4,** 598–606 (2009).

93. Mody, V. V, Siwale, R., Singh, A. & Mody, H. R. Introduction to metallic nanoparticles. *J. Pharm. Bioallied Sci.* **2,** 282–9 (2010).

94. Delyagina, E. *et al.* Improved transfection in human mesenchymal stem cells: effective intracellular release of pDNA by magnetic polyplexes. *Nanomedicine (Lond).* **9,** 999–1017 (2014).

95. Zheng, B. *et al.* Quantitative Magnetic Particle Imaging Monitors the Transplantation, Biodistribution, and Clearance of Stem Cells In Vivo. *Theranostics* **6,** 291–301 (2016).

96. Li, W. *et al.* Enhanced thoracic gene delivery by magnetic nanobead-mediated vector. *J. Gene Med.* **10,** 897–909 (2008).

97. Schade, A. *et al.* Innovative strategy for microRNA delivery in human mesenchymal stem cells via magnetic nanoparticles. *Int. J. Mol. Sci.* **14,** 10710–10726 (2013).

98. El-Sayed, A. & Harashima, H. Endocytosis of gene delivery vectors: from clathrin-dependent to lipid raft-mediated endocytosis. *Mol. Ther.* **21,** 1118–30 (2013).

99. Reilly, M. J., Larsen, J. D. & Sullivan, M. O. Polyplexes traffic through caveolae to the Golgi and endoplasmic reticulum en route to the nucleus. *Mol. Pharm.* **9,** 1280–1290 (2012).

100. Xu, T., Liu, W., Wang, S. & Shao, Z. Elucidating the role of free polycationic chains in polycation gene carriers by free chains of polyethylenimine or N,N,N-trimethyl chitosan plus a certain polyplex. *Int. J. Nanomedicine* **9,** 3231–3245 (2014).

101. Hanzlíková, M. *et al.* Mechanisms of polyethylenimine-mediated DNA delivery:

free carrier helps to overcome the barrier of cell-surface glycosaminoglycans. *J. Gene Med.* **13,** 402–409 (2011).

102. Singh, R. & Lillard, J. W. Nanoparticle-based targeted drug delivery. *Exp. Mol. Pathol.* **86,** 215–23 (2009).

103. Gaebel, R. *et al.* Patterning human stem cells and endothelial cells with laser printing for cardiac regeneration. *Biomaterials* **32,** 9218–9230 (2011).

104. Jaffe, E. a, Nachman, R. L., Becker, C. G. & Miinick, C. R. Culture of Human Endothelial Cells Derived from Umbilical Veins. *J. Clin. Invest.* **52,** 2745–2756 (1973).

105. Kircheis, R. *et al.* Polyethylenimine/DNA complexes shielded by transferrin target gene expression to tumors after systemic application. *Gene Ther* **8,** 28–40 (2001).

106. Klotz, I. M., Royer, G. P. & Scarpa, I. S. Synthetic derivatives of polyethyleneimine with enzyme-like catalytic activity (synzymes). *Proc. Natl. Acad. Sci. U. S. A.* **68,** 263–4 (1971).

107. Miltenyi, S., Müller, W., Weichel, W. & Radbruch, A. High gradient magnetic cell separation with MACS. *Cytometry* **11,** 231–8 (1990).

108. SUTHERLAND, D. R., ANDERSON, L., KEENEY, M., NAYAR, R. & CHIN-YEE, I. The ISHAGE Guidelines for CD34+ Cell Determination by Flow Cytometry. *http://dx.doi.org/10.1089/scd.1.1996.5.213* (2009).

109. Chorny, M. *et al.* Formulation and in vitro characterization of composite biodegradable magnetic nanoparticles for magnetically guided cell delivery. *Pharm. Res.* **29,** 1232–1241 (2012).

110. Macia, E. *et al.* Dynasore, a cell-permeable inhibitor of dynamin. *Dev. Cell* **10,** 839–50 (2006).

111. Seow, W. Y., Yang, Y. Y. & George, A. J. T. Oligopeptide-mediated gene transfer into mouse corneal endothelial cells: Expression, design optimization, uptake mechanism and nuclear localization. *Nucleic Acids Res.* **37,** 6276–6289 (2009).

112. Lemcke, H., Nittel, M. L., Weiss, D. G. & Kuznetsov, S. a. Neuronal differentiation requires a biphasic modulation of gap junctional intercellular communication caused by dynamic changes of connexin43 expression. *Eur. J. Neurosci.* **38,** 2218–2228 (2013).

113. Kuzma-Kuzniarska, M., Yapp, C., Pearson-Jones, T. W., Jones, A. K. & Hulley, P. a. Functional assessment of gap junctions in monolayer and three-dimensional cultures of human tendon cells using fluorescence recovery after photobleaching. *J. Biomed. Opt.* **19,** 15001 (2014).

114. Cheng, K. *et al.* Magnetic targeting enhances engraftment and functional benefit of iron-labeled cardiosphere-derived cells in myocardial infarction. *Circ. Res.* **106,** 1570–81 (2010).

115. Harms, C. *et al.* Certain types of iron oxide nanoparticles are not suited to passively target inflammatory cells that infiltrate the brain in response to stroke. *J. Cereb. Blood Flow Metab.* **33,** e1-9 (2013).

116. Poller, W. *et al.* Magnetic Particle Spectroscopy Reveals Dynamic Changes in the

Magnetic Behavior of Very Small Superparamagnetic Iron Oxide Nanoparticles During Cellular Uptake and Enables Determination of Cell-Labeling Efficacy. *J. Biomed. Nanotechnol.* **12,** 337–346 (2016).

117. Lobsien, D., Dreyer, A. Y., Stroh, A., Boltze, J. & Hoffmann, K. T. Imaging of VSOP Labeled Stem Cells in Agarose Phantoms with Susceptibility Weighted and T2* Weighted MR Imaging at 3T: Determination of the Detection Limit. *PLoS One* **8,** 1–10 (2013).

118. Hernando, D. *et al.* R2* estimation using 'in-phase' echoes in the presence of fat: the effects of complex spectrum of fat. *J. Magn. Reson. Imaging* **37,** 717–26 (2013).

119. Feng, L. *et al.* A releasable disulfide carbonate linker for polyethyleneimine (PEI)-based gene vectors. *New J. Chem.* **38,** 5207–5214 (2014).

120. Hunt, M. A., Currie, M. J., Robinson, B. A. & Dachs, G. U. Optimizing transfection of primary human umbilical vein endothelial cells using commercially available chemical transfection reagents. *J. Biomol. Tech.* **21,** 66–72 (2010).

121. Zhang, J., Wang, Z., Lin, W. & Chen, S. Gene transfection in complex media using PCBMAEE-PCBMA copolymer with both hydrolytic and zwitterionic blocks. *Biomaterials* **35,** 7909–7918 (2014).

122. Lim, J. & Dobson, J. Improved transfection of HUVEC and MEF cells using DNA complexes with magnetic nanoparticles in an oscillating field. *J. Genet.* **91,** 223–7 (2012).

123. Martín de Llano, J. J. *et al.* Birth weight and characteristics of endothelial and smooth muscle cell cultures from human umbilical cord vessels. *J. Transl. Med.* **7,** 30 (2009).

124. Sunshine, J. C., Peng, D. Y. & Green, J. J. Uptake and transfection with polymeric nanoparticles are dependent on polymer end-group structure, but largely independent of nanoparticle physical and chemical properties. *Mol. Pharm.* **9,** 3375–3383 (2012).

125. Ma, Y., Zhang, Z., Wang, X., Xia, W. & Gu, H. Insights into the mechanism of magnetofection using MNPs-PEI/pDNA/free PEI magnetofectins. *Int. J. Pharm.* **419,** 247–254 (2011).

126. Dominska, M. *et al.* Breaking down the barriers: siRNA delivery and endosome escape. *J. Cell Sci.* **123,** 1183–9 (2010).

127. Clamme, J.-P., Krishnamoorthy, G. & Mély, Y. Intracellular dynamics of the gene delivery vehicle polyethylenimine during transfection: investigation by two-photon fluorescence correlation spectroscopy. *Biochim. Biophys. Acta - Biomembr.* **1617,** 52–61 (2003).

128. Lemcke, H., Steinhoff, G. & David, R. Gap junctional shuttling of miRNA — A novel pathway of intercellular gene regulation and its prospects in clinical application. *Cell. Signal.* **27,** 2506–2514 (2015).

129. Valiunas, V. *et al.* A comparison of two cellular delivery mechanisms for small interfering RNA. *Physiol. Rep.* **3,** e12286–e12286 (2015).

130. Seppenwoolde, J.-H. *et al.* Internal radiation therapy of liver tumors: qualitative and quantitative magnetic resonance imaging of the biodistribution of holmium-

loaded microspheres in animal models. *Magn. Reson. Med.* **53,** 76–84 (2005).

131. Voronina, N. *et al.* Non-viral magnetic engineering of endothelial cells with microRNA and plasmid-DNA—An optimized targeting approach. *Nanomedicine Nanotechnology, Biol. Med.* (2016). doi:10.1016/j.nano.2016.06.015

132. Müller, P. *et al.* Magnet-Bead Based MicroRNA Delivery System to Modify CD133 + Stem Cells. *Stem Cells Int.* **2016,** 1–16 (2016).

133. Lee, J. H., Kim, J. W. & Cheon, J. Magnetic nanoparticles for multi-imaging and drug delivery. *Mol. Cells* **35,** 274–284 (2013).

134. Barcelos, L. S. *et al.* Human CD133+ Progenitor Cells Promote the Healing of Diabetic Ischemic Ulcers by Paracrine Stimulation of Angiogenesis and Activation of Wnt Signaling. *Circ. Res.* **104,** 1095–1102 (2009).

135. Bongiovanni, D. *et al.* The CD133+ cell as advanced medicinal product for myocardial and limb ischemia. *Stem Cells Dev.* **23,** 2403–21 (2014).

136. Yerebakan, C. *et al.* Impact of preoperative left ventricular function and time from infarction on the long-term benefits after intramyocardial CD133 + bone marrow stem cell transplant. *J. Thorac. Cardiovasc. Surg.* **142,** 1530–1539.e3 (2011).

137. Manginas, A. *et al.* Pilot study to evaluate the safety and feasibility of intracoronary CD133(+) and CD133(-) CD34(+) cell therapy in patients with nonviable anterior myocardial infarction. *Catheter. Cardiovasc. Interv.* **69,** 773–81 (2007).

138. Colombo, A. *et al.* Myocardial blood flow and infarct size after CD133+ cell injection in large myocardial infarction with good recanalization and poor reperfusion: results from a randomized controlled trial. *J. Cardiovasc. Med. (Hagerstown).* **12,** 239–48 (2011).

139. Tian, S. *et al.* Endothelial cell-targeted pVEGF165 polyplex plays a pivotal role in inhibiting intimal thickening after vascular injury. *Int. J. Nanomedicine* **Volume 10,** 5751 (2015).

140. Chen, Y. *et al.* Development of an MRI-visible nonviral vector for siRNA delivery targeting gastric cancer. *Int. J. Nanomedicine* **7,** 359–68 (2012).

141. Kwok, A. & Hart, S. L. Comparative structural and functional studies of nanoparticle formulations for DNA and siRNA delivery. *Nanomedicine Nanotechnology, Biol. Med.* **7,** 210–219 (2011).

142. Yang, H. *et al.* Cell type and transfection reagent-dependent effects on viability, cell content, cell cycle and inflammation of RNAi in human primary mesenchymal cells. *Eur. J. Pharm. Sci.* **53,** 35–44 (2014).

143. Yue, Y. *et al.* Revisit complexation between DNA and polyethylenimine — Effect of length of free polycationic chains on gene transfection. *J. Control. Release* **152,** 143–151 (2011).

144. Diener, Y. *et al.* RNA-based, transient modulation of gene expression in human haematopoietic stem and progenitor cells. *Sci. Rep.* **5,** 17184 (2015).

145. Scholz, C. & Wagner, E. Therapeutic plasmid DNA versus siRNA delivery: common and different tasks for synthetic carriers. *J. Control. Release* **161,** 554–65 (2012).

146. Nowakowski, A., Andrzejewska, A., Janowski, M. & Walczak, P. Genetic engineering of stem cells for enhanced therapy. 1–18 (2013).

147. Juliano, R. L. The delivery of therapeutic oligonucleotides. *Nucleic Acids Res.* **347,** gkw236 (2016).

148. Osbourne, A. *et al.* Downregulation of connexin43 by microRNA-130a in cardiomyocytes results in cardiac arrhythmias. *J. Mol. Cell. Cardiol.* **74,** 53–63 (2014).

149. Wang, S. *et al.* The endothelial-specific microRNA miR-126 governs vascular integrity and angiogenesis. *Dev. Cell* **15,** 261–71 (2008).

150. Gupta, R., Tongers, J. & Losordo, D. W. Human Studies of Angiogenic Gene Therapy. *Circ. Res.* **105,** 724–736 (2009).

151. Markkanen, J. E., Rissanen, T. T., Kivelä, A. & Ylä-Herttuala, S. Growth factor-induced therapeutic angiogenesis and arteriogenesis in the heart--gene therapy. *Cardiovasc. Res.* **65,** 656–64 (2005).

152. Dakhlallah, D. *et al.* MicroRNA-133a engineered mesenchymal stem cells augment cardiac function and cell survival in the infarct heart. *J. Cardiovasc. Pharmacol.* **65,** 241–51 (2015).

153. Seeger, F. H., Zeiher, A. M. & Dimmeler, S. MicroRNAs in Stem Cell Function and Regenerative Therapy of the Heart. *Arterioscler. Thromb. Vasc. Biol.* **33,** 1739–1746 (2013).

154. Assmus, B. *et al.* Effect of shock wave-facilitated intracoronary cell therapy on LVEF in patients with chronic heart failure: the CELLWAVE randomized clinical trial. *JAMA* **309,** 1622–31 (2013).

155. Bartunek, J. *et al.* Cardiopoietic stem cell therapy in heart failure: The C-CURE (cardiopoietic stem cell therapy in heart failURE) multicenter randomized trial with lineage-specified biologics. *J. Am. Coll. Cardiol.* **61,** 2329–2338 (2013).

156. Ooi, A. G. L. *et al.* MicroRNA-125b expands hematopoietic stem cells and enriches for the lymphoid-balanced and lymphoid-biased subsets. *Proc. Natl. Acad. Sci.* **107,** 21505–21510 (2010).

157. Chen, J., Guo, Z., Tian, H. & Chen, X. Production and clinical development of nanoparticles for gene delivery. *Mol. Ther. Methods Clin. Dev.* **3,** 16023 (2016).

158. Park, J. *et al.* Quantum Dots in an Amphiphilic Polyethyleneimine Derivative Platform for Cellular Labeling , Targeting , Gene Delivery , and Ratiometric Oxygen Sensing. 6511–6521 (2015).

159. Fornasiero, E. F. & Opazo, F. Super-resolution imaging for cell biologists. *BioEssays* **37,** 436–451 (2015).

160. Soenen, S. J. *et al.* Cellular toxicity of inorganic nanoparticles: Common aspects and guidelines for improved nanotoxicity evaluation. *Nano Today* **6,** 446–465 (2011).

161. Kim, Y.-W. *et al.* Oxidative stress in angiogenesis and vascular disease. *Blood* **123,** 625–31 (2014).

162. Carenza, E. *et al.* In vitro angiogenic performance and in vivo brain targeting of

magnetized endothelial progenitor cells for neurorepair therapies. *Nanomedicine* **10,** 225–34 (2014).

163. Wang, Y. *et al.* Regulation of VEGF-induced endothelial cell migration by mitochondrial reactive oxygen species. *Am. J. Physiol. Cell Physiol.* **301,** C695-704 (2011).

164. Mejías, R. *et al.* Long term biotransformation and toxicity of dimercaptosuccinic acid-coated magnetic nanoparticles support their use in biomedical applications. *J. Control. Release* **171,** 225–233 (2013).

165. Wu, X., Tan, Y., Mao, H. & Zhang, M. Toxic effects of iron oxide nanoparticles on human umbilical vein endothelial cells. *Int. J. Nanomedicine* **5,** 385–99 (2010).

166. Wang, Y.-X. J. Superparamagnetic iron oxide based MRI contrast agents: Current status of clinical application. *Quant. Imaging Med. Surg.* **1,** 35 (2011).

167. Bae, J.-E. *et al.* The effect of static magnetic fields on the aggregation and cytotoxicity of magnetic nanoparticles. *Biomaterials* **32,** 9401–9414 (2011).

168. Shaw, J. *et al.* Modulation of cytotoxic and genotoxic effects of nanoparticles in cancer cells by external magnetic field. *Cancer Nanotechnol.* **5,** 2 (2014).

169. Kyrtatos, P. G. *et al.* Magnetic Tagging Increases Delivery of Circulating Progenitors in Vascular Injury. *JACC Cardiovasc. Interv.* **2,** 794–802 (2009).

170. Huang, Z. *et al.* Magnetic targeting enhances retrograde cell retention in a rat model of myocardial infarction. *Stem Cell Res. Ther.* **4,** 149 (2013).

171. Landázuri, N. *et al.* Magnetic targeting of human mesenchymal stem cells with internalized superparamagnetic iron oxide nanoparticles. *Small* **9,** 4017–26 (2013).

172. Vandergriff, A. C. *et al.* Magnetic targeting of cardiosphere-derived stem cells with ferumoxytol nanoparticles for treating rats with myocardial infarction. *Biomaterials* **35,** 8528–8539 (2014).

173. Cheng, K. *et al.* Magnetic enhancement of cell retention, engraftment, and functional benefit after intracoronary delivery of cardiac-derived stem cells in a rat model of ischemia/reperfusion. *Cell Transplant.* **21,** 1121–35 (2012).

174. Fujioka, Y. *et al.* Magnetic Field-Based Delivery of Human CD133(+) Cells Promotes Functional Recovery After Rat Spinal Cord Injury. *Spine (Phila. Pa. 1976).* **37,** E768–E777 (2012).

175. Cheng, K. *et al.* Magnetic Targeting Enhances Engraftment and Functional Benefit of Iron-Labeled Cardiosphere-Derived Cells in Myocardial Infarction. *Circ. Res.* **106,** 1570–1581 (2010).

176. Soenen, S. J. H., Nuytten, N., De Meyer, S. F., De Smedt, S. C. & De Cuyper, M. High Intracellular Iron Oxide Nanoparticle Concentrations Affect Cellular Cytoskeleton and Focal Adhesion Kinase-Mediated Signaling. *Small* **6,** 832–842 (2010).

177. Vandergriff, A. C. *et al.* Magnetic targeting of cardiosphere-derived stem cells with ferumoxytol nanoparticles for treating rats with myocardial infarction. *Biomaterials* **35,** 8528–8539 (2014).

178. Sasaki, H. *et al.* Therapeutic Effects With Magnetic Targeting of Bone Marrow

Stromal Cells in a Rat Spinal Cord Injury Model. *Spine (Phila. Pa. 1976).* **36,** 933–938 (2011).

179. Cheng, K. *et al.* Magnetic antibody-linked nanomatchmakers for therapeutic cell targeting. *Nat. Commun.* **5,** 4880 (2014).
180. Roell, W. *et al.* Engraftment of connexin 43-expressing cells prevents post-infarct arrhythmia. *Nature* **450,** 819–824 (2007).
181. Li, M., Gu, H. & Zhang, C. Highly sensitive magnetite nano clusters for MR cell imaging. *Nanoscale Res. Lett.* **7,** 204 (2012).
182. Heyn, C., Bowen, C. V., Rutt, B. K. & Foster, P. J. Detection threshold of single SPIO-labeled cells with FIESTA. *Magn. Reson. Med.* **53,** 312–320 (2005).
183. Smirnov, P. *et al.* In vivo single cell detection of tumor-infiltrating lymphocytes with a clinical 1.5 Tesla MRI system. *Magn. Reson. Med.* **60,** 1292–7 (2008).
184. Kwon, J.-S. *et al.* Regulation of MMP/TIMP by HUVEC transplantation attenuates ventricular remodeling in response to myocardial infarction. *Life Sci.* **101,** 15–26 (2014).
185. Merx, M. W. *et al.* Transplantation of human umbilical vein endothelial cells improves left ventricular function in a rat model of myocardial infarction. *Basic Res. Cardiol.* **100,** 208–216 (2005).
186. Kovacic, J. C., Mercader, N., Torres, M., Boehm, M. & Fuster, V. Epithelial-to-Mesenchymal and Endothelial-to-Mesenchymal Transition. *Circulation* **125,** (2012).
187. Polchow, B. *et al.* Cryopreservation of human vascular umbilical cord cells under good manufacturing practice conditions for future cell banks. *J. Transl. Med.* **10,** 98 (2012).
188. Polyak, B. *et al.* High field gradient targeting of magnetic nanoparticle-loaded endothelial cells to the surfaces of steel stents. *Proc. Natl. Acad. Sci. U. S. A.* **105,** 698–703 (2008).
189. Kobayashi, H. *et al.* Angiocrine factors from Akt-activated endothelial cells balance self-renewal and differentiation of haematopoietic stem cells. *Nat. Cell Biol.* **12,** 1046–1056 (2010).
190. Li, N. *et al.* Human umbilical vein endothelial cells increase ex vivo expansion of human CD34+ PBPC through IL-6 secretion. *Cytotherapy* (2009).
191. Magin, S. *et al.* Primary cells as feeder cells for clinical co-culture expansion of human hematopoietic stem cells from umbilical cord blood – a comparative study. *Stem Cell Dev.* **18,** (2009).
192. Raynaud, C. M. *et al.* Endothelial cells provide a niche for placental hematopoietic stem/progenitor cell expansion through broad transcriptomic modification. *Stem Cell Res.* **11,** 1074–1090 (2013).
193. Yildirim, S., Boehmler, A. M., Kanz, L. & Möhle, R. Expansion of cord blood CD34+ hematopoietic progenitor cells in coculture with autologous umbilical vein endothelial cells (HUVEC) is superior to cytokine-supplemented liquid culture. *Bone Marrow Transplant.* **36,** 71–79 (2005).

194. Park, B., Yoo, K. H. & Kim, C. Hematopoietic stem cell expansion and generation: The ways to make a breakthrough. *Blood Res.* **50,** 194–203 (2015).

195. Miraglia, S. *et al.* A novel five-transmembrane hematopoietic stem cell antigen: isolation, characterization, and molecular cloning. *Blood* **90,** 5013–21 (1997).

196. Tongers, J., Losordo, D. W. & Landmesser, U. Stem and progenitor cell-based therapy in ischaemic heart disease: promise, uncertainties, and challenges. *Eur. Heart J.* **32,** 1197–206 (2011).

197. Gehling, U. M. *et al.* In vitro differentiation of endothelial cells from AC133-positive progenitor cells. *Blood* **95,** 3106–12 (2000).

198. Invernici, G. *et al.* Human Fetal Aorta Contains Vascular Progenitor Cells Capable of Inducing Vasculogenesis, Angiogenesis, and Myogenesis in Vitro and in a Murine Model of Peripheral Ischemia. *Am. J. Pathol.* **170,** 1879–1892 (2007).

199. Torrente, Y. *et al.* Human circulating AC133+ stem cells restore dystrophin expression and ameliorate function in dystrophic skeletal muscle. *J. Clin. Invest.* **114,** 182–195 (2004).

200. Negroni, E. *et al.* In Vivo Myogenic Potential of Human CD133∓ Muscle-derived Stem Cells: A Quantitative Study. *Mol. Ther.* **17,** 1771–1778 (2009).

201. Brendel, C. *et al.* CD133-targeted Gene Transfer Into Long-term Repopulating Hematopoietic Stem Cells. *Mol. Ther.* **23,** 63–70 (2014).

202. Stamm, C. *et al.* Intramyocardial delivery of CD133+ bone marrow cells and coronary artery bypass grafting for chronic ischemic heart disease: Safety and efficacy studies. *J. Thorac. Cardiovasc. Surg.* **133,** 717–725.e5 (2007).

203. Bartunek, J. *et al.* Intracoronary injection of CD133-positive enriched bone marrow progenitor cells promotes cardiac recovery after recent myocardial infarction: Feasibility and safety. *Circulation* **112,** (2005).

204. Marbán, E. *et al.* Mixed Results for Bone Marrow–Derived Cell Therapy for Ischemic Heart Disease. *JAMA* **308,** 2405 (2012).

205. Genovese, P. *et al.* Targeted genome editing in human repopulating haematopoietic stem cells. *Nature* **510,** 235–240 (2014).

206. Höbel, S. & Aigner, A. Polyethylenimines for siRNA and miRNA delivery *in vivo*. *Wiley Interdiscip. Rev. Nanomedicine Nanobiotechnology* **5,** n/a-n/a (2013).

207. Ohkawa, S. *et al.* Magnetic targeting of human peripheral blood CD133+ cells for skeletal muscle regeneration. *Tissue Eng. Part C. Methods* **19,** 631–41 (2013).

208. Sauvageau, G., Iscove, N. N. & Humphries, R. K. In vitro and in vivo expansion of hematopoietic stem cells. *Oncogene* **23,** 7223–7232 (2004).

209. Yan, M. *et al.* Modulation of Gene Expression by Polymer Nanocapsule Delivery of DNA Cassettes Encoding Small RNAs. *PLoS One* **10,** e0127986 (2015).

210. Jin, H. Y. *et al.* Transfection of microRNA Mimics Should Be Used with Caution. *Front. Genet.* **6,** 340 (2015).

211. Bietenbeck, M., Florian, A., Faber, C., Sechtem, U. & Yilmaz, A. Remote magnetic targeting of iron oxide nanoparticles for cardiovascular diagnosis and therapeutic drug delivery: where are we now? *Int. J. Nanomedicine* **11,** 3191–203 (2016).

212. Kraitchman, D. L., Gilson, W. D. & Lorenz, C. H. Stem cell therapy: MRI guidance and monitoring. *J. Magn. Reson. Imaging* **27,** 299–310 (2008).

213. Wang, S. *et al.* Multifunctional reduction-responsive SPIO&DOX-loaded PEGylated polymeric lipid vesicles for magnetic resonance imaging-guided drug delivery. *Nanotechnology* **27,** 165101 (2016).

214. Burgess, A. *et al.* Targeted delivery of neural stem cells to the brain using MRI-guided focused ultrasound to disrupt the blood-brain barrier. *PLoS One* **6,** e27877 (2011).

215. Weber-Adrian, D. *et al.* Gene delivery to the spinal cord using MRI-guided focused ultrasound. *Gene Ther.* **22,** 568–577 (2015).

216. Muthana, M. *et al.* Use of magnetic resonance targeting to direct cell therapy to target sites in vivo. *Nat. Commun.* **6,** 1–11 (2013).

217. Jain, T. K., Reddy, M. K., Morales, M. A., Leslie-Pelecky, D. L. & Labhasetwar, V. Biodistribution, Clearance, and Biocompatibility of Iron Oxide Magnetic Nanoparticles in Rats. *Mol. Pharm.* **5,** 316–327 (2008).

218. Vasconcelos Braz, S. *et al.* Morphological Analysis of Reticuloendothelial System in Capuchin Monkeys (Sapajus spp.) after Meso-2,3-Dimercaptosuccinic Acid (DMSA) Coated Magnetic Nanoparticles Administration. *PLoS One* **10,** e0140233 (2015).

219. Ricci, M. A., Manzo, C., García-Parajo, M. F., Lakadamyali, M. & Cosma, M. P. Chromatin fibers are formed by heterogeneous groups of nucleosomes in vivo. *Cell* **160,** 1145–58 (2015).

FINANCIAL SUPPORT

This work was carried out at the Reference and Translation Center for Cardiac Stem Cell Therapy (RTC), Department of Cardiac Surgery, University of Rostock and supported by the Federal Ministry of Education and Research Germany (FKZ 0312138A and FKZ 316159) and the State Mecklenburg-Western Pomerania with EU Structural Funds (ESF/IV-WM-B34-0030/10 and ESF/IV-BM-B35-0010/12), by the DFG (DA 1296-1) and the German Heart Foundation (F/01/12).

PUBLICATION LIST

Original publications

1:

Schade A, Müller P, Delyagina E, **Voronina N**, Skorska A, Lux C, et al. Magnetic Nanoparticle Based Nonviral MicroRNA Delivery into Freshly Isolated CD105(+) hMSCs. *Stem Cells Int*. 2014;2014:197154.

2:

Hausburg F, Na S, **Voronina N**, Skorska A, Müller P, Steinhoff G, et al. Defining optimized properties of modified mRNA to enhance virus- and DNA- independent protein expression in adult stem cells and fibroblasts. *Cell Physiol Biochem*. 2015;35(4):1360–71.

3:

Voronina N, Lemcke H, Wiekhorst F, Kühn J-P, Rimmbach C, Steinhoff G, et al. Non-viral magnetic engineering of endothelial cells with microRNA and plasmid-DNA-An optimized targeting approach. *Nanomedicine*. 2016 Jul 4;12(8):2353–64.

4:

Lemcke H, Peukert J, **Voronina N**, Skorska A, Steinhoff G, David R. Applying 3D-FRAP microscopy to analyse gap junction-dependent shuttling of small antisense RNAs between cardiomyocytes. J *Mol Cell Cardiol*. 2016 Jul 29;98:117–27.

5:

Müller P#, **Voronina N**#, Hausburg F#, Lux C, Steinhoff G & David R (#, authorship equally shared) "Magnet-Bead Based MicroRNA Delivery System to Modify CD133 $^{+}$ Stem Cells." *Stem Cells Int.* **2016,** 1–16 (2016).

Review book chapter

Voronina N, Delyagina E, David R, Steinhoff G. Inorganic nanoparticles for gene delivery. In: Advances and Challenges in the Delivery of Nucleic Acid Therapeutics (Volume 1). *Future Medicine*; 2015. p. 108–23.

Patent pending

DE 102016216657.3. "Eukaryotische adulte Zellen umfassend ein Transfektionssystem und deren Herstellung und Verwendung".

Manuscripts in preparation or under revision

1:

Voronina N, Lemcke H, Wiekhorst F, Kühn J-P, Steinhoff G & David R. "Manufacturing and *in vitro* characterization of magnetized miR-modified endothelial cells for regenerative medicine": *JoVE, Invited original publication, under revision.*

2:

Nesteruk J, **Voronina N**, Bubritzki S, Kundt G, Donndorf P, Klopsch C, Kaminski A, Duckers HJ, Steinhoff G. "Stem cell registry program for cardiac patients: what benefits does it derive?": *ESC Heart Failure, under revision.*

3:

Lemcke H, Gäbel R, Sasse S, Zarnico N, **Voronina N**, Ludwig M, Skorska A, Klopsch C, David R, Steinhoff G, Lux C. Gap junctional shuttling of miRNA promotes cardiac differentiation of human mesenchymal stem cells": *manuscript in preparation.*

ABSTRACT PRESENTATIONS AND CONFERENCES

Voronina N*, David R, Steinhoff G. Novel approach for magnetically guided delivery of microRNA to endothelial cells. 10th International Conference on the Scientific and Clinical Applications of Magnetic Carriers, Dresden, 10-14 June 2014 (Poster)

Voronina N*, David R, Steinhoff G. Novel approach for magnetically guided delivery of microRNA to endothelial cells. ESGCT and NVGCT Collaborative Congress, The Hague, 23-26 October 2014 (Poster)

Voronina N*, David R, Steinhoff G. Improving non-viral modification of endothelial cells – magnetically driven approach. ESGCT and FSGCT Collaborative Congress, Helsinki, 17-20 September 2015 (Poster)

Voronina N*, Lemcke H, Wiekhorst F, Kühn JP, David R and Steinhoff G. Improving Virus-Free Modification of Endothelial Cells - Magnetically Targeted Manipulation. ASGCT 19th Annual Meeting, Washington, DC, 4-7 May 2016 (Poster)

ACKNOWLEDGEMENT

Faculty, friends and family members have helped me to complete this dissertation. In the following, I would like to express my gratitude to all of them for their support.

First of all, I would like to express my deep gratitude to Prof. Robert David for supervising this work. He has kindly provided constant scientific guidance, but also the freedom to pursue independent work.

I would like to thank a co-supervisor of this thesis, Prof. Dr. Gustav Steinhoff, Director of the Department of Cardiac Surgery for giving me the opportunity to work in his team on an interesting topic. In addition, I am very grateful for inspiring scientific discussions, motivation and support. It is important also to mention Prof. Dr. Olga Kudritskaya for providing me the initial and fruitful contact with Prof. Dr. Gustav Steinhoff.

I sincerely thank Dr. Cornelia Lux and Dr. Heiko Lemcke for their practical support, constructive criticism, reliability and friendly advice. I am very grateful to my colleagues Paula Müller and Frauke Hausburg for a great time spent together and for their patience.

Furthermore, I would like to extend my thanks to all former and current members of the FKGO research group: Praveen Vasudevan, Dr. Anna Skorska, Dr. Ralf Gäbel, Dr. Christian Rimmbach, Dr. Cajetan Lang, Dr. Marion Ludwig, Dr. Yue Zhang, Evgenya Delyagina, Dr. Anna Schade, Julia Jung, Anita Tölk, Margit Fritsche, Marten Möller, Madeleine Bartsch. Thank you for creating a comfortable working atmosphere and critical discussions.

I am very grateful to all the cooperation partners from other research institutes: Dr. Frank Wiekhorst (Physikalisch-Technische Bundesanstalt, Berlin, Germany), Dr.Jens-Peter Kühn and Stefan Hadlich (Department of Radiology and Neuroradiology, Ernst-Moritz-Arndt-University Greifswald, Greifswald, Germany), Dr. Markus Frank, G. Fulda (Electron Microscopy Center, University of Rostock, Rostock, Germany). These scientists have provided invaluable support which led to extension and strengthening of the obtained data.

I am grateful for the critical evaluation of my results by Prof. Michael Glocker and the members of the structured PhD program “Molecular Mechanisms of Regenerative Processes”.

High gratitude shall be paid to the team of the Department of Cardiac Surgery and Referenceand Translation Center for Cardiac Stem Cell Therapy: Dr. Gudrun Tiedemann, Dr. Ulrike Ruch, Dr. Jana Große, Dr. Sandra Kurzawski, Dr. Frauke Stähler, Jana Gabriel nad Katrin Höfer.

Finally, I would like to give warm thanks to my family and friends, who have always been extremely supportive and patient. Their love and encouragement helped me to complete this thesis.